Neuroanatomical Dysconnectivity in Bipolar Disorder

By

Stefani O'Donoghue, BSc

A thesis submitted to the National University of Ireland Galway, as fulfilment of the requirements for a degree of Doctor of Philosophy

Research Supervisors: Prof Colm McDonald,
Dr. Dara Cannon

Table of Contents

Author's Declaration

I declare that all of the work presented in this thesis was carried out in accordance with the regulations of the National University of Ireland, Galway. This is original work carried out by myself, except where indicated by reference in the text. This thesis has not been submitted previously for any other academic award.

Signature: Date:

11/10/16

Stefani O'Donoghue

Acknowledgements

There are several people I would like to gratefully acknowledge and thank for their continuous encouragement and support during the course of my PhD.

First of all, I would like to thank my supervisor, **Prof. Colm McDonald**, for giving me the opportunity to work in the Clinical Neuroimaging Lab. His expert advice and guidance has tremendously supported my progress during the PhD. I owe my achievements in the past four years to his dedicated mentorship.

Dr. Dara Cannon, has generously gone above and beyond the role of co-supervisor. She has committed an immense amount of time to my work and progress. I am indebted to her for the support she has shown me during the challenging times of this PhD process.

There are two people in particular I would like to acknowledge for their contribution to the development of the rich-club measure. **Liam Kilmartin** and **Dr. Denis O'Hora** have offered me tremendous assistance in the engineering and statistics components of this complex and novel analysis technique. Collaborating with these scientific experts has given me the appreciation of knowing when and how to ask for guidance.

I would also like to thank the members of the **Clinical Neuroimaging Lab** for being a family to me during the last four years. I thank all of the lab members for their kindness, **Marian Fannon** for her positivity and encouragement, and **Dr. Brian Hallahan** for his advice and professional support.

I would like to acknowledge the **Hardiman Research Scholarship** for allowing me to carry out my research at NUI Galway.

I would like to thank the international research centres for their contribution in collecting the data presented in this thesis. I would also like to note, the multi-centre collaboration would not have been possible without **Prof. McDonald's** organisation. The clinical and neuroimaging data for the Galway Bipolar Study was collected by **Dr. Camilla Langan** and **Dr. Louise Emsell**. The acquisition of data for the three centre study was supervised by **Dr. Josselin Houenou, Prof. Michele Wessa, and Prof. Mary Phillips**.

Most importantly, I would like to acknowledge and gratefully thank the patients and healthy volunteers for dedicating their time to participating in this research.

Personal Thanks

There are a number of people who deserve significant mention for their moral support during the course of my PhD.

My mammy, **Moyra**, for always encouraging me to follow my passion and go for it with full force. Thank you for teaching me to solve any task by crossing off the stickies one by one.

My dad, **John**, for always being proud of me regardless of achievement. His continuous encouragement to "not limit myself to a 40-hour work week" helped push this thesis to completion.

My friends **Nora, Laura, Chelsey, and Ali** for being my pen pals over the last four years. They have endured emails and messages that potentially read longer than this thesis. I would like to thank them for their unwavering friendship, support, and love.

Most significantly, I would like to acknowledge my sisters, **Kerry and Sandra**. It is through them I have been inspired to pursue a career in neuroscience and psychology. Over the past 26 years, they have been my mirror image and polar opposite. They are my motivators and support system. Therefore, I dedicate this thesis to them.

List of Figures

Chapter 1

Chapter 2

Chapter 3

List of Tables

Chapter 1

Chapter 3

Abstract

Bipolar Disorder (BD) is a major psychotic illness characterized by cyclic mood dysregulation. The dysconnectivity hypothesis suggests that psychotic illnesses arise not from regionally specific focal pathophysiology, but rather from impaired neuroanatomical integration across networks of brain regions. Decreased white matter organization has been hypothesized to be a feature of psychotic illnesses in general, and is supported by meta-analyses of Diffusion Tensor Imaging (DTI) studies in BD and schizophrenia. Although repeatedly associated with white matter microstructural alterations, predominantly among frontal-limbic and posterior parietal white matter, BD has been relatively unexplored through complex network analysis. This method combines structural and diffusion magnetic resonance imaging (MRI) to model the brain as a network and evaluate its topological properties. Few graph analyses investigations to date have probed neuroanatomical connectivity in BD and findings are inconsistent. This thesis utilizes graph analyses to examine features of structural integration and segregation in a moderate sized euthymic bipolar cohort, and then further in a large multi-centre collaboration.

Three main methodological approaches were employed: global and regional graph analysis, sub-network analysis, and rich-club connectivity analysis. Through the investigation into the topology of brain networks this work aims to elucidate the extent of neuroanatomical dysconnectivity in BD. The statistical approaches included ANCOVA and independent t-tests in the moderate size cohort. In the multi-centre investigations

linear mixed effects modeling was employed to account for the inherent differences due to research centre scanner hardware. Next, our sub-network and rich-club analyses implemented permutation testing to identify between group differences.

Results of the current work demonstrate neuroanatomical dysconnectivity as a feature of BD, supported through measures of integration and segregation. Regional dysconnectivity was most prominent in fronto-limbic and posterior parietal nodes across cohorts with BD compared with healthy volunteers. Sub-networks were more weakly connected in left fronto-temporal connections in the larger cohort with BD compared with controls. Rich-club connectivity findings indicated weak deficits in BD across the samples. Furthermore, analysis of rich-club membership provided evidence for impaired organization of right frontal structures.

Taken together, the findings suggest that neuroanatomical dysconnectivity in BD is present, diffuse and extends beyond fronto-limbic regions. Neuroanatomical dysconnectivity could be contributed to by impaired integration between neighboring brain regions. The application of graph theory to diffusion tensor imaging data can identify abnormalities of large scale networks associated with BD and help to elucidate the underlying neurobiology of the condition.

Manuscript Organization

Chapter 1 begins with an introduction to the clinical background and application of neuroimaging to detect neuroanatomical dysconnectivity in BD. Following, the neuroimaging background covers the principles of MRI and diffusion, the neuroimaging advances into the investigation of white matter, and describes standardized techniques implemented in the field. Next, the major diffusion meta-analyses to date in psychosis are selectively reviewed. Following, the origin of graph theory and components of network analysis are reviewed. Standardized graph theory properties applied in psychiatric cohorts are further defined. Following a review of the structural network analysis investigations to date in BD, the introduction chapter concludes with an overview of DTI findings in BD, leading into the aims and hypotheses of the thesis.

Chapter 2 addresses the methodological approaches of the research carried out in the thesis. To avoid repetition of complex network techniques, each section consists of the parameters implemented in the Galway Bipolar Study, and modifications made in the study across the four research centres. The graph theory study across the four centres consists of data from three international research centres and the re-analysed Galway data.

Chapter 3 presents the results of the methodological approaches employed across the cohorts of individuals with BD. The removal of the re-analysed Galway data from the four-centre study is also considered in the results. The results chapter is divided into five sections. First, the clinical and socio-demographic details are defined for the participant groups. The second section reports the findings of integration and segregation properties

of connectivity. The third section reports the findings of the sub-network analyses across research centres. The fourth results section describes differences in the normalized rich-club connections and rich-club membership. Finally, the associations of clinical characteristics in the patient group are related to measures of connectivity.

The discussion of the findings is carried out in Chapter 4. This chapter aims to interpret the findings in light of the current literature. The discussion is divided into multiple sections. The first discusses the global and regional connectivity properties, and how these are consistent across the datasets and tied together. The second addresses the findings from the sub-network analyses across all datasets. The third section explores the rich-club connectivity differences and structural rich-club membership. In addition, a general discussion will tie together these multiple measures of connectivity as a potential marker of BD. In addition, the methodological considerations and limitations are addressed. Finally, the thesis concludes with recommendations for future research.

Chapter 1

Introduction

Advances in diffusion Magnetic Resonance Imaging (MRI) allow for neuroanatomical connectivity to be assessed *in vivo* in populations with major psychotic illnesses. Neuroanatomical connectivity techniques model the brain as a network by mapping the set of grey matter structures with their linked white matter connections. Network science then applies graph theory to interpret features of neuroanatomical integration in debilitating brain disorders. To date, a paucity of research has employed graph theory based network analysis in Bipolar Disorder (BD). Of the few studies to date, the findings are variable. Therefore, this work sought to explain the pattern and extent of neuroanatomical dysconnectivity in a moderate sized euthymic bipolar cohort, and then further in a large multi-centre collaboration of individuals with BD.

Clinical Background

BD is a major psychiatric disorder characterized by intermittent episodes of mania and depression and is present in approximately 1% of the population(Belmaker 2004). Psychotic features are commonly observed in individuals with BD, which can clinically resemble other psychotic disorders like schizophrenia(Dunayevich & Keck 2000). These overlapping clinical features include delusions and disorganized thought form (Marneros

et al. 2009; Dunayevich & Keck 2000), with shared cognitive deficits such as inattention and working memory dysfunction.

In 1899, Emil Kraepelin first distinguished BD from schizophrenia, by highlighting the clinically separable features of BD as "manic-depressive insanity" from dementia praecox or schizophrenia(Kraepelin 1904; Zivanovic & Nedic 2012). The distinction between these two major psychotic disorders has been controversial for over a century with most research focusing on overlapping clinical features, genetics and neuroimaging rather than distinctive neurobiological features(McDonald et al. 2004; Craddock et al. 2005). These overlapping clinical features include delusions and disorganized thought form (Marneros et al. 2009; Dunayevich & Keck 2000), with shared cognitive deficits such as inattention and working memory dysfunction. Following, in 1957 Leonhard coined the term "bipolar" referring to individuals who experienced cyclic phases of mania and depression, and thereby patients present with two opposite poles of mood states (Leonhard 1957).

Bipolar Disorder Type I is diagnosed when an individual experiences at least one or more manic episodes along with subsequent depressive episodes. Bipolar Disorder Type II is diagnosed when an individual experiences one or more severe depressive episodes, along with periods of hypomania.

Defining characteristics of manic episodes include euphoric or irritable mood, excessive energy with a reduced need for sleep, impulsivity, grandiosity, and rapid speech(APA 1994). Individuals experiencing mania are typically hospitalized when symptoms interrupt their interpersonal or work functions. Hypomania can occur when a change in

behaviour is shown, and may be shorter in duration, but patients do not demonstrate functional impairment to the extent of manic episodes.

Defining characteristics of depressive episodes include low mood, anhedonia, feeling worthless or hopeless, changes in appetite and weight, psychomotor disruption, and further changes in sleeping patterns, poor concentration, and suicidal thoughts or behaviour(APA 1994). The most typical of these symptoms is anhedonia referring to the loss of ability to experience pleasure in previously enjoyable experiences(Velthorst & Meijer 2012). In addition, patients display psychomotor disruption that results in moving or thinking more slowly. Individuals must present with these characteristics of depressive disorder for 2 weeks in order to make a diagnosis(APA 1994).

In between these cyclic mood states are periods of mood stability termed euthymia. Investigating individuals with BD during a euthymic phase of illness allows for the investigation of persistent trait related abnormalities of the illness. The recent literature supports the existence of structural and functional brain abnormalities in remitted patients with BD (Langan & McDonald 2009; Chen et al. 2011).

To understand the components of graph theory based network analysis in more detail the principles of MRI, diffusion and neuroimaging advances in white matter orientation and organization are introduced in this section.

Magnetic Resonance Imaging Principles

Magnetic resonance imaging is a medical technique used to visualize the internal tissue of the body. The resolution of the MR image is dependent on the strength of the magnet, the frequency of the electromagnetic current, acquisition parameters, and the environment of the hydrogen protons. MRI uses hydrogen protons, present in both water and tissue, to create a small electromagnetic field. This is due to the magnetic moment (μ) in protons, which reflect the strength and direction of the inherent magnetic field surrounding the proton nucleus. These protons have a spinning charge and when placed in a strong magnetic field, B_0, they will align either parallel or anti-parallel to the magnetic field. Due to the magnetic moment (μ), the hydrogen protons interact with the magnetic field causing the protons to precess. They precess in two directions: parallel (low energy) and anti-parallel (high energy). The frequency of the precession is proportional to the strength of the magnetic field, given by the equation:

$$\omega_0 = \gamma B_0$$

where ω_0 is the Larmor frequency, γ is the gyromagnetic ratio, and B_0 is the main magnetic field measured as 1.5 or 3 Tesla in the current research(Figure 1.1).

Figure 1.1. Larmor precession

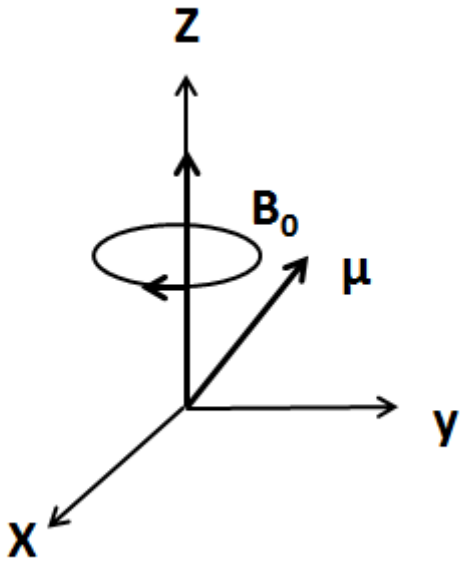

Figure 1.1. Legend. The precession of hydrogen protons is due to magnetic moment (μ) and magnetic field (B_0).

Alignment of the protons with the magnetic field can be altered by changing the radio frequency (RF) pulse. At rest, protons will spin at random about the B_0 along the z-axis. Then, when the RF pulse is applied, the protons will precess. As the RF pulse is turned off, the protons will return to equilibrium. The time it takes for protons to return from high energy states to equilibrium in the low energy state is considered the T1 relaxation

time. The T2 relaxation time refers to the time at which the precessing protons become more random.

A contrast image is produced by changing the strength, duration and sequence of RF pulses. This changes the angle at which the protons are flipped. Varying contrasts between tissues can be visualized by the relaxation properties of the protons, revealing differences in the brightness of voxels.

Figure 1.2. Illustration of T1 Image Contrast

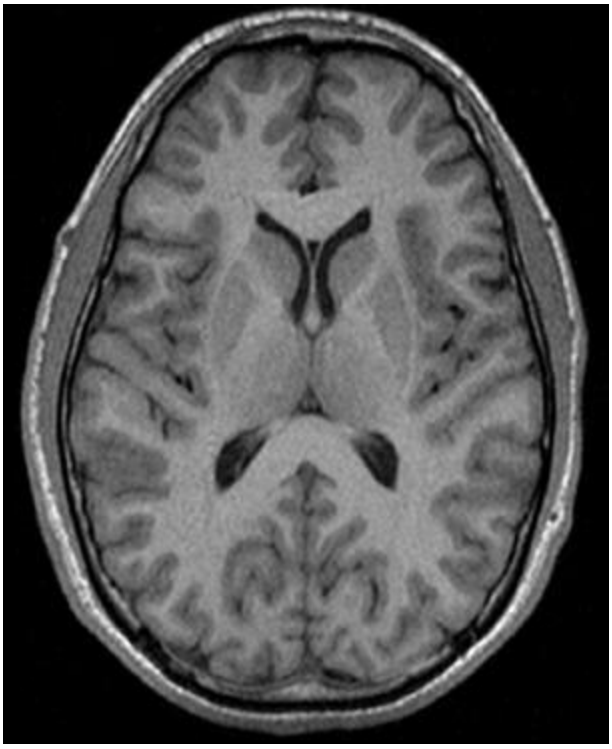

Using reconstruction techniques, structural MR images can be rendered into a 3D representation.

Diffusion MRI

A diffusion weighted MR image uses a modified sequence to the standard acquisition parameters of a T1 MR image. The standard MRI sequence is sensitized to the anisotropic properties of water molecules within axons to quantify the extent of microstructural white matter changes. In contrast to standard structural MRI acquisition, diffusion MR image sequencing includes magnetic field gradients to encode the spatial location of protons. The signal in the presence of diffusion is dependent on gradient strength and direction. The area of the diffusion weighted gradients and diffusion time both determine the b value, which characterizes the MR sensitivity to diffusion. The b-value refers to the degree of diffusion-weighting due to the signal intensity. The b-value will be higher if the diffusion gradient pulses have higher amplitudes over longer durations.

The process of diffusion is repeated in multiple directions to estimate a three-dimensional model (tensor). Stejskal and Tanner introduced the gradient spin echo sequence(Stejskal & Tanner 1965). This initial spin echo sequence shows two gradient applications.

Figure 1.3. Gradient Spin Echo diffusion-weighted MRI Sequence

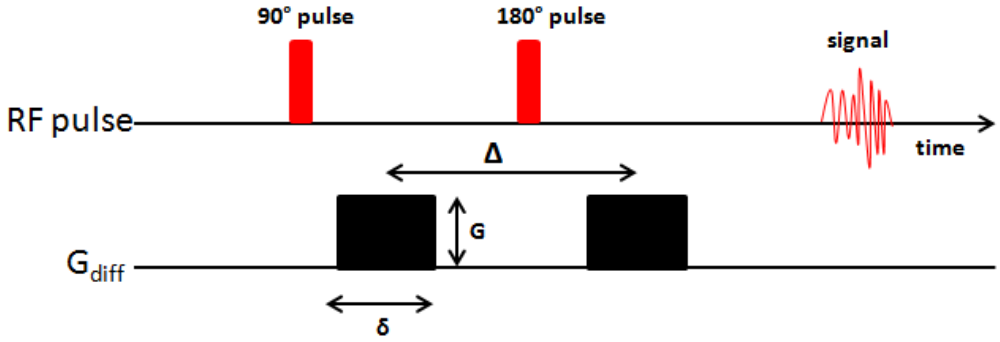

Figure 1.3 Legend. The typical spin echo sequence is characterized by: G the gradient strength, δ and Δ reflects the time of and time between the applied gradient. Dephasing occurs after the first 90° RF pulse. Each proton begins to precess at different rates. After second gradient application following 180° RF pulse the protons undergo rephasing. The rephasing completes when the protons do not diffuse during the time Δ between the two gradient applications.

Brownian motion

In 1905, Einstein suggested there was an inherent thermal motion surrounding water molecules(Jones 2008). He also believed this inherent motion of particles was related to properties of diffusivity. Einstein modeled the process of diffusion as a statistical "random walk," and determined that diffusion is reflected by the mean square distance traveled by molecules in a given interval of time (m^2/s), given by Einstein's equation:

$$< X >^2 = 2DT_d$$

Where $<X>^2$ is the mean-squared diffusion distance along one direction and T_d is the diffusion time. This equation laid the groundwork for developing the diffusion coefficient in biological tissue. In biological tissues, water molecules are restricted by intracellular and extracellular spaces. The diffusion in white matter is then considered anisotropic, where the displacement of water molecules is hindered along its boundaries and exhibits greater directionality(Beaulieu 2002). Anisotropic diffusion may be represented by coherently organized tissue. The diffusivity or displacement of water molecules in grey matter tissue will be more isotropic (Figure 1.4).

Figure 1.4. Isotropic and Anisotropic Diffusion

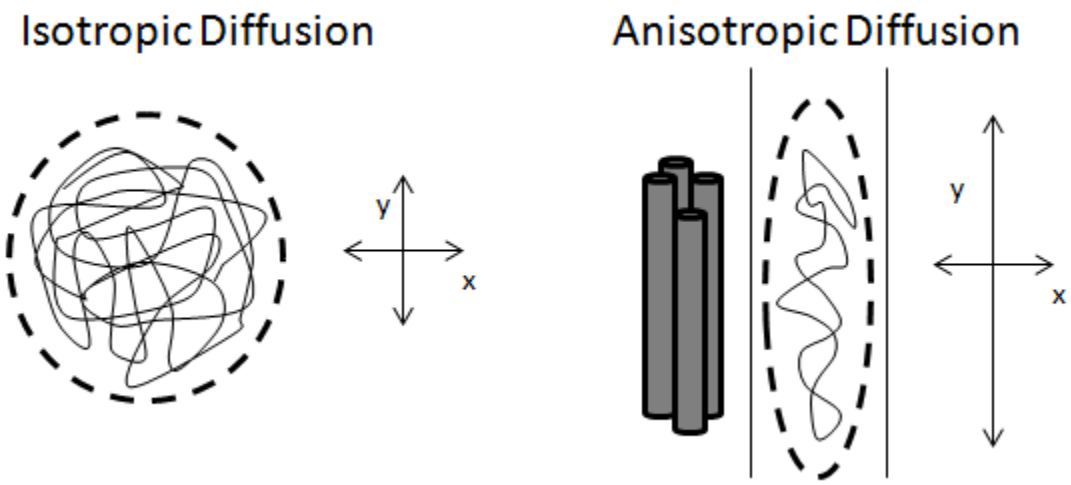

Figure 1.4 Legend. Isotropic diffusion reflects the displacement of molecules moving freely in every direction. Anisotropic diffusion is restricted parallel to its boundaries.

Diffusion Tensor

The diffusion tensor model allows for the quantification of the diffusion coefficient at every voxel in the brain. The diffusion coefficient, *D*, defines the displacement of molecules at each axis x, y, z, which relates to the principle directions of diffusion.

$$D = \begin{bmatrix} D_{xx} & D_{xy} & D_{xz} \\ D_{xy} & D_{yy} & D_{yz} \\ D_{xz} & D_{yz} & D_{zz} \end{bmatrix}$$

Measurements along 6 axes are needed to produce the 3D ellipsoid. The tensor then contains three eigenvalues reflecting the length of the shortest, middle and longest length of the ellipsoid, and the eigenvectors represent their orientations. Estimates of the diffusion tensor's eigenvalues measure the magnitude of the diffusion. The next section on neuroimaging advances investigating white matter orientation and organization cover the most commonly used measure of anisotropic diffusion, fractional anisotropy.

Neuroimaging Advances Investigating White Matter Orientation and Organization

Diffusion magnetic resonance imaging (dMRI) allows for a non-invasive investigation of microstructural alterations in white matter tracts through quantification of white matter connectivity *in vivo*(Jones 2008). Specifically, dMRI sequences are sensitized to measures the diffusion of water molecules in the brain which is hindered or restricted due to the local cellular environment (Le Bihan et al., 2001, Beaulieu, 2002).

This hindered or restricted diffusion pattern is influenced by cellular components such as cell density and packing, the integrity of the cell membrane, myelin sheath, and cytoskeleton, extracellular glial cells and the surrounding vasculature (Le Bihan et al., 2001). In white matter, water molecules diffuse along a preferential direction that is parallel to the axons located within tract bundles. Measuring this preferential or anisotropic diffusion pattern is used to estimate fibre orientation and reconstruct white matter pathways providing unique, clinically relevant white matter microstructural information that is not available using conventional MRI methods.

The diffusion tensor model is the most widely used method to characterise white matter organisation *in vivo*. Fractional anisotropy (FA), the most consistently reported tensor metric, reflects the degree of anisotropic diffusion (or level of organisation) within a fibre bundle (Pierpaoli et al., 1996, Jones, 2010). It has been proposed that the presence of intact cell membranes and myelination modulate anisotropy(Jones 2008), where differences in FA may reflect neuroinflammation or changes in myelination(Derek K. Jones et al. 2013; Jones 2010). However, the precise interpretation of FA is controversial because it is widely accepted that FA does not specifically correlate with a single component of the underlying microstructure. In addition, radial diffusivity (RD) has been employed as an alternative measure of white matter organization. RD quantifies the diffusion perpendicular to the principle diffusion direction.

To date, dMRI provides the most accurate reconstruction of white matter connectivity *in vivo*, and is therefore viable as a potential marker of white matter microstructural abnormality across brain disorders.

Standard techniques

Standard methods of analysing diffusion MRI data include whole brain voxel based analysis and deep white matter voxel-based analysis. Voxel based morphometry (VBM) is a classical technique for measuring volume related pathology in structural MRI, wherein localized and whole brain grey and white matter volume can be assessed(Ashburner & Friston 2000). This quantitative measure allows for the investigation at the voxel (volume and pixel) level, providing insight into volumetric

differences in specific regions of the brain(Ashburner & Friston 2000). Voxel-based analysis of diffusion data is distinct from voxel-based morphometry of structural data as voxel-based analysis of diffusion data is employed to examine localized differences in fractional anisotropy values between groups. One advantage of voxel-based techniques is that it is not biased to grey matter morphometry of structures with greater volume or surface area (Ashburner & Friston 2000). VBM output is susceptible to methodological variations during the process of spatially normalizing the MR images; therefore, other voxel based methods were developed to specifically explore white matter pathology, including Tract Based Spatial Statistics (TBSS). This technique statistically compares FA between groups in deep white matter voxels along the core of the tracts(Smith et al. 2006). Tract based spatial statistics create an average FA map common to the study participant group, wherein case-control differences can be calculated(Smith et al. 2006). Investigation into neuroanatomical differences in BD compared to healthy volunteers using VBM and TBSS indicate some inconsistencies in results between these methodologies (Vederine et al. 2011; Nortje et al. 2013).

A further approach to interrogating white matter structural pathology is through tractography, which presents structure, geometry and morphometry of diffusive properties of white matter(Tournier et al. 2007). Tractography analysis of particular white matter bundles relies on anatomical knowledge of a tract for reconstruction(Johansen-Berg & Behrens 2006; Johansen-Berg et al. 2004). Analysis of whole tract and segmented white matter tracts using tractography can identify focal white matter alterations in the brain when comparing groups of participants, for example patients with psychotic illness and healthy volunteers.

Finally, functional MRI (fMRI) is used to quantify functional connectivity or the synchronized activity between two or more spatially separated brain regions. Given that functional connectivity between anatomically separated regions indicates the existence of structural connections, there is also a considerable interest in probing anatomical connectivity using structural neuroimaging techniques.

Recent meta-analyses of diffusion MRI studies in BD

Recent meta-analyses collated white matter deficits reported in BD and schizophrenia independently. Reports of reduced organisation of white matter tracts in BD has been generally implicated (Vederine et al. 2011; Nortje et al. 2013), with support for limbic dysconnectivity in the illness. Most consistent aberrant microstructural organisation of white matter has been reported in the anterior limb of internal capsule, temporal-parietal white matter, and left posterior cingulum in patients with BD(Vederine et al. 2011; Nortje et al. 2013). A summary of these meta-analyses is provided in Table 1.

An initial meta-analysis of 10 voxel based studies in BD reveal clusters of decreased FA in participants with BD compared with healthy controls(Vederine et al. 2011). These clusters of reduced FA in patients were identified in white matter near the parahippocampal gyrus, and near the right anterior and subgenual cingulate cortex. These structures are likely to play a role in altered emotional processing and functional limbic connectivity in BD(Wessa & Linke 2009; Wessa et al. 2014). The area identified near the right parahippocampal gyrus is crossed by the superior longitudinal fasciculus (SLF), the inferior longitudinal fasciculus (ILF), the inferior occipital fasciulus (IFOF), and the

posterior thalamic radiations. This abnormality is consistent with dysconnectivity of association pathways having a role in the pathophysiology of BD, predominantly within leftward hemispheric asymmetry (Vederine et al. 2011). The second cluster combined the right anterior cingulate cortex (ACC) and subgenual cingulate cortex (SgCC), considered to present critical roles in automatic and conscious emotional processing(Phillips et al. 2008). Furthermore, cingulate deficits indicate impaired integration of cortico-subcortical connections (Emsell & McDonald 2009). The cingulum bundle has been repeatedly implicated as a neural substrate in BD and represents a central component of the limbic network(Benedetti et al. 2011; Lu et al. 2011; Heilbronner & Haber 2014; Wang et al. 2009).

Another meta-analysis of 15 DTI studies including both VBM and TBSS analysis identified 61 clusters of reduced FA in BD compared to healthy controls (Nortje et al. 2013). Additionally, sub-analysis of clinically homogenous participants with bipolar I disorder identified more robust clusters. The voxel-based analyses revealed white matter alterations of three frontal, three occipital, three parietal, and two temporal clusters in patients (Nortje et al. 2013). In comparison, the TBSS analysis identified reduced FA in right temporal-parietal white matter, suggesting dysconnectivity of the ILF and IFOF(Nortje et al. 2013). The main findings were consistently driven by the bipolar I disorder subgroup. Additionally, left cingulum and anterior cingulate white matter were identified as in the prior meta-analysis (Vederine et al., 2011). The most robust findings supporting the previous meta-analysis include larger clusters of reduced FA in right posterior white matter involving longer distance association tracts(Nortje et al. 2013).

Therefore, the findings are consistent with diffuse rather than discretely regional white matter alterations.

Table 1.1. Review of Diffusion tensor imaging meta-analyses in BD and SZ

Author	HC (n)	SZ (n)	BD (n)	Imaging Method	Findings
Ellison-Wright & Bullmore (2009)	383	407	N/A	Co-ordinates of FA differences	Alterations of left frontal deep white matter and left temporal deep white matter
Veredine et al. (2011)	279	N/A	289	Anatomical Likelihood Estimation	Two clusters of reduced FA One involving SLF, IFOF, ILF and posterior thalamic radiations. Second cluster included the uncinate, the IFOF and corpus callosum forceps minor
Nortje et al. (2013)	256 98	N/A	252 138	VBA TBSS	Widespread white matter involvement in BD Decreased FA in BD (right posterior tempoparietal cluster and two left cingulate clusters) anterior limbic.

Table 1.1 Legend. VBA: Voxel-based analysis; TBSS: Tract-based Spatial Statistics

Studies Directly Comparing White Matter Pathology between BD and Schizophrenia

Meta-analyses to date have focused upon individual illnesses, and few studies directly compare white matter organization using dMRI between BD and schizophrenia (Skudlarski et al., 2013; Sussmann et al., 2009; Wheeler et al., 2015b). Standard diffusion MR techniques applied in the investigation of structural alterations in vivo in schizophrenia and BD report common FA reductions within callosal and fronto-temporal regions (Table 2). Specifically, reduced white matter organization common to both BD and schizophrenia were reported in the callosal genu, anterior limb of the internal capsule, uncinate fasciculus, and anterior thalamic radiation supporting cortico-thalamic dysconnectivity (Sussmann et al., 2009). A comparison of paranoid schizophrenia and bipolar mania using diffusion MRI noted reduced connectivity among fronto-parietal and cortical-thalamic networks suggesting these networks are affected in symptomatic patients(Cui et al. 2011). Decreased white matter organization was associated with age in both psychotic BD and schizophrenia, however this observation was prominent in the schizophrenia group, which could reflect a more pervasive developmental feature in schizophrenia as compared to BD (Kirkpatrick et al. 2008). In BD, the anatomical location of white matter dysconnectivity may be clinically informative for disrupted networks responsible for the regulation of mood. Recently, a direct comparison of BD and major depression report reduced white matter organization in the genu of the corpus callosum possibly representing a shared substrate underpinning mood disorder, whereas reduced FA in the left posterior cingulum appeared specific to BD (Wise et al. 2015). Moreover, these direct comparison findings support the independent meta-analyses of BD and schizophrenia, suggesting that white matter microstructural abnormalities represent a

common phenotype across psychosis(Vederine et al. 2011; Nortje et al. 2013; Ellison-Wright & Bullmore 2009).

Taken together, these studies demonstrate shared callosal and frontal white matter dysconnectivity across BD and schizophrenia in focal analysis of FA at the voxel-level and along major white matter pathways. Further studies that would assess connectivity in patients with and without psychotic features in BD may assist in elucidating trait abnormalities associated with the development of psychotic symptoms as distinct from the core mood symptoms of bipolar affective disorder. Previously in a three-centre study, Sarrazin and colleagues reported differences in FA when they assessed differences in patients with and without a history of psychotic features(Sarrazin et al. 2014).These reported focal deficits within white matter highlight the scope for a network based approach to explore dysconnectivity. Network analysis has the potential to advance prior focal tractography analyses by mapping the series of connections in the brain through their anatomical elements to assess neuroanatomical connectivity. The following sections of this chapter describe the origin of graph analysis and some of the methodological challenges in this evolving discipline of in vivo neuroanatomical analysis.

Table 1.2. Direct DTI Comparison Studies of BD to Other Samples

Author	HC (n)	SZ (n)	BD (n)	Imaging Method	Findings
Sussman et al. (2009)	38	28	42	VBA	Alterations in ALIC, uncinate fasciulus, ATR common to both schizophrenia and BD.
Cui et al. (2011)	30	25	18	VBA	Reduced FA in left posterior corona radiate common to both bipolar mania and paranoid schizophrenia. Bipolar mania cohort showed reductions in FA in right posterior corona radiata and right ATR.
Sui et al. (2011)	62	54	48	DTI fMRI CAA, ICA	Both BD and schizophrenia shared reduced WM in anterior thalamic radiation and uncinate fasciulus. Differences in WM in occipital and frontal lobes.
Skudlarski et al. (2013)	104	125	82	TBSS	Lower FA in multiple regions; genu and body of corpus callosum common to both cohorts. FA in left SLF correlated with Schizophrenia-Bipolar Scale. Schizophrenia cohort had marked WM differences compared to BD.
Wise et al. (2015)	668 489	736	536	VBA and TBSS Meta-analysis	Both BD and major depression participants exhibited FA alterations in the genu of the corpus callosum. Differences in the left posterior cingulum demonstrated by reduced FA.
Wheeler et al. (2015)	130 43	128	39	Network analysis	Greater fronto-parietal and fronto-temporal coupling found in deficit schizophrenia compared to non-deficit schizophrenia, and in deficit schizophrenia compared with HC, as well as increased density of connections relative to controls and non-deficit schizophrenia. No differences between non-deficit schizophrenia and BD.

Table 1.2. Legend. Voxel Based Analysis (VBA), Tract Based Spatial Statistics (TBSS), Indepependent Component Analysis (ICA), White Matter (WM), Superior Longitudinal Fasiculus (SLF), Anterior Limb of Internal Capsule (ALIC), Anterior Thalamic Radiation (ATR)

Origin of Graph Theory Based Network Analyses

The origin of graph theory begins with the mathematician Euler, and his formula for the Seven Bridges of Konigsberg Problem, when in 1736 Euler represented the map of the city of Koningsberg, Russia as a graph(Bullmore & Sporns 2009; Fornito et al. 2013; Debnath 2010). The city holds seven bridges crossing the river Pregel, where he argued it was impossible to complete a path crossing over all seven bridges and return to their starting point by crossing every bridge only once(Bullmore & Sporns 2009; Fornito et al. 2013). He argued that there is no resolution due to the odd number of edges, wherein edges are not retraceable(Debnath 2010). Euler's formula of representing the land masses as vertex points and bridges as arcs conceived the branch of mathematics known as graph theory(Sporns 2013c). The application of graph theory has expanded to evaluate empirical networks as well as brain networks(Sporns 2013c; Sporns et al. 2005; Hagmann et al. 2008). One feature termed "small-worldness" describes a network with many short path lengths and high clustering. In social networks this has been described as the "six degrees of separation" phenomenon, wherein people can be linked to any other person by six or less steps. In addition, the rich-club phenomenon addresses how highly influential people are more likely to be well-connected with other highly influential people. Many properties of empirical networks have inspired their utility in the interpretation of brain networks, e.g. small-worldness and the rich-club

phenomenon(Sporns et al. 2000; Senden et al. 2014). Graph theory provides measures of topology, examining a structures' positioning in a network and its connectivity through an anatomical structure(Rubinov & Sporns 2010; Hagmann et al. 2008).

What is a brain network?

A structural brain network can be defined by both structural and diffusion weighted MRI to map neuroanatomical connectivity(Sporns 2013c; Bullmore & Sporns 2009; Rubinov & Sporns 2010; Crossley et al. 2013; Achard & Bullmore 2007). Alternatively, graph analyses can be readily applied with physiological data acquired using fMRI and EEG. Reconstruction of brain networks (or "connectome") maps a set of neuroanatomical landmarks and their structural connections. At the macro-scale, network analysis uses structural MRI to model the cortical and subcortical structures as "nodes", along with dMRI to reconstruct the set of white matter connections as "edges"(Zalesky, Fornito, Harding, et al. 2010; Fornito et al. 2013). Alternatively, functional networks can be implemented with correlativity time series data to represent edges.

A brain network models complex interactions between neuroanatomical elements, characterizing hierarchical ordering and clustering of connections as topological features which shape global integration(Bassett et al. 2009; Hagmann et al. 2008; Griffa et al. 2013). Brain networks by their nature should display small-world features, depicting high clustering and many short paths(He et al. 2007). This small-world feature of brain

networks describes connectivity that is non-random and highly efficient(He et al. 2007; Bassett et al. 2008).

The application of graph theory to brain networks is a novel and quickly evolving field, however comes with challenges. The components of complex network analysis lack standardization in node definition and edge weights(Fornito et al. 2013). A utility of this is that this allows for hypotheses to be probed by varying features of anatomical elements and connection strengths.

Node Definition

Node definition is known to have a marked sensitivity to the resulting findings from network data(Zalesky, Fornito, Harding, et al. 2010). Nodal parcellation may be atlas based, hold subject specific volumetric information, voxel-based, or defined by subject specific cortical thickness(Zalesky, Fornito, Harding, et al. 2010; de Reus & van den Heuvel 2013b; Wheeler et al. 2015). Applying a standardized atlas template has the benefit of reproducibility, however may lack anatomical sensitivity (Fornito and Bullmore, 2014; Johansen-berg, 2013). Atlas based parcellations run efficiently and are optimal for automated quantitative analysis(Tzourio-Mazoyer et al. 2002). Alternatively, subject specific parcellations map the participant's diffusion-weighted MR image with the anatomical MR image in order to link specific volumetric information with reconstructed white matter connections between each structure(Fischl 2012). Voxel-based definition has also been implemented in graph analysis (Zalesky, Fornito, Harding,

et al. 2010; Crossley et al. 2014). Recently, cortical thickness has been utilised in graph analysis studies in psychiatric illness, however this cortical thickness approach limits network reconstruction to cortical maps alone(Wheeler et al. 2015).

In summary, the majority of studies to date define a node based on subject-specific parcellation, however limit this to cortical mapping(Guusje Collin et al. 2015; van den Heuvel et al. 2013; Collin et al. 2014; G. Collin et al. 2015; Hagmann et al. 2008; Griffa et al. 2013). In BD most reports use cortical maps alone, which given the importance of the limbic system in emotional regulation, may limit the scope of network approaches in mood disorders.

Edge definition and weighting

Edges reflect the quantitative measure of connectivity between elements(Sporns 2013a; Sporns et al. 2005). Edges may define structural or functional measures of connectivity(Fornito et al. 2013). Tractography reconstruction of white matter connections using diffusion MRI – based tractography can be represented as edges. The quantification of edges are weighted by the number of reconstructed streamlines, fractional anisotropy, or percentage of tracts (Fornito et al. 2013). Streamlines refers to the number of reconstructed tracts between two nodes. These tracts are reconstructed from the eigenvector directions being orientated in the same direction. Standardized selection of connection weights remain unresolved, with most studies reporting the number of reconstructed streamlines or a defined threshold of streamlines to be

optimal(Fornito et al. 2013). Fractional anisotropy as a connection weight describes the mean FA between two nodes. These connection weights have been used to identify network abnormalities in brain disorders, however more neurobiologically valid models of connectivity could likely improve understanding of the mechanisms underpinning the network differences between patient populations and healthy individuals(Fornito et al. 2013; O'Donnell & Pasternak 2015). Current recommendations suggest presentation of findings from multiple edge weights(Fornito et al. 2013; O'Donnell & Pasternak 2015).

Graph thresholding is another topic of debate for graph analysis. The aim is to identify connections greater than a defined threshold in order to remove spurious or unlikely connections(Fornito et al. 2012). Optimal group thresholding in network analysis can be defined from 30-90% (de Reus & van den Heuvel 2013a). Some network approaches implement connection-weight or density-based thresholds (Fornito et al. 2012; Zalesky et al. 2011).

Lastly, edge connections can be defined by "pass" or "end" parameters when generating connection maps. Networks may be defined by connections that pass from one node to another node through a third node, assisting connections that integrate information(Fornito et al. 2013). Alternatively, networks may separately consider connections from one node that end at the following node(Fornito et al. 2013). While these connectivity parameters are critical to the interpretation of brain networks, relatively few investigations report which connectivity parameter has been implemented(Fornito et al. 2013). Therefore, it is difficult to ascertain the effect this choice may have on resulting analyses.

Graph Theory Measures

Following network reconstruction, graph theory properties are quantified to describe brain networks(Rubinov & Sporns 2010). These topological properties provide quantitative measures of network connectivity as a whole or can define a specific node's connectivity within the network. Definitions of the more commonly used measures are provided in Table 1.3.

Table 1.3. Standard Graph Theory Measures

Measure	Definition
Degree	Degree is the number of edges connected through a given node
Density	Density is the fraction of existing connections to possible connections
Betweenness Centrality	Betweenness is the fraction of all shortest paths in the network that contain a given node.
Characteristic Path Length	Defines the number of shortest path length in the network
Clustering Coefficient	Clustering is the equivalent to the fraction of node's neighbours that are neighbours to each other
Global Efficiency	The global efficiency is the average inverse shortest path length in the network, the inverse of path length
Local Efficiency	Local efficiency is the global efficiency but computed on node neighbourhoods. Related to clustering coefficient, it is a measure of segregation
Rich Club Coefficient	The rich club at density k is the fraction of edges that connect nodes of degree k or higher, these nodes are more likely to be highly connected than the rest of the network

Table 1.3 Legend. Definitions of standard regional graph measures. These measures characterize features of integration and segregation. Graph properties are used to interpret network models.

The *degree* within a network reflects the number of reconstructed edges through a given node(Rubinov & Sporns 2010). The mean degree of a network represents the average degree across all nodes. This may be skewed by low degree nodes and alternatively degree values may be calculated as the proportion of their degree corrected to the volume of the neuroanatomical structure they connect(Zalesky & Fornito 2009; van den Heuvel & Sporns 2011). A measure of global integration is the characteristic *path length* which defines the number of shortest paths across a given node, and is primarily influenced by longer paths (Rubinov & Sporns 2010; Bullmore & Sporns 2009). *Global efficiency* is mathematically the inverse of the shortest path length, with the global efficiency being affected or influenced by shorter paths(Rubinov & Sporns 2010; Achard & Bullmore 2007).

Local or regional graph properties examine connectivity patterns of specific nodes. In particular, local topological properties such as *local efficiency* and *clustering coefficient* represent paths of information processing specific to neuroanatomical elements(Rubinov & Sporns 2010). The extent of communication between neighbouring nodes indicates structural integration of related functional processes (Achard & Bullmore 2007; Bullmore & Sporns 2009; Rubinov & Sporns 2010). The nodal efficiency measures the capacity for information transfer of a particular node in the network. Another local property, clustering coefficient, measures the frequency of connection with neighbouring nodes,

determining how structures are segregated into communities (Crossley et al., 2013)(Table 1.3). Additionally, various in-house metrics have been developed by research groups to depict complex features of local connectivity patterns including measures of inter-hemispheric efficiency (Leow et al. 2013) and path length within and between communities to reveal patterns of hierarchical communities within networks(Gadelkarim et al., 2014).

Generated measures of centrality reflect structural integration between communities and regional networks. *Betweenness centrality* describes the minimum number of shortest paths through a node, thereby measuring quantitatively structural integration between communities(Caeyenberghs & Leemans 2014; Newman & Girvan 2004; van den Heuvel et al. 2010). Topologically central nodes are considered "hubs" in a network. These "hubs" are critical for information flow between communities and sub-networks(Rubinov & Bullmore 2013; van den Heuvel & Sporns 2013). If these "hubs" are affected by a pathophysiological process, this can undermine the efficiency of the network structure locally and globally.

Recently, a measure titled the *rich-club* identifies a group of structures more densely interconnected compared to the rest of the network i.e. by more than chance alone (McAuley et al., 2007; van den Heuvel and Sporns, 2011; Sporns and Van Den Heuvel, 2013; Senden et al., 2014a). Taken from empirical networks, the rich-club phenomenon describes the influential role of those rich in connections. This network property has been a recent focus of investigation across various brain disorders including Alzheimer's disease, Huntington's disease, schizophrenia, and BD (Collin et al., 2013; Collin et al.,

2015; Daianu et al., 2015; McColgan et al., 2015; van den Heuvel et al., 2013). Measures of networks may be critical for understanding complex network interactions and graph properties are advancing to describe such complex behaviours of brain networks(Ajilore et al. 2015).

Figure 1.5. Graphical representation of key graph theory metrics

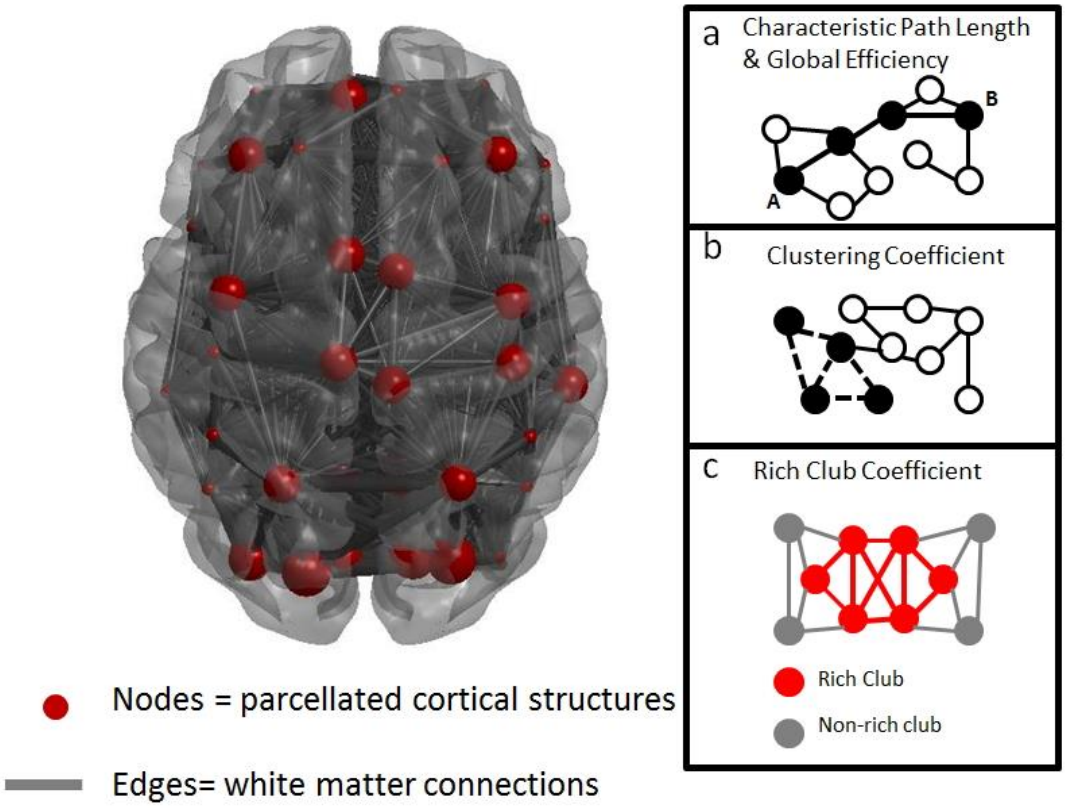

Figure 1.5. Legend. This brain map expresses the series of connections as a network, with white matter connections (edges) linking parcellated cortical regions (nodes). (a) characteristic path length: a measure of the graphs average shortest distance between node A and node B; global efficiency: measured as the inverse of path length. (b) clustering coefficient: the number of connections that exist between the nearest neighbours of a node as a proportion of the maximum number of possible connections. (c) rich club coefficient: highlights nodes that are more highly interconnected among themselves than with the rest of the nodes in the network.

The Potential Network Analysis Provides for Advancing the Field

Network analysis advances standard techniques by extending focal measures and assesses the influence of connectivity on communication and efficiency parameters globally. Recently, large-scale initiatives have been implemented to map the series of structural connections in the healthy brain, such as the Human Connectome Project(Van Essen 2011; Van Essen et al. 2013).

Graph theory measures may detect pathology contributing to deficits in global integration or mediating functional deficits(Bullmore & Sporns 2009; Derrible & Kennedy 2011; Fornito et al. 2013). The quickly advancing field of network analysis makes its application to investigating psychiatric illnesses timely. This technique infers anatomical integration which may also reflect physiological differences between healthy participants and individuals with psychiatric illness. Initial investigations into the interpretation of organizational patterns in healthy individuals demonstrate hierarchical relationships in neuroanatomical networks(Bassett et al. 2009; Hagmann et al. 2008; Meskaldji et al. 2013). Interpretation of these connectivity patterns define how altered integration of potentially vulnerable structures may contribute to whole brain dysconnectivity.

Functional connectome analysis advances standard fMRI techniques which infer connectivity based on time series data acquired during fMRI tasks(Bullmore & Sporns 2009). Functional network analysis can relate functionally relevant connectivity patterns

under specific cognitive tasks, or resting-state activity(Sporns 2013b). Functional connectivity measures the statistical relationship between two neuroanatomical regions(Sporns 2013a; Sporns 2013b). Functional activation is known to fluctuate during the MRI scan(Chiang et al. 2015). Recently, a methodological investigation tested graph theory measures stationarity over time, revealing global integration measures and betweenness centrality to be more stationary and therefore more robust measures to describe properties of functional networks(Chiang et al. 2015).

Structural-functional coupling has also been implemented in network applications in psychotic illnesses, wherein measures of structural connectivity have been related proportionally with functional connectivity measures(van den Heuvel et al. 2013). Moreover, structural connectivity measures have been correlated with findings from functional MRI time series data to elucidate the structure-function relationship(Ajilore et al. 2015). Advances in these neuroimaging modalities can aid in interpretation of directionality and intensity within connectivity alterations.

Review of structural network findings in BD

Most complex network investigations in BDs investigate trait related features of *well* patients with BD. An initial application of graph theory in 25 euthymic individuals with BD and 25 healthy controls reported global and nodal dysconnectivity, predominantly affected by reductions in fronto-limbic and inter-hemispheric connectivity(Leow et al. 2013). Global alterations were defined by reduced overall network clustering and global

efficiency, as well as increased characteristic path length(Leow et al. 2013). Moreover, measures of segregation revealed regional connectivity alterations. In this investigation, regional deficits in clustering and nodal efficiency measures converge across left fronto-limbic regions, specifically the left orbitofrontal gyrus, left hippocampal gyrus, and bilateral isthmus cingulate gyrus(Leow et al. 2013). In addition, alterations of inter-hemispheric path length suggests intra-hemispheric connectivity was more densely connected than inter-hemispheric connectivity (Leow et al. 2013). Inter-hemispheric dysconnectivity was identified mostly in the bilateral frontal lobes, with evidence for widespread deficits across temporal, parietal and occipital lobes.

In a further investigation of 25 euthymic patients with BD, node-level community structure was determined by an "in-house" measure Path Length Associated Community Estimation (PLACE)(Gadelkarim et al., 2014). PLACE measures the differences between inter-community and intra-community path lengths. These alterations were identified in a community containing the right paracentral gyrus, right posterior cingulate, left precentral gyrus and left posterior cingulate (Gadelkarim et al., 2014). Alterations in the left isthmus cingulate and left precuneus were associated with the number of depressive episodes, a potentially clinically relevant marker of illness prognosis. This study suggested left-right decoupling to be a trait feature of BD.

Another study implemented complex network analysis in multiply affected bipolar I disorder families, incorporating 19 patients with BD and 21 of their unaffected first degree relatives(Forde et al. 2015). This study probed structural connectivity by modeling cortical and subcortical regions, and their reconstructed connections. In contrast to early

investigations, this study did not identify deficits in global integration(Forde et al. 2015). However, nodal analysis based on prior focal DTI results identified reductions in clustering and local efficiency in left superior frontal and right medial superior frontal connections(Forde et al. 2015). Unaffected relatives displayed intermediate levels of clustering and local efficiency between patients with BD and healthy volunteers that did not significantly differ from either group.

Recent neuroimaging network analyses have also sought to identify the structure-function relationship in brain disorders, and particularly how measures of structural interaction are associated with function. The first network analysis study in BD to investigate this structure-function relationship utilized measures of structural inter-hemispheric integration in 24 individuals with BD compared to 23 healthy volunteers(Ajilore et al. 2015). They further identified measures of neuropsychological performance and signals of fMRI activation(Ajilore et al., 2015). The study included a neuropsychological battery assessing processing speed, verbal memory, working memory and cognitive flexibility, as well as a functional MRI task assessing response inhibition(Ajilore et al. 2015). Structural measures of path length, clustering coefficient, nodal efficiency and PLACE were tested as predictor variables for activation of the lateral orbitofrontal cortex during the response inhibition task(Ajilore et al. 2015). Results of the analyses identified structural connectome associations of functional activation in the lateral orbitofrontal cortex, predominantly nodal path length in the left orbitofrontal gyrus and nodal clustering in the right orbitofrontal gyrus. Most prominently, path length was associated with neurocognitive performance during the response inhibition fMRI task(Ajilore et al. 2015). This study suggested that functional deficits of processing speed and working

memory in BD are associated with reduced neuroanatomical network properties of efficiency and clustering(Ajilore et al. 2015).

The first investigation of rich-club connectivity was recently carried out in a large cohort of 216 participants with bipolar 1 disorder and 144 healthy volunteers(Collin et al., 2015). This investigation aimed to characterize central regions known as "hubs", rich club connections, and inter-hemispheric connectivity. Hubs were highly central consisting of the top 10% most connected and central brain regions(Collin et al., 2015). No significant differences were observed between BD patients and controls in hub connectivity or rich club connections within cortico-cortical networks, and the authors concluded that structural integration of these central structures appear to be preserved in the illness (Collin et al., 2015). However an association was identified between interhemispheric streamline density and IQ, suggesting commissural connections to be related to cognitive performance(Collin et al., 2015).

To date, research in this field demonstrates that abnormal global integration, fronto-limbic and inter-hemispheric connectivity may be trait features of BD. Disrupted global integration supports previous literature suggesting BD to be characterized by widespread disrupted white matter organization. Furthermore, fronto-limbic and posterior involvement have been supported as features of BD in smaller but relatively clinically homogenous samples (Forde et al., 2015; Gadelkarim et al., 2014; Leow et al., 2013b). In addition, reduced inter-hemispheric efficiency and longer inter-hemispheric path length can be considered a reproducible feature of BD(Collin et al., 2015; Leow et al., 2013). Furthermore, deficits in inter-hemispheric efficiency have been related to poorer

processing speed, working memory and IQ. Therefore, reductions in inter-hemispheric efficiency may be a marker of cognitive dysfunction associated with BD.

Direct comparisons

Wheeler and colleagues (2015b) directly compared neuroanatomical connectivity in schizophrenia and BD using graph analysis. Investigation of connection density between measures of thickness in cortical regions was compared between deficit schizophrenia, non-deficit schizophrenia, BD and healthy volunteers. Deficit schizophrenia characterizes individuals who have a poorer prognosis, course of illness, and are less responsive to treatment as compared to non-deficit schizophrenia(Wheeler et al. 2015). No differences were identified between BD and non-deficit schizophrenia and healthy volunteers, however pervasive white matter dysconnectivity was identified in deficit schizophrenia(Wheeler et al. 2015). White matter dysconnectivity was predominantly identified among fronto-temporal connections in deficit schizophrenia(Wheeler et al. 2015).

BD graph theory studies to date largely report decreased global and regional structural connectivity; however, there is limited consistency in defining global dysconnectivity. In BD, the largest network investigation to date supports impaired inter-hemispheric dysconnectivity is associated with reduced global efficiency, and preserved rich-club connectivity (Collin et al., 2015). Impaired posterior cingulate and parietal connectivity has been consistently identified in BD. Of interest, these regions support a central core

identified in investigations of topological hubs(van den Heuvel & Sporns 2011; Gollo et al. 2015).

Overview of DTI analyses in BD

Disruption of microstructural white matter organization and associated impaired integration present as neuropathophysiological features of psychotic illnesses. Converging evidence from standard diffusion neuroimaging techniques supports impaired callosal organization and limbic dysconnectivity in BD(Vederine et al. 2011; Nortje et al. 2013). Some voxel-based analyses reported deficits in ALIC, supporting current theories of BD relating to disruption of the dorsal-cognitive network, resulting in defective emotional regulation(Linke et al. 2013). Specifically, disruption of the anterior limb of the internal capsule (ALIC) has been related to impaired connectivity of fronto-thalamic and thalamo-cortical projections (Levitt, 2012; Linke 2013). Findings from voxel-based analyses also implicate anterior projection fibres and alterations in posterior projection fibres(Nortje et al. 2013). As proposed in the most recent meta-analysis, differentiation in findings among methodological analyses might indicate microstructural abnormalities in the core white matter compared to peripheral portions of tracts(Nortje et al. 2013; Smith et al. 2006).

Recent evidence supports network analysis as a neuropathophysiologically relevant measure extending focal deficits to represent neuroanatomical integration patterns, identifying inter-hemispheric as well as altered default mode network dysconnectivity in

BD(Ajilore et al., 2015; Collin et al., 2015; Gadelkarim et al., 2014; Leow et al., 2013b). Moreover decreased organization of posterior white matter appears related to impaired cognitive function rather than affective symptoms of BD(Nortje et al. 2013). Specifically, inter-hemispheric connectivity has been related to cognitive measures of premorbid IQ and current IQ, with interhemispheric connectivity related to current IQ(Collin et al., 2015). Additionally, clinical measures have been related to aberrant connectivity, where in-house metrics reported connectivity of the left isthmus cingulate gyrus and left precuneus was related to the number of depressive episodes(Gadelkarim et al., 2014). While in-house measures may identify specific characteristics to BD, these novel graph metrics limit reproducibility across investigations.

In summary, DTI studies in BD suggest node-level and inter-hemispheric connectivity patterns are distinctive abnormalities in BD. Aberrant microstructural organization of commissural pathways is consistent with reports of inter-hemispheric dysconnectivity. Decreased white matter organization of anterior limbic system tracts have been supported by reductions in efficiency and clustering connecting cingulate and subcortical limbic structures. Furthermore, alterations in posterior limbic and parietal connectivity have been reported, although these key regions do not appear to be affected as a central core in BD.

Despite multiple indicators across a range of neuroimaging modalities suggesting impaired anatomical connectivity in BD, the research using graph theory techniques remains limited with inconsistent findings. Graph theory represents a novel area of

research with uncertain optimal methods of processing and analysis, but can be readily employed to assess network level rather than focal abnormalities in DTI data.

Study Rationale

The heterogeneity of network analysis techniques and graph properties available makes comparison between studies and meta-analyses challenging. The present investigation utilized certain commonly employed graph metrics, such as global efficiency and clustering coefficient, in order to facilitate comparison of our results with those of other studies. These graph properties were selected as they specifically quantify a node's influence in network integration and segregation. In addition, certain more novel metrics, involving subnetwork and rich-club connectivity, were employed given their recent application to other disorders and the convergent evidence for regional neuroanatomical dysconnectivity as a core feature of bipolar disorder. Therefore, this study aims to improve upon prior studies with

Aims and Hypotheses of the Thesis

Aims

The overall aim of this thesis is to assess neuroanatomical dysconnectivity as a trait related feature of BD. Two patient cohorts with age and gender matched healthy controls are employed for this purpose: (i) a clinically homogenous sample of prospectively confirmed euthymic bipolar 1 disorder patients on whom diffusion tensor imaging was acquired as part of the Galway Bipolar Study, and (ii) an international collaborative multicentre study of largely remitted patients with BD on whom diffusion tensor imaging was acquired with the same model scanner and acquisition protocol. The aim of the thesis is to assess neuroanatomical connectivity using graph theory to explore parameters of global and local integration and segregation, neuroanatomical subnetworks, rich club connection density and structural members of the rich club, as well as any clinical association of these parameters in the participant groups.

Hypotheses

1. There will be impaired features of integration and segregation connectivity measures indicated by longer characteristic path length, reduced global and local efficiency, reduced global mean and regional clustering and reduced density in BD compared with healthy controls.

2. There will be weaker connected components in areas of impaired regional segregation in BD compared with healthy controls, in particular incorporating fronto-limbic regions.

3. Neuroanatomical connectivity in sub-networks will be more likely to be affected in patients with a positive history of psychotic features compared to patients with an absent history of psychotic features.

4. There will be reduced rich-club connectivity in patients with BD compared with healthy controls as hubs are generally implicated to be affected across brain disorders.

Chapter 2

Methods

This chapter outlines the neuroimaging methodology first implemented in the Galway Bipolar Study data and reproduced in a multi-centre study across three and four research centres. To avoid repetition of complex network techniques, the recruitment section consists of the parameters implemented in A. Galway Bipolar Study and B. The three centre study. The diffusion data from the Galway Bipolar Study was then re-analysed to be included with the three centre data and presented as a study across four centres. Therefore, sections reporting pre-processing, complex network analysis and statistical approaches will report on A. the Galway Bipolar Study and B. The multi-centre study, which includes identical approaches for the three centres and four centres.

Participants Recruitment

Participants of the Galway Bipolar Study

Eighty-five participants between 18 and 60 years of age were recruited as part of the Galway Bipolar Study(Emsell, Leemans, et al. 2013; Emsell, Langan, et al. 2013). Forty-two patients were recruited from in and out-patient services at the University Hospital Galway (UHG) and Health Service Executive (HSE) services in the West of Ireland. Seven of the patients with remitted BD were included after participation in a follow-up imaging of a first episode psychosis study and underwent an identical scanning procedure(Scanlon et al. 2014; Kenney et al. 2015). Forty-three age and gender matched

healthy volunteers were recruited from the local community. In patients, BD type 1 was confirmed using the DSM-IV Structured Clinical Interview for DSM Disorders(APA 1994). Exclusion criteria for all participants included a history of medical or neurological illness, history of head injury resulting in loss of consciousness for over 5 minutes, history of substance abuse in the past year, learning disability, and oral steroid use in previous 3 months, and any other MRI contraindications. Further exclusion criteria for controls included personal or family history of psychotic or affective disorder in first or second-degree relatives. Additional patient exclusion criteria included a lifetime comorbid DSM-IV Axis 1 disorder. All patients were euthymic at the time of scanning, defined as a score ≤ 7 on both the Hamilton Rating Scale for Depression and Young Mania Rating Scale(Hamilton 1960; Young et al. 1978). Ethical approval was granted from the National University of Ireland Galway and University Hospital Galway research ethics committees. After a complete description of the study was presented to participants written informed consent was obtained.

Participants of Three-Centres

The collaborative effort involved the following three centres: Western Psychiatric Institute and Clinic in Pittsburgh, Pennslyvania led by Professor Mary L. Phillips at the School of Medicine, University of Pittsburgh, USA; Neurospin Lab and Assistance Publique-Hopitaux de Paris Hopital Henri Mondor-Albert Chenevier in Creteil, Hopital Fernand Widal-Lariboisiere in Paris, France led by Dr. Josselin Houenou; and Central Institute for Mental Health in Mannheim, Germany led by Dr. Michele Wessa and Dr. Julia Linke.

The collaboration was established to investigate white matter dysconnectivity in BD. The study design allowed for shared data access between the three centres and our Galway Bipolar Study data. This coordinated research implemented identical scanner and image acquisition protocols, and has previously published a tractography analysis in 118 patients with BD and 86 healthy volunteers. The present study included 109 participants with BD and 103 volunteers were recruited from the three international research centers(Sarrazin et al. 2014; Laidi et al. 2015; Sarrazin et al. 2015).

Participants recruited from the French research centre underwent assessment using the Diagnostic Interview for Genetic Studies. Participants from the United States and Germany were assessed through the Structured Clinical Interview for DSM-IV. Participants were between 18 and 65 years of age.

Participants were included in the study if diagnosed with DSM-IV BD Type I. Healthy participant criteria included having no personal or family history of Axis I mood disorder, schizophrenia, or schizoaffective disorder. Exclusion criteria for all participants included a history of neurological disease or traumatic brain injury with loss of consciousness, as well as any MRI contraindications.

Image Acquisition

MRI Acquisition of Galway Bipolar Study

Diffusion-weighted and structural magnetic resonance images were obtained for all participants. Structural MRI data was acquired on a 1.5 Tesla Siemens Magnetom

Symphony Scanner using a 4-channel head coil. Volumetric T1-weighted magnetization prepared acquisition of gradient echo (MPRAGE) sequence was acquired with imaging parameters repetition time(TR): 1140 ms, echo time(TE): 4.38ms, inversion time(TI): 600 ms, flip angle 15; matrix size 256x256; an in-plane pixel size 0.9x0.9 mm^2; slice thickness of 0.9 mm.

Diffusion MRI data was acquired using an 8-channel head coil with an echo planar image diffusion sequence acquired with parallel imaging, 64 optimized diffusion gradient directions with b=1300 s/mm^2, 7 non-diffusion weighted images, repetition time=8100 ms, echo time=95 ms, field of view = 240 x 240 mm^2, matrix = 96 x 96, in-plane voxel size of 2.5x2.5 mm^2, slice thickness=2.5 mm, 60 slices.

MRI Acquisition of Three-Centres

Diffusion-weighted imaging (DWI) and structural T1 scans were obtained for all participants using the same model 3T Magnetom Triotim syngo MR B17 with 12-channel head coil from Siemens Medical Solutions. Structural MRI acquisition includes a high-resolution T1-weighted acquisition (echo time, 2.98 ms; repetition time, 2300 milliseconds; 160 sections; voxel size, 1.0 x 1.0 x 1.0 mm).

A shared DW sequence along 41 gradient directions (voxel size, 2.0 x 2.0 x 2.0 mm; b = 1000 s/mm2 plus 1 b=0 image; echo time, 87 or 84 ms; repetition time, 14000 ms; 60 or 64 axial sections).

Diffusion Pre-processing

Pre-processing is carried out to ensure adequate quality of the data is assessed and data with substantial artefacts are further removed from the analysis. Additional measures can be implemented to reduce artefacts during MRI acquisition such as reduced scanning time, alternative sequences, and cardiac gating(Soares et al. 2013). Artefacts acquired during acquisition such as signal drop outs, can lead to further errors in tractography reconstruction and subsequent analyses. Therefore, further measures are needed to correct for possible geometric distortions and subject motion. The raw data was processed as outlined in Figure 2.1.

Figure 2.1. Pre-processing Quality Assessment Pipeline

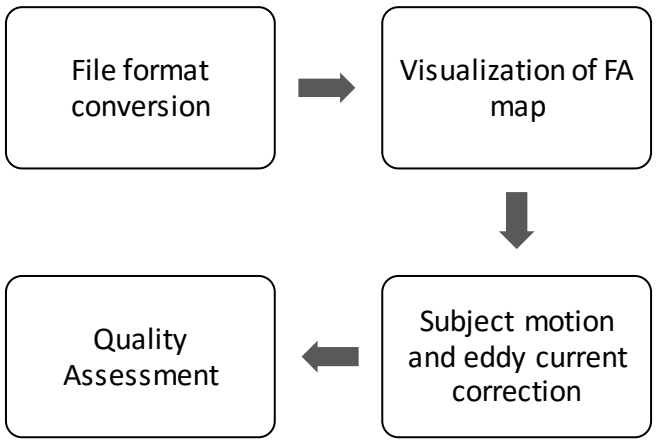

File Format Conversion

The initial step in pre-processing DTI data includes format conversion of raw DICOM files. Raw DICOM files were converted into ExploreDTI compatible (DTI.mat) format to run pre-processing and analysis. Following file conversion, assessment of accuracy in format conversion can be shown when we visualize the colour-coded FA maps.

Colour-coded FA Maps

Colour-coded maps are used to visualize information about the direction of diffusion from colour-coding principle eigenvalues. Colour encoding of the diffusion signal consists of three colour definitions: anterior-posterior in green, inferior-superior in blue, and left-right in red. FA values are determined based on the major eigenvectors, presenting the magnitude of the diffusion. Errors in estimation of tensor orientation can cause flipped diffusion and gradient information. Here, DWI data was converted to appropriate ExploreDTI file format, and visualization of colour-encoded FA maps was carried out for inspection. Diffusion orientation errors were identified in interhemispheric and association tracts, while projection tract orientation was preserved (Figure 2.2). Failure to correct for these distortions can lead to inaccuracies in analysis of diffusion data(Soares et al. 2013). Therefore, the gradient table was modified and reconstruction of the diffusion weighted data was repeated for all participants.

Figure 2.2. Orientation Correction of DW signal during format conversion

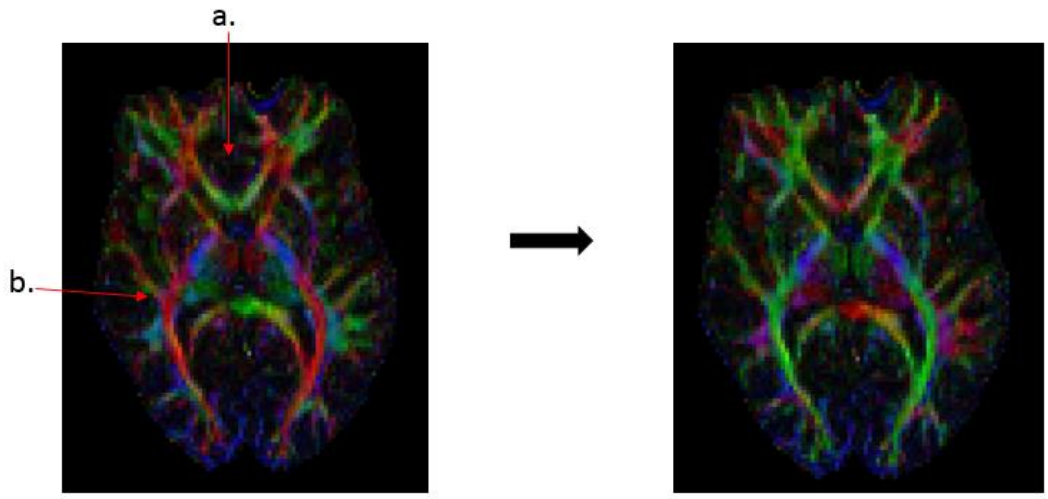

Figure 2.2 Legend. Major white matter pathways are colour-coded to indicate diffusion orientation direction produced using *ExploreDTI* software. a. Interhemispheric fibre pathways should be displayed by the colour red indicating "left-right" diffusion. Visualization of the genu of the corpus callosum in green signals DW images warrant correction. b. Association tracts such as the superior longitudinal fasciculus should be coloured green indicating anterior-posterior direction of diffusion. Therefore, we corrected for the associated fibre direction with rotation of gradient information within voxels.

Motion Distortion Correction

Conversion of raw DICOM data to images appropriate for analysis requires pre-processing to remove potential artefacts. These pre-processing steps correct for subject motion and geometric distortions. Next, *ExploreDTI* software was used to perform subject and geomentric distortion correction and quality assessment of diffusion MRI data across all centres(Leemans et al. 2009). Visual inspection was carried out across all raw data to check for poor acquisition, which can result in missing slices and artifacts in images. Following conversion of acquired data to ExploreDTI format, visual inspection of raw DW images was implemented for the additional three-centres, as well as data from the Galway Bipolar Study.

Pre-processing steps of DW data consist of subject motion and EPI correction(Leemans et al. 2009; Jones & Cercignani 2010). Quality control assessed for movement, susceptibility, and noise artefacts. Movements from involuntary cardiac pulsation and small head movements can bias resulting diffusion-weighted data. Therefore, to achieve optimal DW images, we corrected for head motion during acquisition. Rigid-motion and eddy current induced distortions were corrected with a six parameter remapping of DW images to structural scans (Figure 2.3). Diffusion weighted data contains diffusion gradient orientation information within voxels defined by the b-matrix; therefore, overlooking rotation the b-matrix can result in errors in fibre reconstruction (Leemans & Jones 2009). Previously, standard rotation of DW images was employed, however evidence suggests rotation of the b-matrix must be implemented for accurate representation of diffusion orientation.

Figure 2.3. Subject Motion Correction across DW images

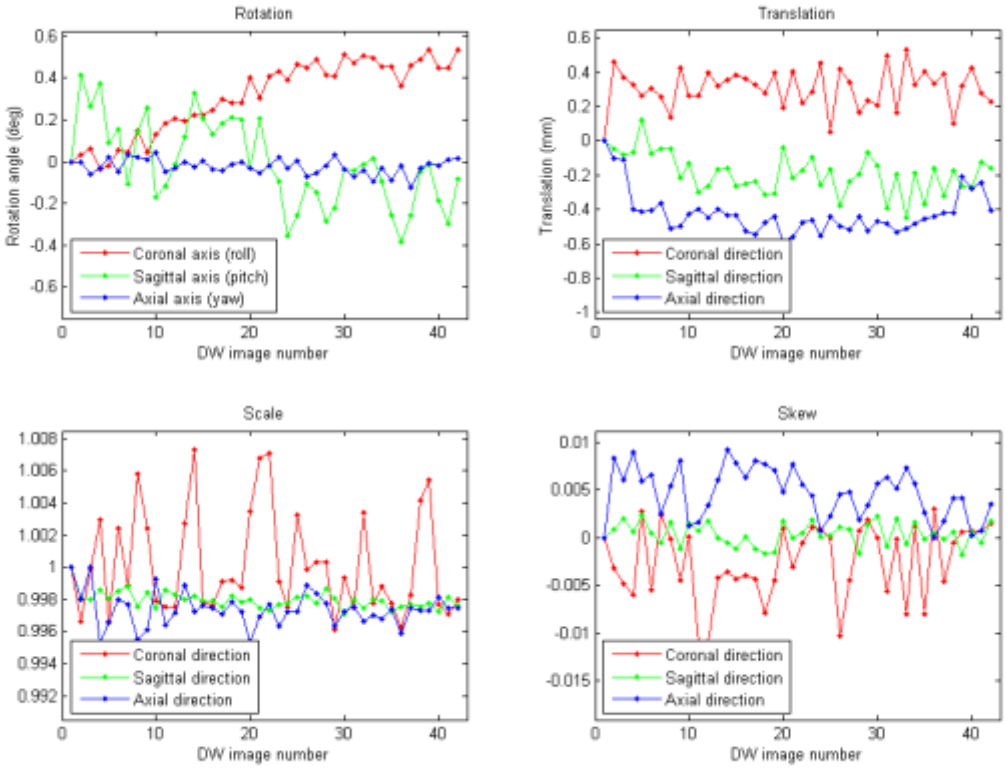

Figure 2.3 Legend. Using *ExploreDTI* software v8.4.3 & v8.4.4 we produced outlier profiles to detect the extent of subject head movement across all slices.

Eddy Current Induced Distortion

Eddy currents are inherent in diffusion acquisition and can be identified by image distortion. In diffusion-weighted imaging geometric distortions can be induced during long acquisition sequences due to gradient system hardware or long gradient acquisition times. These susceptibility effects are visualized by misregistration between images,

signal loss, shift in images, and ghosting(Jones & Cercignani 2010). An example of a DW image before and after correction for subject motion and eddy current correction are shown below in Figure 2.4.

Figure 2.4. DW image before and after subject motion and eddy current correction

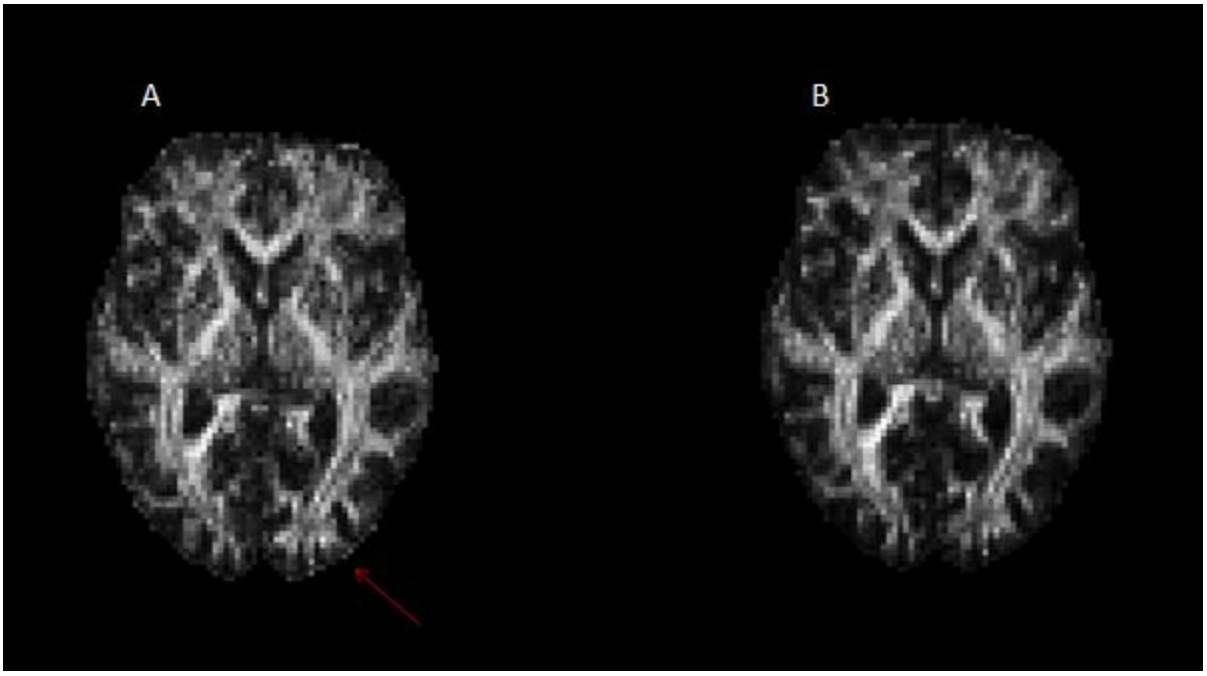

Figure 2.4. Legend. Using *ExploreDTI* software v4.8.3 we show a participant DTI image A. Before correction shows bright rims before correction produced by eddy currents, which are B. removed following correction of subject motion and eddy current distortions.

Quality Assessment

Quality assessment involves visual inspection, known as "looping" across each orthogonal direction across all DW images to identify the following artifacts: geometric distortions, hypointensities, and signal dropout. Switching between DW images was carried out to look for drift or movements. Quality control was assessed for all participants within the Galway Bipolar Study and the multi-centre study.

To benchmark quality control across datasets in the multi-centre study, we inspected cases of poor and mild image quality as reported in assessments received from the international centres. Next, all DW images were given a quality rating of i. mild, ii. moderate and iii. severe level following assessment of "looping" through all DW images, residual maps and outlier profiles. Residual maps indicate hypointensities and signal drop out across all three orthogonal views (Figure 2.5), and outlier detection defines the slice number at which the signal was lost (Figure 2.6). Due to cases of poor data quality, ten DW images were removed from analysis. An example of a participant with three forms of artifacts, failed connectivity density thresholding upon further connectivity analyses processing steps is displayed in Figure 2.5.

Figure 2.5. Quality assessment of residual maps

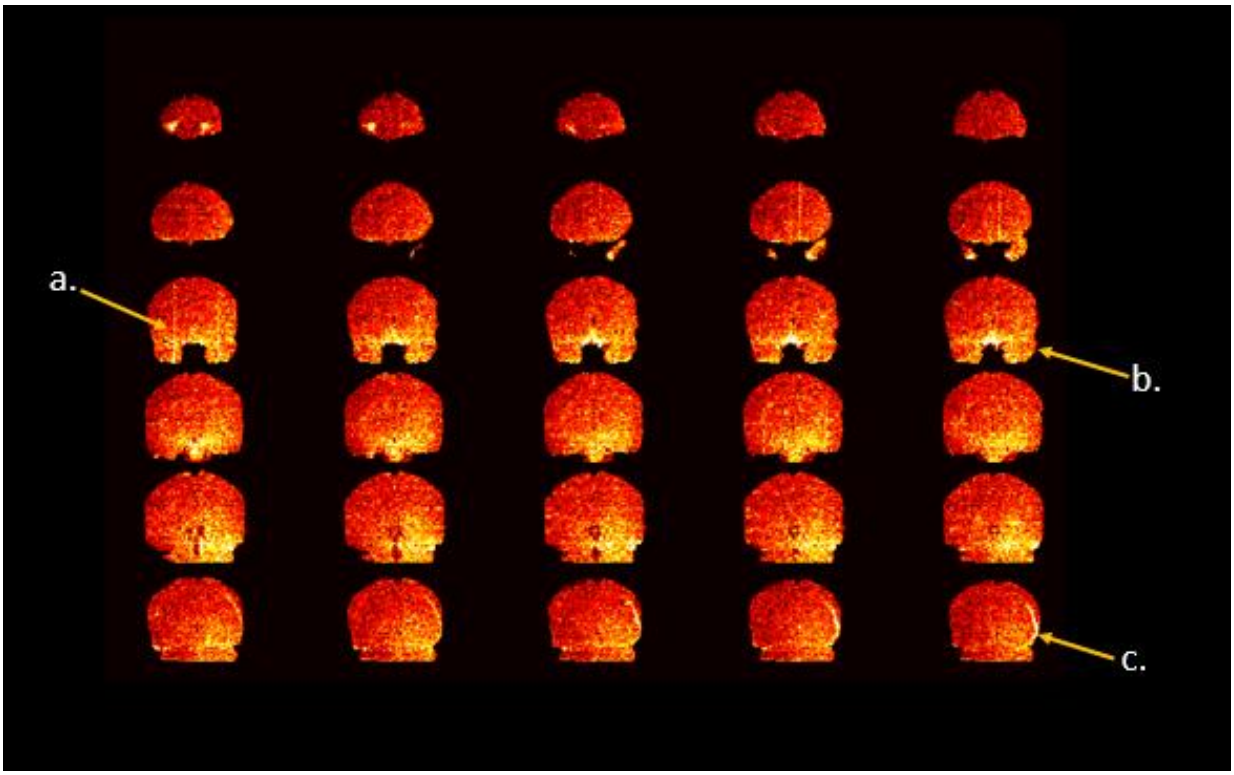

Figure 2.5. Legend. Examination of signal intensity at every slice and orientation allows for the assessment of residuals. Residual map of this DW image in coronal plane indicate a poor fit of the diffusion tensor model. A. signal dropout. B. hypointensity due to cardiac pulsation. C. scanner artifacts indicated by bright rim.

Figure 2.6. Outliers across DW images

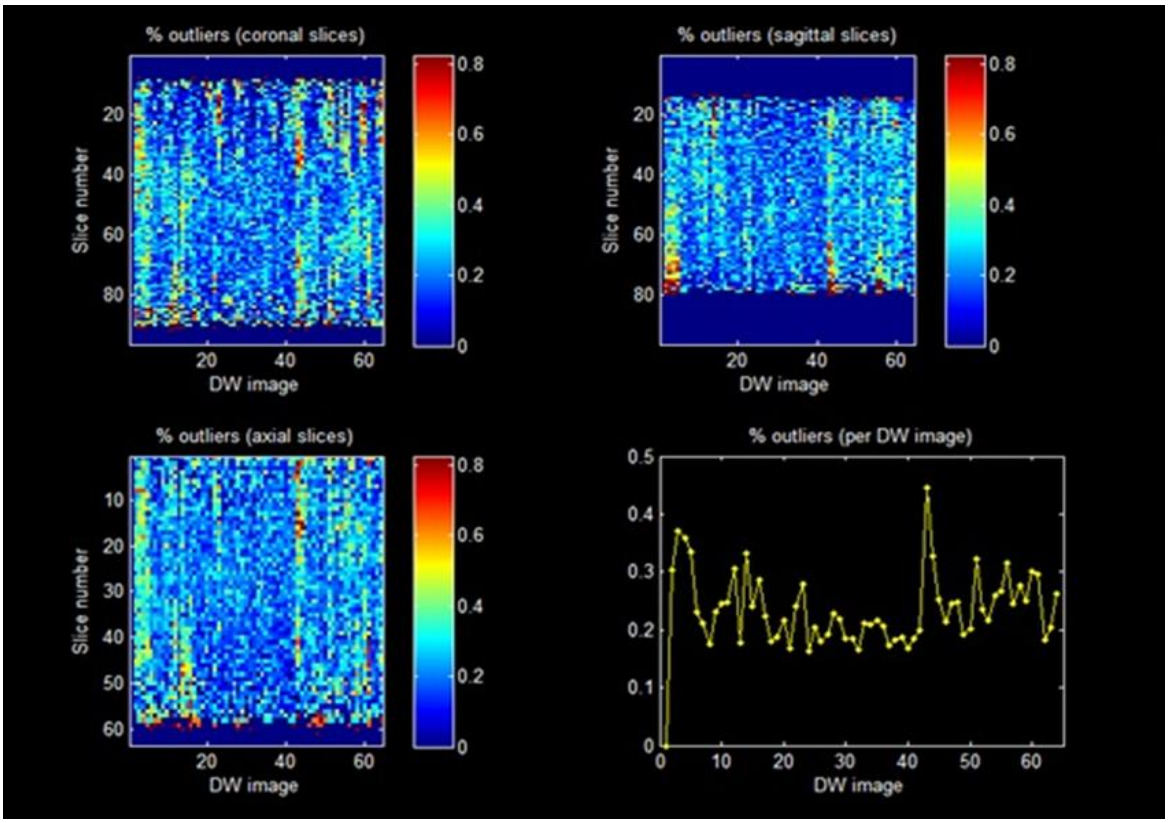

Figure 2.6 Legend. A plot of the DW image slice outlier percentage was generated to identify outliers across all DW images per participant.

Whole Brain Tractography

Deterministic Streamline Tractography

White matter trajectories were reconstructed using the deterministic streamline tractography method using *ExploreDTI* v.4.8.3(Leemans et al. 2009). A step-wise fibre tracking algorithm calculates the fibre path along each voxel. Extending DTI

tractography reconstruction of the principle fibre orientation defined by the largest eigenvalue, constrained spherical deconvolution (CSD) examines the multiple diffusion directions within each voxel as an ellipsoid(Jeurissen et al. 2011; Tournier et al. 2007; Tournier et al. 2011).

Constrained Spherical Deconvolution

A Constrained Spherical Deconvolution (CSD) algorithm was implemented to account for crossing fibers present within voxels(Tournier et al. 2007; Jeurissen et al. 2011). Diffusion tensor tractography defines the diffusion signal for a single fibre population, however may be subjected to partial volume effects from smaller fibre orientations. CSD provides a better estimate of fibre orientation within voxels containing crossing fibers. As over 90% of voxels are shown to contain crossing fibres, CSD was implemented to overcome the limitations of DTI tractography(Jeurissen et al., 2011; Wedeen, 2012).

Spherical Harmonics

The spherical harmonic order estimates the number of diffusion directions present within voxels. The extent of possible diffusion directions is dependent on the number of gradients applied during acquisition. The L_{max} parameter of the spherical harmonic order was adapted across analyses. The spherical harmonic order can be computed for L_{max} values ranging from 2-8.

Acquisition of gradient directions more than 45 directions is optimal to meet the signal-to-noise ratio of the reconstruction model(Mohlenkamp 2011; Tournier et al. 2011). In the Galway dataset, the number of encoding gradient directions was a high value of 64.

Therefore, the maximum number of diffusion orientations (8) was applied. Next, the three international centres applied 41 gradient directions during acquisition of diffusion data. Therefore, the optimal l_{max} was defined at a value of 6.

Tractography Settings of Galway Bipolar Study

In the Galway Bipolar Study (GBS) analysis, CSD fiber tracking was initiated in each voxel and continued with a step size of 1 mm until the following threshold was exceeded: fiber orientation distribution >.15, angle threshold curvature >30◦, minimum length <20 mm, and maximum length > 300 mm. A spherical harmonic order of L_{max}=8 was applied. Angle threshold curvature of 30◦ was applied to restrain spurious streamline production.

Tractography of Three-Centre Study

The same fibre tracking parameters defined in the Galway Bipolar Study was applied in the three additional research centres. In addition, due to updates in ExploreDTI software from v4.8.3 to v.4.8.4 recursive calibration was applied in subsequent tractography reconstruction. Recursive calibration of the response function accounted for partial volume effects present within voxels of multiple fibre orientation directions (Tax, 2014). The number of diffusion weighted gradient directions acquired in order to implement CSD during tractography reconstruction was defined as an l_{max} of 6.

Tractography of Galway Bipolar Study re-analysed for a Four-Centre Study

Data from the Galway Bipolar Study was re-analysed to be included in the multi-centre study. Therefore, the Galway Bipolar Study tractography data was recursively calibrated and applied an altered l_{max} value for reconstruction of the same possible fibre orientations as the three international centre analysis. The l_{max} was altered from a possible value of 8, to a value of 6 to match the three-centre parameters.

Figure 2.7. Complex Network Analysis Pipeline

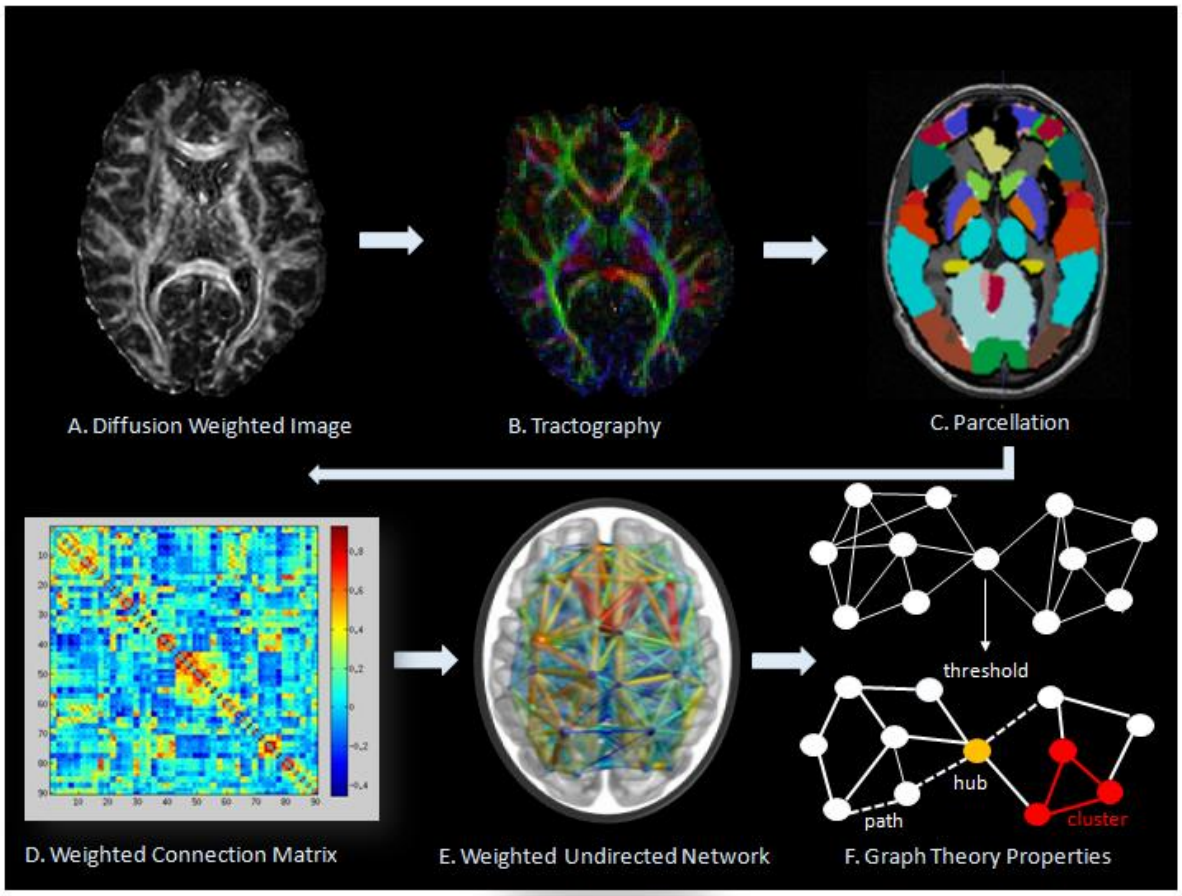

Figure 2.7 Legend. Detailed information of each step is described below. Images reconstructed using BrainNet Viewer and *ExploreDTI* software.

Complex Network Analysis

Generating Connectivity Matrices

Following tractography reconstruction, connectivity matrices were generated using an ExploreDTI plugin, connecting the set of reconstructed streamlines with a structural parcellation atlas, consisting of automated anatomical labeling atlas (AAL) coordinates, labels, and volumes.

A connection matrix can take two forms of connectivity, defined by settings "pass" and "end". This "pass" selection reconstructs connections originating in one node A through node B and terminating at node C. Alternatively, the "end" setting defines connections originating in node A terminating at node B, and a new connection is formed between node B and terminating at node C (Figure 2.8). The pass setting defines the integrative properties of anatomical pathways relaying through nodes, which represent the patterns of neuroanatomical circuits. The "end" setting refers to separate connections terminating at every subsequent node and a newly characterized connection reported thereafter. The selection of "pass" compared to "end" is not yet standardized, however analyses may implicitly select "pass" as reported in ExploreDTI manual(Leemans et al. 2009). In this research presented, the "pass" setting was used to define the connectivity matrices. This

was chosen as our hypotheses aimed to investigate features of integration in brain networks.

Figure 2.8. Pass and End connections

Figure 2.8 Legend. "Pass" shows one pathway connecting three nodes. "End" selection shows two separate connections both connected to node b.

Selection of Edges

Undirected and Weighted Edges

Connection weights were generated from tractography reconstruction. When implementing complex network analysis it is essential to report the connection weight (strength) and whether connectivity is directed or undirected(Parker et al. 2014; Rubinov & Sporns 2010). Investigating neuroanatomical connectivity using DTI assumes

connections are undirected, as knowledge of afferent and efferent connectivity is unknown. Additionally, connection weights can be unweighted or weighted. Unweighted connectivity examines whether a connection is present or not, resulting in binary graphs. Unweighted connectivity may be useful for the investigation of false-positive and false-negative effects. Weighted connection matrices define the extent to which two nodes are well or weakly connected(Bullmore & Sporns 2012). Moreover, weaker connectivity strength may be contributed by topologically vulnerable structures or microstructural alterations in white matter. This will be addressed in the Discussion chapter. An example of binary and weighted connection matrices are displayed below in Figure 2.9.

Figure 2.9. Binary and Weighted Connection Matrices

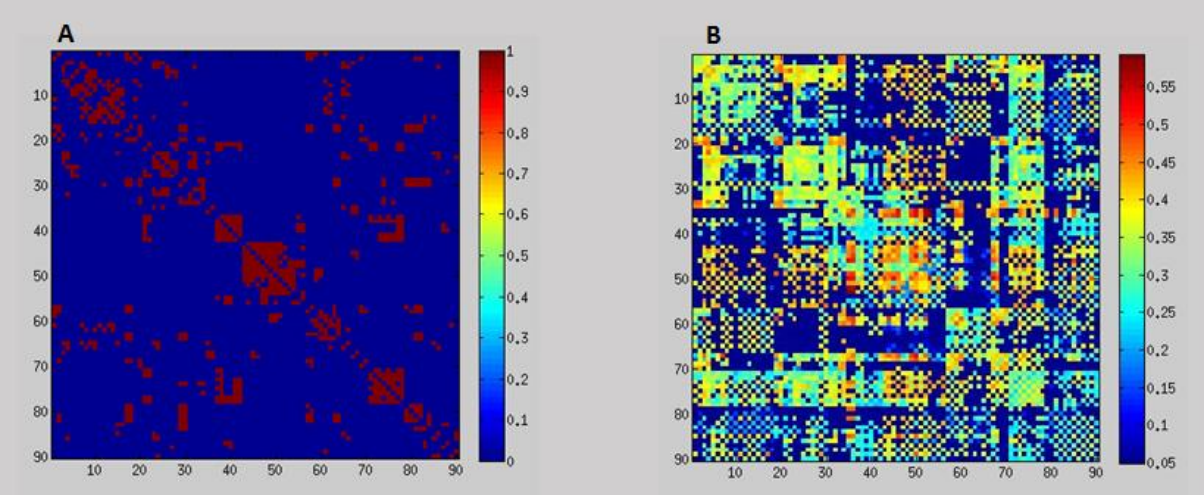

Figure 2.9 Legend. A represents the binary graph, depicting whether a connection exists or not. Present connections displayed in red, with absent connections in blue. B. represents the weighted connection matrix. Values approaching red on the scale describe greater connection density. Data was visualized using BrainNet Viewer software.

Analysis of undirected and weighted edges included streamline count between nodes and mean fractional anisotropy(FA) between nodes(Levitt et al. 2012). The strength of connections refers to the number of reconstructed streamlines connecting two nodes. Streamline count represents the total number of reconstructed streamlines interconnecting two nodes, uncorrected for volume. Challenges occur when connection strength defined by reconstructed streamlines is an abstract reconstruction of the fibre tracking algorithm and is dependent on the number of possible reconstructed diffusion directions and voxel size. In addition, FA connection weight is a voxel-wise measure of microstructural organization averaged across the reconstructed streamlines between two regions(Fornito et al. 2013). To extend the previous DTI analysis in this cohort reporting widespread FA reductions, we implemented FA edge weights in graph theory and sub-network analyses.

Graph Thresholding

Thresholding connections graphs are applied to remove false positive connections that can occur with tractography data. Therefore it is critical to threshold graph data to remove spurious connections. Standardized graph thresholding parameters are not yet routinely implemented, with arbitrary thresholds selected(Drakesmith et al. 2015). The relationship between thresholding, connectivity weights, and resulting graph theory metrics is an area of current investigation(Fornito et al. 2012; Drakesmith et al. 2015).

Some investigations select a minimum mean degree that has to be maintained across all groups, however this assumption may produce approximately equal mean degree between

groups(Fornito et al. 2012). Low thresholds include effects from false positives while high thresholds include highly disconnected networks that may not be reflective of an accurate sparse connectome. Some studies remove an edge with T or less streamlines, modeled from 0 to 10 streamlines(Drakesmith et al. 2015).

Patients with aberrant microstructural organization may likely have connection values that shift towards lower streamline count compared to healthy volunteers. Therefore, graph thresholding must be considered with caution, as certain thresholds may limit the ability to detect an effect between groups which are present, although subsequently removed from analysis. A connection weight-based threshold, T, or a connection density-based threshold, k, can be applied. The correlation matrix after T matched thresholding sets the minimum connection weight in the matrix for both the patient and healthy volunteer, resulting in approximately equal mean weights, although differences in connection density. Alternatively, the connection matrix can be matched for density, but allows minimum and mean weight to vary across participants.In the research presented here we set k in both groups and allowed T to vary. Therefore, connection matrices thresholded at a density value 0.2, resulted in similar connection densities between groups but allowed connection weights to vary, minimizing false-positive streamline count(Fornito et al. 2012).

Selection of Nodes

The Automated Anatomical Labeling Atlas(AAL) was utilized for cortical and subcortical parcellation(Tzourio-Mazoyer et al. 2002). The AAL is a macro-anatomical parcellation atlas based on a single subject brain template set in MNI space(Tzourio-Mazoyer et al. 2002). The AAL atlas applies spatial coordinates and associated volume for 90-120 cortical and subcortical structures. The cerebellum was excluded resulting in a 90 node parcellation scheme (45 nodes bilaterally). Visual inspection of the cortical parcellation atlas to T1 images was carried out with MRIcron(Rorden et al. 2007). Prior to mapping images take form below in Figure 2.10.

Figure 2.10. Visual inspection of AAL and participant diffusion data

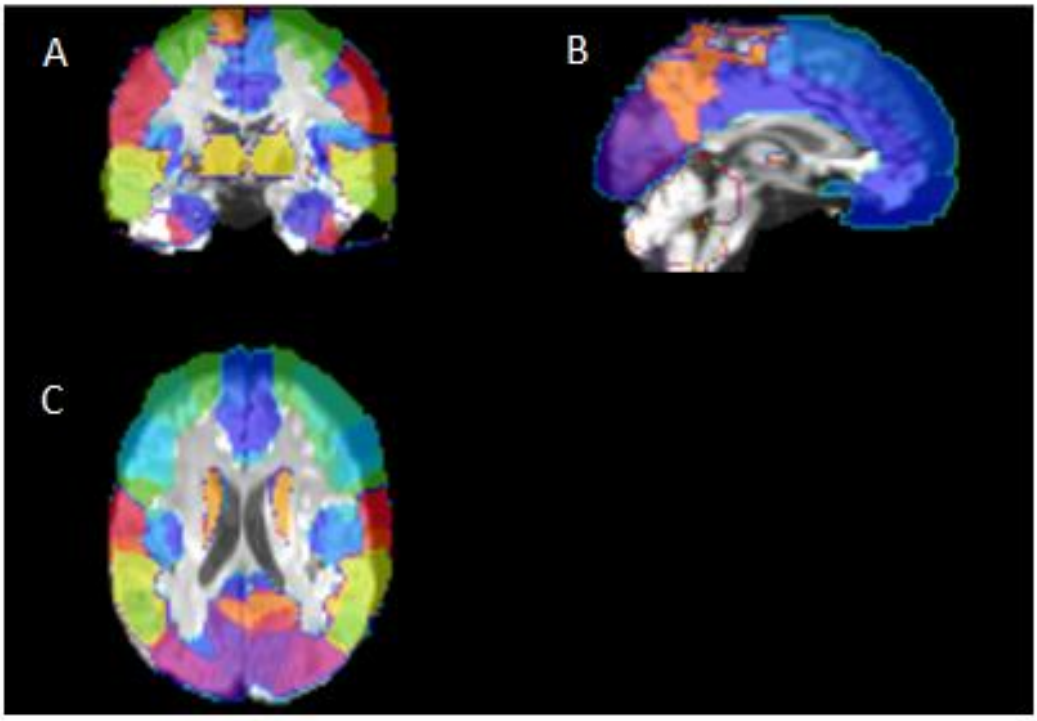

Figure 2.10 Legend. Overlay of AAL coordinates and atlas over participant volume data using MRIcron before connectivity mapping.

Brain Connectivity Toolbox

Network metrics were generated using the Brain Connectivity Toolbox through MATLAB(Rubinov & Sporns 2010). The Brain Connectivity Toolbox (BCT) consists of graph theory property measures. Graph functions are performed across all connectivity matrices, which considered all non-numbers equal to 0 (when a tract does not pass

through a node), and resulted in graph metric values defined for every participant connection matrix.

Global and Local Metrics

Global and local metrics were derived to investigate properties of integration and segregation(Rubinov & Sporns 2010; Bullmore & Sporns 2009). A weighted connection approach was implemented in the graph theory analyses. Metrics of degree, clustering coefficient, characteristic path length, global efficiency and betweenness centrality were investigated in the following analyses.

Figure 2.11. Topological features of networks

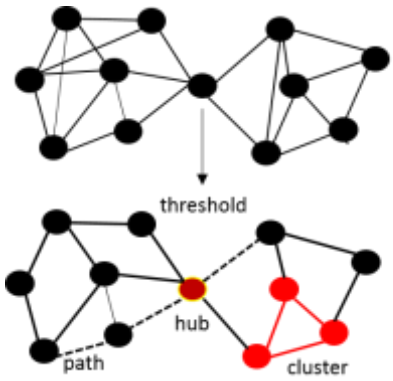

Figure 2.11 Legend. Graph properties used to describe brain topology. Thresholded graphs remove spurious or unlikely connections to reveal sparse complex networks. A path is denoted by the dashed line to represent a possible reconstructed streamline course connecting a minimum of four nodes. Next, the cluster highlighted in red indicates connections of one node that are also connected with its neighbours. A hub node takes a

central position in the network and is intersected by many paths and integrates information between communities.

The metrics chosen for analysis in the study were defined by the following equations reported in (Rubinov & Sporns 2010):

(i) Weighted degree (strength): the number of streamlines through a node, defined by the following equation:

$$k_i^w = \sum j \in N^{ij} ,$$

Where k is the weighted number of links connected to node i.

(ii) Weighted clustering coefficient: the frequency of connections between a node and its neighboring nodes, defined by:

$$C^w = \frac{1}{n}\sum i \in N \frac{2t_i^w}{k_i(k_i-1)},$$

Where C_i is the clustering coefficient of node i ($C_i = 0$ for $k_i < 2$).

(iii) Weighted characteristic path length: measures the average shortest path length, i.e. the minimum number of edges that must be traversed to go from one node to another, measured by:

$$L^w = \frac{1}{n}\sum i \in N \frac{\sum j \in N, j \neq i d_{ij}^w}{n-1},$$

Where L_i is the average distance between node *i* and all other nodes.

(iv) Weighted global efficiency: mathematically proportional to the average inverse of the shortest path length, measures:

$$E^w = \frac{1}{n}\sum i \in N \frac{\sum j \in N, j \neq i (d_{ij}^w)^{-1}}{n-1},$$

Where E_i is the efficiency of node *i*.

(iv) Weighted local efficiency: the length of the shortest path between two nodes, containing only neighbors of the node of interest, shows:

$$E_{loc}^w = \frac{1}{2}\sum i \in N \frac{\sum j,h \in N, j \neq i (w_{ij} w_{ih} [d_{jh}^w (N_i)]^{-1})^{1/3}}{k_i (k_i - 1)},$$

Where $E_{loc,i}$ is the local efficiency of node *i*, and $d_{hj}(N_i)$ is the length of the shortest path between *j* and *h*, that contain only neighbors of *i*.

(v) Weighted betweenness centrality: describes nodes that participate in many short paths have high centrality, reflecting a nodes influence in a network (Rubinov & Sporns 2010; Bullmore & Sporns 2009). Nodes with high

betweenness have a high influence among nodes in a network (Girvan and Newman, 2002).

$$b_i^w = \frac{1}{(n-1)(n-2)} \sum_{\substack{h,j \in N \\ h \neq j, h \neq i, j \neq i}} \frac{p_{hj}^w(i)}{p_{hj}^w},$$

Where p_{hj} is the number of shortest paths between h and j, and p_{hj} (i) is the number of shortest paths between h and j that pass through i.

Regional Analysis of Galway Bipolar Study

Prior tractography analysis of this cohort was implemented in anatomically segmented subdivisions of the corpus callosum, cingulum, and fornix in 35 individuals with BD and 43 age and gender matched healthy volunteers(Emsell, Leemans, et al. 2013). Radial diffusivity increases and FA decreases were identified in the right dorsal anterior and left subgenual portion of the cingulum and throughout the corpus callosum. FA was significantly reduced in patients in the left fornix and diffusivity was increased in the fornix bilaterally in patients compared with controls. We therefore examined fronto-limbic sub-network connections more closely to investigate local clustering and efficiency patterns in BD. Next, previously identified altered radial diffusivity (RD) along the splenium led to a further investigation of posterior connections(Emsell, Leemans, et al. 2013). Nodal analyses were selected *a priori* from this previous data driven analysis (Emsell, Langan, et al. 2013; Emsell, Leemans, et al. 2013). Nine bilateral nodes were selected(listed in Table 3) as regions connected by prefrontal white matter, cingulum, and callosal splenium connections(Emsell, Langan, et al. 2013).

Regional Analysis of Four-Centre Study

Previously, a tractography study was carried out across three centres; including 118 bipolar I disorder patients and 86 healthy controls(Sarrazin et al. 2014). Twenty-two deep white matter tracts were reconstructed using Q-ball imaging and an automated white matter segmentation technique. Q-ball imaging is a technique used to render the multiple fibre orientation directions present in voxels. Patients with bipolar I disorder had reduced mean FA along the anterior segment of the left arcuate fasciculus, the body and splenium of the corpus callosum, and long fibres of the left cingulum (Sarrazin et al. 2014). Therefore eight nodes were selected for analysis of degree, clustering coefficient and local efficiency. In addition, we investigated nodes reported in the GBS study to identify if these effects were more robustly identified in this larger participant group.

Galway Bipolar Study Statistics

Galway Bipolar Study

MANCOVA tests, co-varied for age and gender, were performed across measures of degree, clustering coefficient, betweenness centrality, characteristic path length, global efficiency and local efficiency using IBM SPSS statistics software version 22(IBM SPSS Amos 2012). Calculations of global values from nodal measures were performed by averaging the values across all 90 nodes to generate a global average for each measure (e.g., degree, clustering & betweenness centrality). Global analyses and regional comparisons underwent False Discovery Rate(FDR) correction for multiple comparisons(Benjamini & Hochberg 1995).

Partial correlations were performed between clinical parameters (age of onset, illness duration, symptom scores) and graph theory metrics indicating significance.

Multi-Centre Study

Linear mixed effects models were implemented for the multi-centre study to account for variance contributed by scanners employed at 4 research centres. The same model scanner was used for three of the four research centres. The linear mixed effects model implemented research centre as a random-effects factor. Age was considered a confounding covariate, and gender was included as a confounding variable. Partial correlations among graph theory metrics and clinical variables accounted for research centre, age, and gender as covariates.

This analysis also examined the effect of scanner versus research centre, identifying low variability between research centres in three-centre analysis, with high variability by scanner in the four-centre analysis.

Network Based Statistic

Following pre-processing steps and complex network analysis steps of generated connectivity matrices and connectome maps, the NBS toolbox was employed to detect an effect at the sub-network level (https://sites.google.com/site/bctnet/comparison/nbs). We examined sub-network connectivity to elucidate impaired integration within groups of connected regions. The NBS identifies collections of interconnected nodes (connected components), which differ in density between groups(Fornito et al. 2012).

The statistical technique implemented in the toolbox identifies an experimental effect at the cluster level by performing mass univariate testing controlling for Family Wise Error (FWE) rate. First a p-value threshold was selected at $p<0.05$, next permutation testing performed 5000 permutations, and all connected components supra-threshold were compared between healthy volunteers and participants with BD(Zalesky, Fornito & Bullmore 2010). The NBS requires selection of a threshold to determine supra-threshold connections: as this threshold setting is quite arbitrary, investigation across three supra-threshold values was employed, as has been most commonly implemented(Zalesky, Fornito & Bullmore 2010; Zalesky et al. 2012). The NBS overcomes the problem of multiple comparisons typically shown when comparing data across every connection. This method examines connections at the component level using the FWER correction, thereby correcting for the number of components.

Figure 2.12. Identifying components using Network Based Statistics

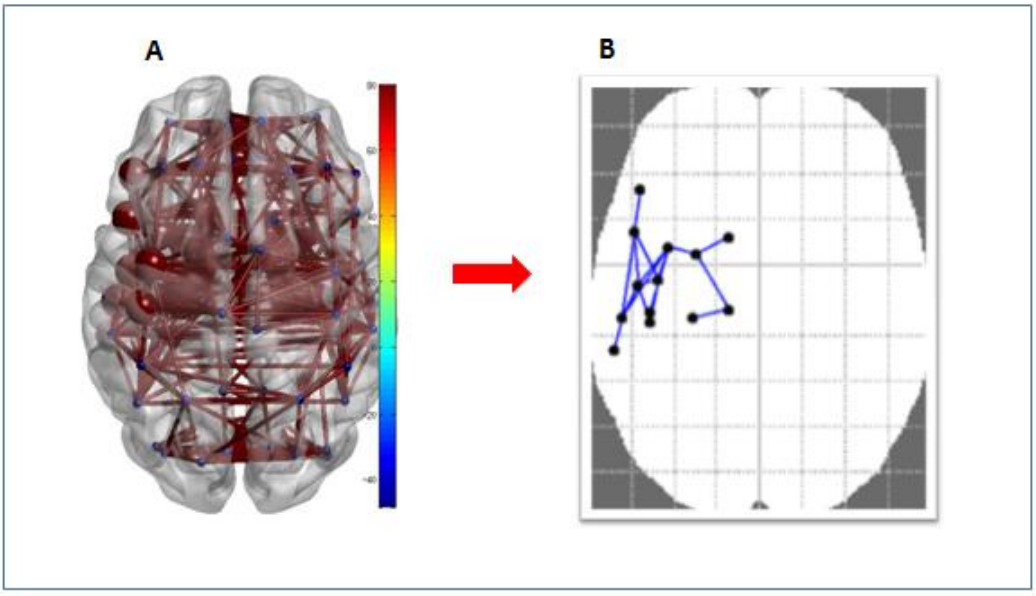

Figure 2.12 Legend. The series of connections supra-threshold >1 were identified as shown in Figure A. Figure B, shows connected component difference between groups in a sub-network of connected regions.

Network Based Statistic Statistical Analysis

Galway Bipolar Study

NBS software applied a t-test at every connection to run a permutation analysis. This analysis co-varied for age and gender. Design matrices included diagnosis as a main effect variable, with a contrast indicating the connectivity was reduced in patients compared to healthy controls.

Multi-Centre Study

An F-test was used to model differences between groups with additional covariates to account for research centre, and age and gender as covariates. Nuisance variable encoding was implemented to model research centre. An F-test implemented a connectivity threshold at 1. The permutation test ran 5,000 permutations. Multiple design matrices were included to test for post-hoc analyses examining psychotic features within the patient group, as well as tests between healthy controls and patients with psychotic features, as well as tests between healthy controls and patients without psychotic features.

Rich Club Coefficient

Finally, we explored the "rich-club" coefficient among cortico-subcortical connections. The "rich-club" refers to a set of nodes that are rich in connections and densely inter-connected among themselves forming a club(McAuley et al. 2007; van den Heuvel & Sporns 2011). This integrative sub-unit is critical for coherent integration spanning multiple cortices.

Figure 2.13. Rich-Club Organization

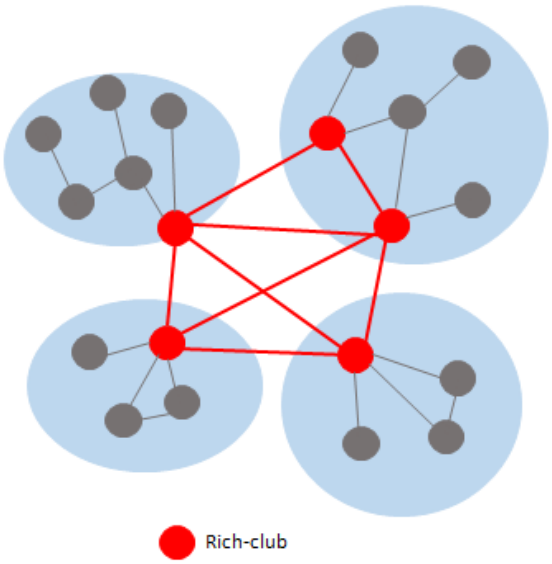

Figure 2.13 Legend. Red nodes and dense red connections depict the dense connections between rich-club structures as opposed to peripheral nodes.

We investigated rich-club connectivity differences between groups, as well as rich-club structural membership. A weighted rich-club coefficient measures the extent of dense connections within high-density structures. We investigated rich club connectivity differences between groups, as well as rich club node membership. The rich club coefficient $\Phi(k)$ is defined as:

$$\phi(k) = \frac{2E_{>k}}{N_k(N_k-1)},$$

whereby, E>*k* represents the number of connections greater than *k* present within a subgraph degree >*k*, as N>*k* indicates the number of nodes in the subgraph(McAuley et al. 2007; Collin et al. 2013). The measure Φ reflects the level of interconnectivity between nodes. (McAuley et al. 2007; van den Heuvel & Sporns 2011; Collin et al. 2014).

Weighted rich-club networks

The weighted rich-club parameter $\Phi^w(k)$ was computed to define the extent of connection density across participants. In this analysis, all connections were defined and ranked by connection strength (number of streamlines), resulting in a metric W^{ranked}. Therefore, within M, for each value *k*, the group of nodes with a degree larger than *k* was selected. Following, the number of links $E_{>k}$ was computed between members of the subset and the collective weight $W_{>k}$, which resulted in summation of the strongest $E_{>k}$ connection

weights of the whole network, defined by the top $E_{>k}$ number of connections of the collection of ranked connections in W^{ranked}. $\Phi^{w}(k)$ is computed by the following equation:

$$\phi^{w}(k) = \frac{W_{>k}}{\sum_{l=1}^{E_{>k}} W_{l}^{ranked}}$$

Normalised Rich-Club Networks

$\Phi(k)$ presents an increasing function, such that nodes with a higher degree will also have a higher probability of being interconnected by chance alone, $\Phi(k)$ is then normalized relative to a set of comparable random networks of equal degree and similar connectivity distribution(van den Heuvel & Sporns 2011).

Normalization adjustment takes the degree distribution of each participant and randomizes the degree connection matrix over a number of rewirings or re-shuffles. Following testing of a sufficient number of rewirings revealing low variance, a number of iterations for the rewiring was determined. As the sufficient number of rewirings lacks standardization with re-arrangements ranging from 100 to 1000(Daianu et al. 2015; Kocher et al. 2015; van den Heuvel & Sporns 2011), selection of number of random rewirings (m=500) revealed a standard deviation(SD) that converges below .001 (Figure 2.13). Testing of the number of rewiring iterations revealed low variance and consistency when fixed at n=10 iterations (Figure 2.13). For each network, *m*=500 random networks were computed and from each of the randomized connection networks, for every level of

k, the rich-club $\Phi_{random}(k)$ was computed as the average rich-club coefficient over the m random networks (Figure 2.13). A normalized rich-club coefficient $\Phi_{norm}(k)$ is then computed as:

$$\phi_{norm}(k) = \frac{\phi(k)}{\phi_{random}(k)}$$

Figure 2.14. Number of sufficient re-wirings and iterations

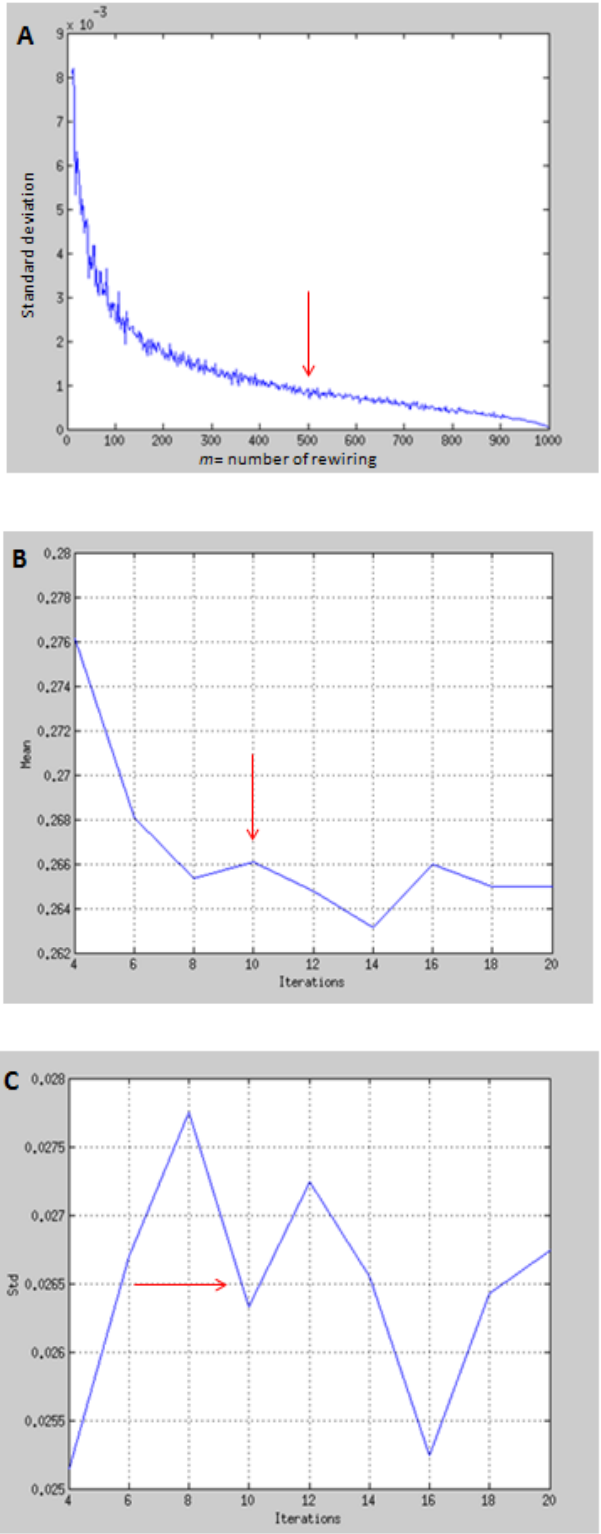

Figure 2.14 Legend. **A**. Graph of the possible number of rewiring and standard deviation. At *m*=500, low variance was estimated. The possible number of mean iterations of rewirings shown in (**B**.), with the standard deviation are shown in graph (**C**.). A low number of iterations with minimal variance is optimal for efficient processing across all datasets.

The measure $\Phi > 1$ over a range of k suggests the presence of rich-club organization. (Colizza et al., 2006; McAuley et al., 2007; Collin et al., 2014). A value of Φ was then estimated across a range of *k* for all participants' connectivity data. Within the Galway dataset, the range of *k* values for rich club coefficient was 27-64, while the range of *k* values for normalized rich club coefficient was 28-56. Among the four-centre dataset, the range of *k* at which $\Phi>1$ was determined for *k* value of 21-30.

Figure 2.15 Normalized Rich-Club Curve

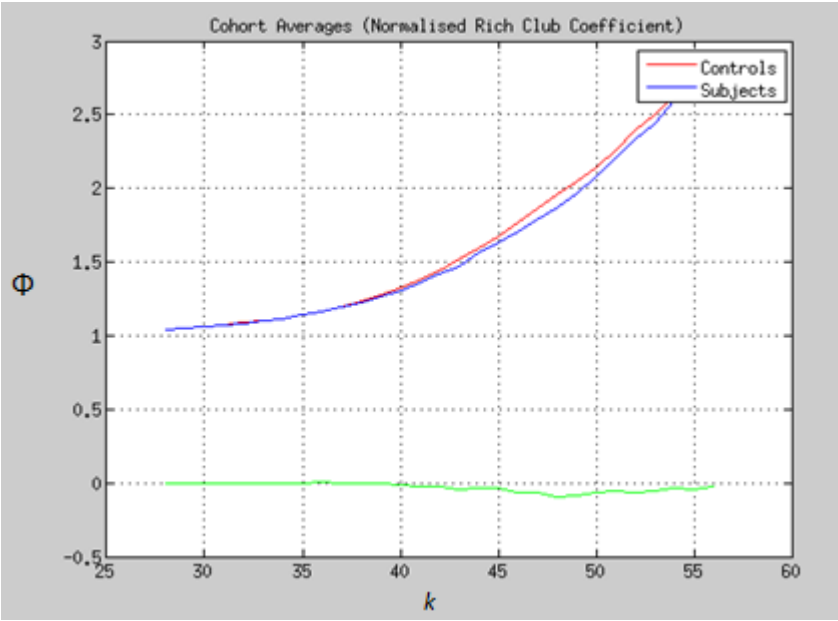

Figure 2.15. Rich-club curve >1 across a range of k values. Healthy controls defined in red, with patients in blue, and absolute difference defined in green.

Rich-Club Statistical Analysis

Galway Bipolar Study

Between group effects were determined using 9999 Monte Carlo resamples performed in R(RStudio 2012). Multiple comparisons corrected for 28 possible values of *k* density was implemented using the FDR method(Benjamini & Hochberg 1995). Additionally, a partial correlation was performed, correcting for age and gender, examined whether there was an association between these critical structures and measures of global integration.

Multi-Centre Study

The Fisher-Pitman permutation test was implemented to detect a difference in rich-club connectivity across a range of k (the rich-club regime). This statistical test is employed when comparing non-normally distributed means(Neuhäuser & Manly 2004). This was implemented in the analysis due to the variance in data contributed by scanner variation. Therefore, this permutation analysis accounted for research centre variation in means, and included age and gender as covariates. Additionally, a Holm-Bonferroni correction was implemented for multiple comparisons to provide adjusted p-values. Additionally, similarly with the analysis of the Galway dataset, a partial correlation was used to investigate the relationship between rich-club density and global efficiency measures.

Chapter 3

Results

This chapter is divided into four results sections. First, the results will cover clinical and socio-demographic details of the participant groups. The second section will cover findings of global and local graph theory properties of neuroanatomical connectivity. The third section reports the sub-network findings across research centres. The fourth results section describes the normalized rich-club connections and rich-club membership. These results sections will be given for the Galway Bipolar Study and the study across four-centres, with additional presentation of the effects when the re-analysed Galway research centre findings are removed.

Clinical and socio-demographic details of participants

Galway Bipolar Study participants

Participants were aged between 22-60 years. Participants and healthy volunteers were age and gender matched. The BD group received significantly less years of education than healthy volunteers ($t=3.29$, $p=0.001$). The socio-demographic and clinical details of the GBS participants are outlined in Table 3.1.

Table 3.1. Clinical and socio-demographic details of GBS participants

	Healthy Controls	Bipolar Group	Group Comparison (Test Statistic, p)
Number of Participants	43	42	
Age, mean ± SD	40.3 ± 9.5	39.3 ± 10.3	t= 1.497, 0.138
Gender, male/female, n	20/22	23/19	χ^2=.110, 0.740
Years of Education, mean ± SD	17.9 ± 2.9	15.4 ± 3.6	t= 3.329, 0.001
Age of Onset, years, mean ± SD		28.7 ± 7.9	
Illness Duration, years, mean ± SD		10.9 ± 8.8	
Number of Hospitalizations, mean ± SD		1.5 ± 1	
Hamilton Depression Rating Scale (HDRS), mean ± SD, [range]		0.9 ± 1.4 [0-7]	
Young Mania Rating Scale (YMRS), mean ± SD, [range]		0.45 ± 1 [0-4]	
Global Assessment of Functioning (GAF), mean ± SD		84.5 ± 5.3	

Table 3.1 Legend. Participants were age and gender matched. All participants in the bipolar group were confirmed euthymic with clinical rating scales of mania and depression less than a score of 7.

Psychotropic Medication

Most patients were medicated at the time of scanning. Thirty-three of the patients were taking mood stabilizers at the time of scanning with most on lithium (29); twenty-two of the patients were taking antipsychotics with most taking olanzapine (15); and 8 participants were taking antidepressants. Four participants in the bipolar group were unmedicated at time of MRI scan. Two measures of lithium use were included for analysis. First, we investigated lithium status (patients who never took lithium, patients who previously took lithium, and patients currently taking lithium) and secondly years of lithium use. The average length of lithium use was 8.55 years ± 7.72.

Participants across four-centres

The study across four centres consisted of 296 participants, including 152 individuals with BD and 144 healthy controls. The clinical and sociodemographic details are provided in Table 3.2.

Table 3.2. Clinical and socio-demographic details of participants across four-centres

	Healthy Control					BD					Group Comparison (Test statistic, p value)
	Galway	**USA**	**France**	**Germany**	**Total**	**Galway**	**USA**	**France**	**Germany**	**Total**	
Number of Participants	42	21	45	36	144	43	43	25	41	152	
Participants Age in Years, Mean ± SD	41.07 ± 9.25	32.78 ± 6.68	36.17 ± 11.55	42.11 ± 11.83	38.59 ± 10.85	39.95 ± 10.96	33.76 ± 8.26	35.66 ± 12.13	41.40 ± 11.18	38.00 ± 10.80	t=0.466, 0.642
Gender, male/female, n	23/19	7/14	21/24	17/19	68/76	22/21	10/33	16/9	18/23	66/86	X^2=.431, 0.511
Illness Duration, Years, Mean ± SD						10.75 ± 8.83	15.51 ± 6.81	14.00 ± 10.90	14.87 ± 10.99	14.63 ± 8.64	
Age on onset, Years, Mean ± SD						28.92 ± 7.86	18.25 ± 6.62	21.52 ± 5.29	23.09 ± 10.24	20.06 ± 5.84	
Young Mania Rating Scale, Mean ± SD						0.46 ± 1.05	2.95 ± 2.71	4.42 ± 7.03	1.29 ± 1.79	4.0 ± 5.08	
Hamilton Depression Rating Scale, Mean ± SD						0.92 ± 1.36	9.95 ± 8.47	6.33 ± 7.77	1.85 ±2.91	6.4 ± 8.69	
Psychotic Features, n						38	23	16	13	90	

Table 3.2 Legend. There were no differences between groups in terms of age and gender. The BD group had an average age of onset of 20 years old, and had an illness duration of 15 years. Participants with BD displayed low symptoms scores in YMRS, and HDRS/MADRS depression rating scales. Approximately 60% of the BD group had a positive history of psychotic features.

Psychotropic Medications

BD participants of the four-centre study were taking up to 4-5 medications at time of scanning. Features of medication history are described for total medication use for each centre.

Table 3.3. Psychotropic Medications

	BD Group				
	Galway	**USA**	**France**	**Germany**	**Total**
Medication Class, frequency, n					
Antidepressants	8	23	8	19	58
Lithium	29	12	12	10	63
Mood Stabilizer (other)	4	26	12	28	70
Antipsychotic	22	27	17	16	82
Benzodiazepine		5	7	2	14
Medication Load, frequency, n					
0	n/a	4	1	0	5
1	n/a	52	24	51	127
2	n/a	55	24	35	114
4	n/a		1		1

Table 3.3 Legend. Medication classes are reported for each centre and collectively. Medication load was given for the three international centres. The psychotropic medication load was calculated for all medications taken at time of scanning. Therefore, the medication load will include a higher total frequency than the number of BD participants.

Patients within the three international centres took up to five medications at time of scanning. Their medication class type and medication load was recorded for all patients. Medication load was included as a variable to reflect the number and dosage of different medications taken. The methods for calculating medication load have been described previously for one of the international research centres included in this study(Versace et al. 2008). Their calculations for medication load are as follows: Mood stabilizers and antidepressant medications were categorized into low-dose or high-dose groups. Low-doses were recorded as load levels 1 and 2, and patients taking high doses were recorded at load levels 3 or 4. Patients not currently taking medications were reported to take load level 0. Antipsychotics were converted to effective daily dose chlorpromazine equivalent levels and then coded load 0 if not taking any medication, load 1 if the dose was equal to or below chlorpromazine equivalent, and load 2 if above the chlorpromazine equivalent dose. Benzodiazapine medication load levels were coded as 0, 1 or 2 relative to the midpoint of the recommended daily dose range for each of the medications recommended in the *Physicians' Desk Reference*(Thomson 2007). Then, a combined medication load measure is determined by summing all individual medication codes for each medication category for each patient.

The majority of patients were on a low medication load. Most patients were taking antipsychotics, mood stabilizers (other than lithium), and lithium. Few patients were taking up to four psychotropic medications. Most patients taking four medications were on a low medication load. Three patients were taking a 5^{th} psychotropic medication, with two patients taking benzodiazepines and one patient taking a mood stabilizer.

Participants across three-centres

When the re-analysed Galway Bipolar Study participants were removed, there were 109 individuals with BD and 103 healthy controls. Participants had a mean YMRS score of 4, and HDRS score of 9. A proportion of patients were symptomatic at time of scanning, as a number of patients were reported to have HDRS symptoms scores > 9. Mean Montogomery-Asberg Depression Rating Scale (MADRS)(Montgomery & Asberg 1979) and Young Mania Rating Scale (YMRS)(Young et al. 1978) scores were on average <4, and Hamilton Depression Rating Scale 17 (HDRS)(Hamilton 1960) average was <9. Symptomatic patients were considered those with symptomatic scores >7 across mood scales. History of psychotic features was considered at least one manic or one depressive episode with hallucinations or delusions (DSM-IV-R criteria). The average illness duration was approximately 20 years' illness.

Global and regional graph theory metrics

Results of global connectivity in Galway Bipolar Study

There were statistically significant group differences in global measures, whereby the BD group displayed increased characteristic path length and reduced global efficiency and clustering coefficient compared with the healthy volunteer group when connections were weighted by FA. Table 3.4 displays the descriptive statistics in global connectivity measures when edges are weighted by FA, and Figure 3.1 shows the spread of the data between groups. In addition, global metrics were corrected for global connectivity defined by the density measure to account for possible differences in reduced connection density globally. Differences in disrupted anatomical integration were unchanged when corrected for global connectivity. This is also indicated by relatively similar average degree between groups. There were no statistically significant group differences in measures of betweenness centrality and degree ($F=0.060$, $p=0.807$, $F=0.021$, $p=0.885$). When global measures were defined by number of streamlines between nodes, no global differences were observed (Table 3.5, Figure 3.2).

Table 3.4. Global measures in patients and healthy controls weighted by FA

Global Measures	**Healthy Control (Mean ± SD)**	**BD (Mean ± SD)**	**Group Comparison F[p value]**
Betweenness Centrality	64.75 ± 5.52	64.52 ± 6.93	0.060 [0.807]
Clustering Coefficient	0.23 ± 0.01	0.22 ± 0.02	4.083 [0.047]*
Characteristic Path Length	4.10 ± 0.16	4.21 ±0.26	5.975 [0.017]*
Degree	45.49 ± 2.45	45.27 ± 2.38	0.021 [0.885]
Global Efficiency	0.27 ± 0.01	0.26 ± 0.02	6.137 [0.015]*

Table 3.4 Legend. * Indicates significant p-value after multiple comparison correction. All analyses accounted for age and gender. Three of five global measures were deemed significant following at $p<0.05$.

Figure 3.1. Disrupted anatomical integration in BD

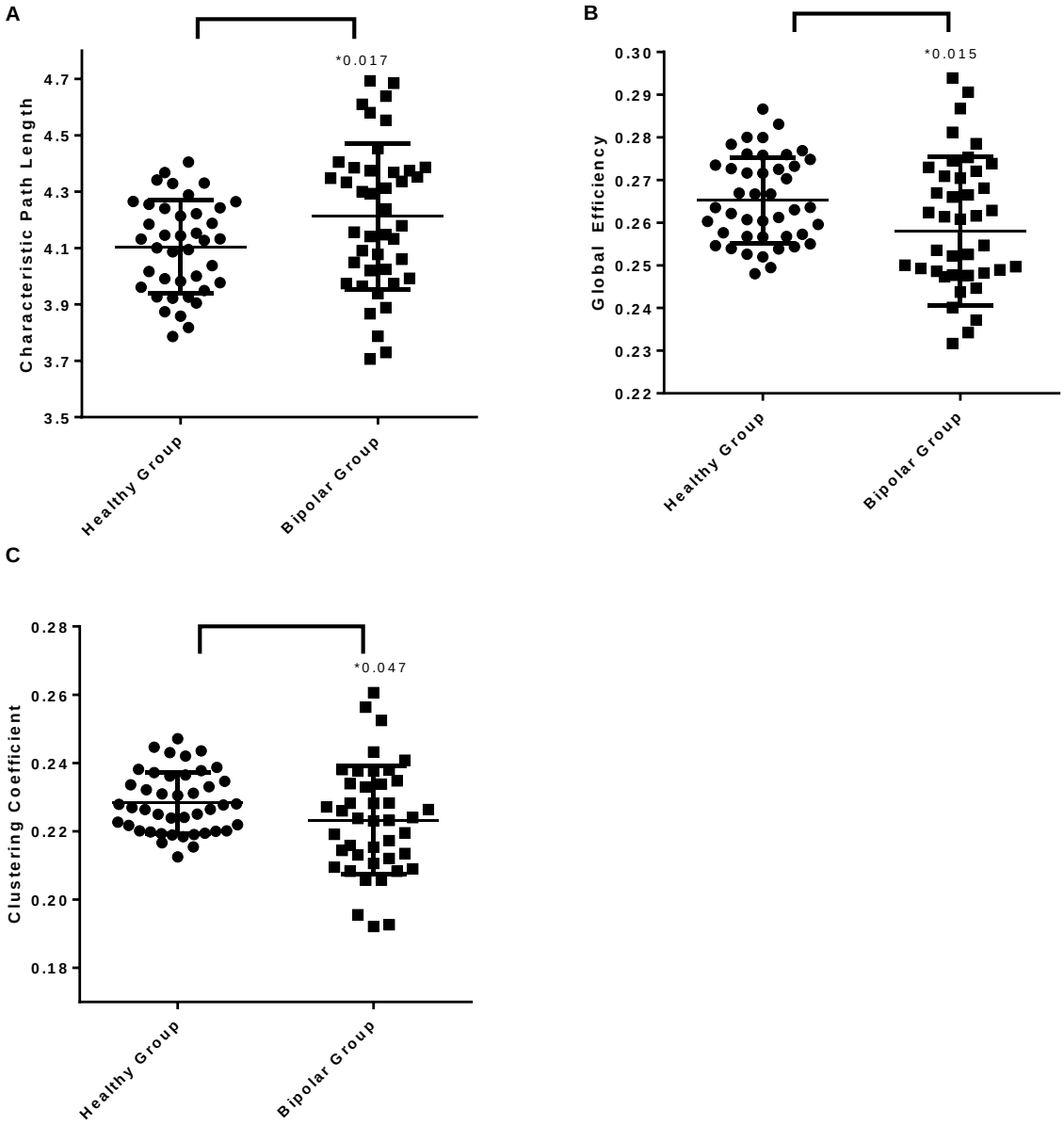

Figure 3.1. Legend. Global metrics defined by FA connection weight in patients and controls show unadjusted values for A) Characteristic Path Length B) Global Efficiency and C) Clustering Coefficient. The mean is represented by the middle line, with bars representing standard error.

Table 3.5. Global measures in patients and controls weighted by number of streamlines

Global Measures	Healthy Control (Mean ± SD)	BD (Mean ± SD)	Group Comparison F [p value]
Betweenness Centrality	144.86 ± 7.05	142.86 ± 8.13	2.732[0.102]
Clustering Coefficient	52.62 ± 8.14	51.86 ± 9.20	0.834[0.364]
Characteristic Path Length	0.008 ± 0.002	0.008 ± 0.003	0.831[0.365]
Degree	45.48 ± 2.45	45.26 ± 2.37	0.007[0.933]
Global Efficiency	182.39 ± 34.27	176.66 ± 33.04	1.290[0.259]

Table 3.5 Legend. No global measures were deemed significant when weighted by number of streamlines.

The differences in magnitude shown between weighting connections by FA and number of streamlines can be contributed by the quantification of these measures. FA represents a scalar value between isotropic diffusion (0) to anisotropic diffusion (1). The FA edge weight reflects the average FA across all voxels between two nodes. The number of reconstructed streamlines is an average measure of reconstructed fiber tracts between two nodes. The FA connection weight might be a more sensitive measure as it relates to the microstructural differences specific to the surrounding voxels. This topic will be addressed further in the discussion chapter.

Figure 3.2. Preserved connection density in BD

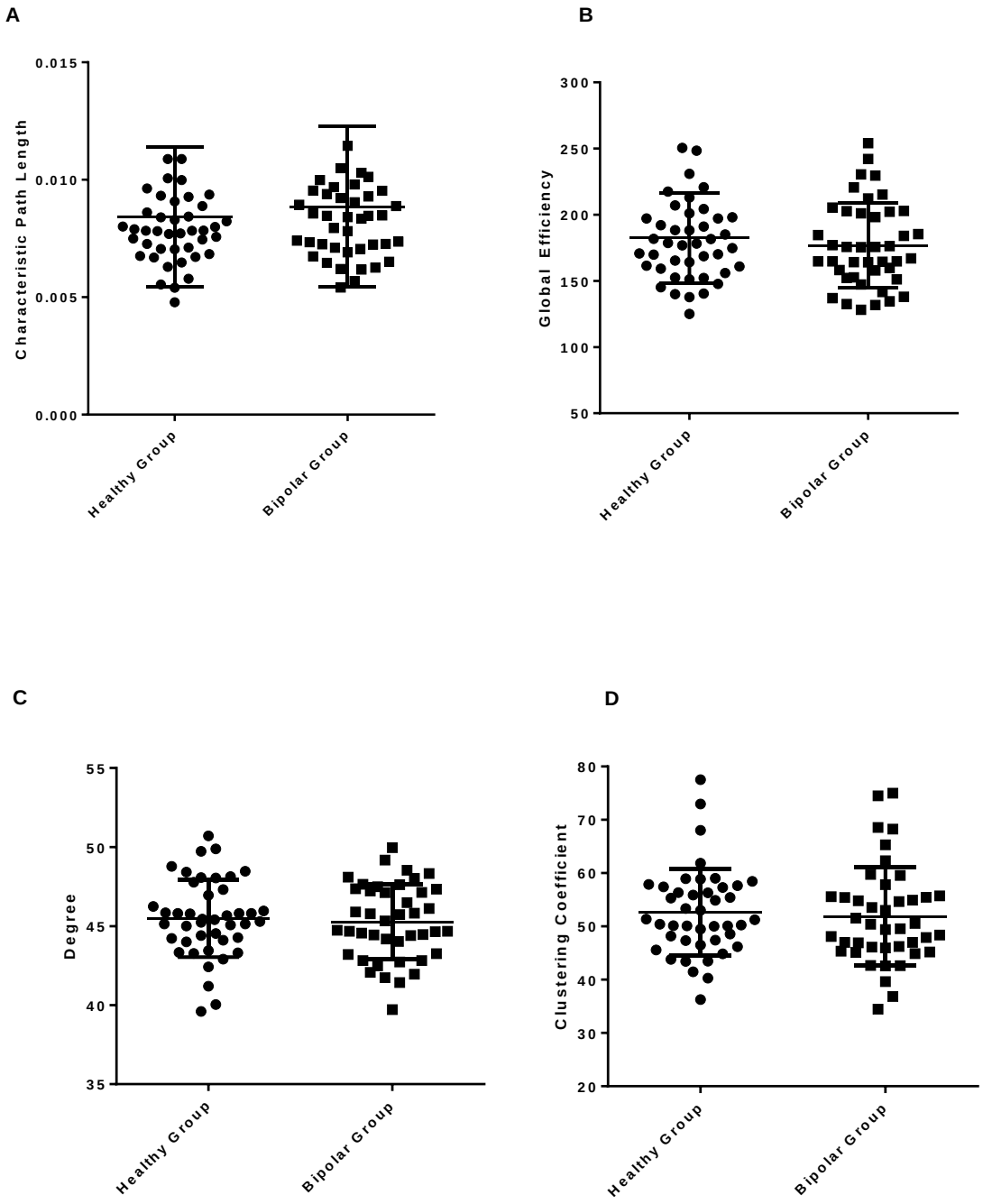

Figure 3.2 Legend. Preserved global connectivity in patients with BD when connection weights are defined by the number of streamlines.

Results of regional connectivity in Galway Bipolar Study

We examined regional connectivity through measures of clustering and local efficiency in order to examine local connectivity patterns potentially implicated in BD. Seven of the regions connected by fronto-limbic and parieto-occipital areas revealed significant connectivity differences surviving multiple comparison correction, where all significant regions demonstrated reduced clustering and local efficiency in BD compared with the healthy control group. The statistically significant regional differences predominantly incorporated the superior and middle frontal nodes and superior and middle occipital nodes, again identified most prominently by the FA connection weight [Table 3.6 & 3.7].

Table 3.6. Regional clustering coefficient in the BD and HC groups weighted by FA

Clustering Coefficient Region		**Healthy Control Mean ± SD**	**BD Mean ± SD**	**Group Comparison F[p value]**
Precentral Gyrus	Left	0.22 ± 0.022	0.21 ± 0.021	2.641 [0.108]
	Right	0.21 ± 0.014	0.21 ± 0.019	5.078 [0.027]
Superior Frontal Gyrus	Left	0.22± 0.014	0.21 ± 0.017	6.575 [0.012]
	Right	0.21 ± 0.011	0.21 ± 0.018	0.049 [0.825]
Middle Frontal Gyrus	Left	0.21 ± 0.016	0.20 ± 0.017	5.464 [0.022]
	Right	0.20 ± 0.013	0.20 ± 0.018	3.174 [0.079]
Medial Superior Frontal	Left	0.21 ± 0.014	0.21 ±0.020	6.422 [0.013]
	Right	0.22 ± 0.018	0.21 ± 0.021	4.323 [0.041]
Anterior Cingulate Gyrus	Left	0.22 ± 0.016	0.21 ± 0.022	6.402 [0.013]
	Right	0.22 ± 0.017	0.21 ± 0.023	4.978 [0.028]
Middle Cingulate Gyrus	Left	0.21 ± 0.016	0.20 ± 0.022	0.654 [0.421]
	Right	0.21 ± 0.015	0.20 ± 0.021	1.818 [0.181]
Superior Parietal Gyrus	Left	0.21 ± 0.012	0.21 ± 0.019	2.955 [0.089]
	Right	0.22 ± 0.015	0.21 ± 0.018	5.258 [0.024]
Superior Occipital Gyrus	Left	0.24 ± 0.021	0.23 ± 0.021	15.371 [0.000*]
	Right	0.25 ± 0.021	0.24 ± 0.024	6.929 [0.010]
Middle Occipital Gyrus	Left	0.23 ± 0.016	0.22 ± 0.020	6.185 [0.015]
	Right	0.25 ± 0.023	0.24 ± 0.022	4.669 [0.034]

Table 3.7. Local efficiency in the BD and HC group weighted by FA

Local Efficiency Region		**Healthy Control Mean ± SD**	**BD Mean ± SD**	**Group Comparison F[p value]**
Precentral Gyrus	Left	0.31 ± 0.019	0.30 ± 0.022	3.415 [0.068]
	Right	0.30 ± 0.015	0.29 ± 0.020	7.819 [0.006]
Superior Frontal Gyrus	Left	0.32 ± 0.015	0.31 ± 0.019	9.411 [0.003*]
	Right	0.32 ± 0.015	0.31 ± 0.023	4.147 [0.045]
Middle Frontal Gyrus	Left	0.30 ± 0.017	0.29 ± 0.019	10.937 [0.001*]
	Right	0.30 ± 0.014	0.29 ± 0.022	8.271 [0.005*]
Medial Superior Frontal	Left	0.30 ± 0.016	0.30 ±0.023	5.042 [0.027]
	Right	0.30 ± 0.017	0.29 ± 0.025	5.499 [0.021]
Anterior Cingulate Gyrus	Left	0.30 ± 0.018	0.30 ± 0.022	4.897 [0.030]
	Right	0.30 ± 0.016	0.29 ± 0.023	4.30 [0.040]
Middle Cingulate Gyrus	Left	0.30 ± 0.016	0.30 ± 0.021	2.415 [0.124]
	Right	0.31 ± 0.016	0.30 ± 0.022	5.084 [0.027]
Superior Parietal Gyrus	Left	0.32 ± 0.016	0.31 ± 0.026	3.400 [0.069]
	Right	0.32 ± 0.018	0.319 ± 0.027	3.786 [0.055]
Superior Occipital Gyrus	Left	0.34 ± 0.019	0.32 ± 0.024	12.913 [0.001*]
	Right	0.34 ± 0.017	0.33 ± 0.025	9.870 [0.002*]
Middle Occipital Gyrus	Left	0.34 ± 0.015	0.33 ± 0.023	8.527 [0.005*]
	Right	0.33 ± 0.023	0.32 ± 0.025	5.097 [0.027]

Table 3.7 Legend. This analysis examined two different local graph measures in FA connections. MANCOVAs were carried out between groups, co-varying for age and gender. * indicates significant p-value after FDR correction. Nine nodes bilaterally were selected a priori from a previous data driven DTI analysis(Emsell, Leemans, et al. 2013; Emsell, Langan, et al. 2013) for analyses of local graph theory measures.

Table 3.8. Regional connectivity in the BD and HC groups weighted by the number of streamlines

Clustering Coefficient Region		**Healthy Control Mean ± SD**	**BD Mean ± SD**	**Group Comparison F [p value]**
Precentral Gyrus	Left	78.56±23.01	78.03±25.02	0.164[0.687]
	Right	77.77±22.42	79.93±27.92	0.004[0.947]
Superior Frontal Gyrus	Left	67.97±19.15	69.35±24.82	0.094[0.760]
	Right	71.06±21.22	74.43±22.35	0.065[0.800]
Middle Frontal Gyrus	Left	57.79±14.40	55.64±17.66	0.826[0.366]
	Right	56.47±20.57	58.32±22.47	0.003[0.955]
Medial Superior Frontal Gyrus	Left	56.44±16.62	55.41±21.92	0.793[0.376]
	Right	57.62±17.47	54.95±21.17	1.252[0.266]
Anterior Cingulate Gyrus	Left	61.01±17.40	56.32±21.37	3.031[0.085]
	Right	64.37±17.03	59.33±19.82	3.593[0.062]
Middle Cingulate Gyrus	Left	58.40±18.69	58.93±18.00	0.089[0.766]
	Right	66.81±17.19	66.55±16.46	0.411[0.523]
Superior Parietal Gyrus	Left	44.60±14.41	41.80±13.08	0.859[0.357]
	Right	47.41±15.98	43.75±12.42	1.705[0.195]
Superior Occipital Gyrus	Left	70.21±16.29	64.53±18.79	2.692[0.105]
	Right	72.40±14.99	68.20±20.49	1.653[0.202]
Middle Occipital Gyrus	Left	62.33±17.27	58.59±15.63	1.596[0.210]
	Right	46.61±12.07	47.36±16.86	0.069[0.793]

Table 3.8 Legend. There were no statistically significant differences between groups in regional connectivity when we examined regional clustering by the number of streamlines.

Table 3.9. Regional connectivity in the BD and HC groups weighted by number of streamlines

Local efficiency Region		**Healthy Control Mean ± SD**	**BD Mean ± SD**	**Group Comparison F [p value]**
Precentral Gyrus	Left	123 ± 34	123 ±41	0.133[0.716]
	Right	121±	124±40	0.003[0.953]
Superior Frontal Gyrus	Left	113±30	116±39	0.022[0.884]
	Right	124 ±35	125±34	0.061[0.805]
Middle Frontal Gyrus	Left	96±23	94±33	0.623[0.432]
	Right	93±33	94±33	0.050[0.824]
Medial Superior Frontal Gyrus	Left	89±23	88±31	0.511[0.477]
	Right	88±24	84±28	1.473[0.228]
Anterior Cingulate Gyrus	Left	97±23	90 ±28	3.469[0.066]
	Right	101 ±24	93 ±25	4.140[0.045]
Middle Cingulate Gyrus	Left	97±27	97±25	0.171[0.680]
	Right	115±26	114±25	0.575[0.450]
Superior Parietal Gyrus	Left	75 ±22	71±20	1.029[0.313]
	Right	80±24	75±19	1.633[0.205]
Superior Occipital Gyrus	Left	106 ±20	98±24	2.910[0.092]
	Right	109 ±21	104±28	1.461[0.230]
Middle Occipital Gyrus	Left	107±30	102±26	0.976[0.326]
	Right	74±18	76±26	0.109[0.742]

Table 3.9 Legend. Regional connectivity remains intact when connection weights are defined by number of streamlines. There were no differences between patients and controls in regional measures of clustering coefficient. Subtle between group differences in local efficiency were identified in the right anterior cingulate gyrus.

Relationship between graph properties and clinical characteristics

There were no significant relationships between graph theory measures and clinical characteristics. Partial correlations did not reveal any significant association between graph theory properties and clinical measures including: age of onset (r=0.196, p=0.71), illness duration (r=-0.196, p=0.710), YMRS (r=-0.188, p=0.722) and HDRS (r=0.655, p=0.158) scores.

Differences in characteristic path length were not explained by lithium status (r=-0.169, p=0.410) or number of years taking lithium (r=-0.62, p=0.76).

Global and regional connectivity in the study across four centres

BD patients exhibited longer CPL (F=8.995, p=0.003) and reduced global efficiency (F=5.614, p= 0.018) compared to controls when connectivity was defined by FA edge weight [Table 3.10, Figure 3.3]. Similarly to the results from the Galway Bipolar Study data, patients displayed reduced clustering coefficient compared to healthy controls. Global metrics of degree, density, and betweenness centrality did not statistically differ. One statistical outlier was removed as data was more than 2.5 SD away from the mean.

Global property findings withstood correction for global density, however there was also an effect of density when included as a confounding covariate (CPL: F=7. 295, p=0.007; Density: 47.96, p<0.001), (Eglobal: F= 3.961, p=0.048; Density: F= 117.15, p<0.001), but no effect on Clustering Coefficient: F=4.195, p=0.041; Density: F=0.194, p=0.660).

Table 3.10. FA-weighted global connectivity measures across four-centres

Global Measures	**Healthy Control Mean± SD**	**BD Mean ±SD**	**Group Comparison F[p value]**
Characteristic Path Length	4.90 ± 0.52	5.04 ± 0.62	8.995[0.003]*
Global Efficiency	0.228 ±0.029	0.222 ± 0.028	5.614[0.018]*
Degree	31.43 ± 9.31	30.64 ± 9.505	1.639[0.201]
Density	0.364 ± 0.104	0.355 ± 0.106	1.617[0.204]
Clustering Coefficient	0.218 ± 0.016	0.215 ± 0.016	4.367[0.038]*

Table 3.10 Legend. Edge weights were defined by the mean FA between nodes. * Indicates measures statistically significant between groups. Three of five graph properties displayed significant between-group differences. Two measures of global connectivity were preserved.

Table 3.11. Streamline-weighted global connectivity measures across four-centres

Global Measures	**Healthy Control Mean± SD**	**BD Mean ±SD**	**Group Comparison F[pvalue]**
Characteristic Path Length	0.052 ± 0.036	0.059 ± 0.046	0.755[0.448]
Global Efficiency	84.23 ± 78.36	77.41 ± 73.73	3.617[0.149]
Degree	30.38 ± 7.88	29.63 ± 8.14	1.281[0.337]
Density	0.34 ± 0.085	0.34 ± 0.091	0.360[0.590]
Clustering Coefficient	32.61 ± 22.50	30.43 ± 21.47	7.098[0.072]

Table 3.11 Legend. Trend-like reductions in average clustering were observed in the BD group compared with the HC group when connectivity was assessed using number of streamlines edges weights.

Figure 3.3. FA-weighted global connectivity measures across four-centres

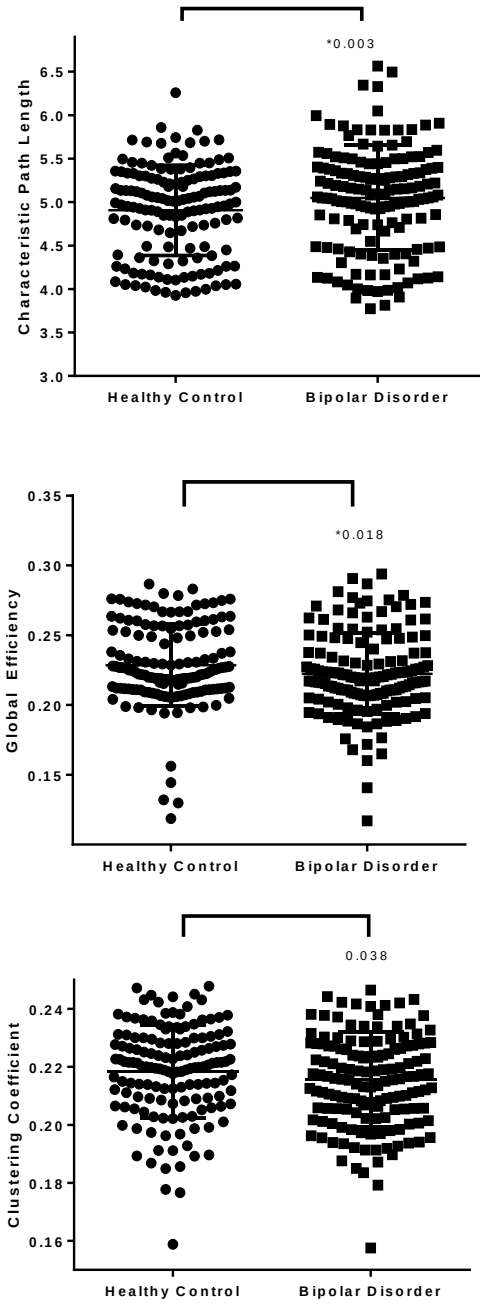

Figure 3.3 Legend. Patients display group differences across 3 of 5 global measures of integration. These graphs are unadjusted for variations due to research centre, age and gender. Patients displayed longer characteristic path length, reduced global efficiency and clustering compared to healthy controls.

Regional connectivity across four-centres

Nodes identified for a regional or local analysis were those previous implicated in the Galway Bipolar Study findings and additionally a prior tractography analysis of the three centre dataset that identified dysconnectivity in limbic, callosal, and leftward anterior arcuate fasciculus(Sarrazin et al. 2014). Therefore, 14 nodes were selected for further investigation due to their connectedness to these white matter pathways.

The patients with BD across the four-centres exhibited reduced clustering coefficient measure among connections traversing the superior frontal gyri, left middle cingulate gyrus, frontal medial gyri orbital part, posterior cingulate, bilateral superior occipital and parietal gyri using FA as the connection weight [Table 3.12]. Similar differences were observed when regional connectivity was assessed by the number of streamlines [Table 3.13]. When we examined local efficiency between groups, patients displayed reduced nodal efficiency of the bilateral superior frontal gyri, anterior, middle, and posterior cingulate gyri, as well as parietal-occipital gyri using FA connection measures [Table 3.14]. Consistent with the results from the clustering coefficient measure, findings were more robust using the FA edge weight compared with the number of streamlines [Table 3.15]. Local efficiency exhibited a greater extent of dysconnectivity across nodes compared to clustering measures. Following multiple comparison correction, the left middle cingulate and right anterior cingulate displayed the greatest connectivity deficits. Regional measures of connectivity displayed bilateral dysconnectivity locally.

Table 3.12. FA-weighted clustering differences between BD and HC groups across four-centres

Clustering Coefficient Region		**Healthy Control Mean ± SD**	**BD Mean ± SD**	**Group Comparison F[pvalue]**
Superior Frontal Gyrus	Left	0.207 ± 0.026	0.198 ± 0.024	7.987[0.005]*
	Right	0.195 ± 0.022	0.190 ± 0.024	4.464[0.035]
Inferior Frontal Gyrus, orbital part	Left	0.212 ± 0.037	0.211 ± 0.035	0.313[0.576]
	Right	-	-	-
Anterior Cingulate Gyrus	Left	0.207 ± 0.026	0.201 ± 0.028	2.597[0.108]
	Right	0.212 ± 0.025	0.204 ± 0.026	6.964[0.009]
Middle Cingulate Gyrus	Left	0.201 ± 0.026	0.194 ± 0.030	5.995[0.015]
	Right	0.193 ± 0.026	0.187 ± 0.033	4.148[0.043]
Posterior Cingulate Gyrus	Left	0.215 ± 0.034	0.210 ± 0.035	4.184[0.042]
	Right	0.224 ± 0.036	0.218 ± 0.035	2.890[0.090]
Superior Parietal Gyrus	Left	0.232 ± 0.036	0.225 ± 0.036	5.849[0.016]
	Right	0.227 ± 0.034	0.219 ±0.033	5.144[0.024]
Superior Occipital Gyrus	Left	0.217 ± 0.038	0.209 ± 0.034	6.401 [0.012]
	Right	0.222 ± 0.034	0.215 ± 0.034	7.183[0.008]*

Table 3.12 Legend. Thirteen nodes were narrowed for investigation of regional connections. Frontal, limbic and parietal connections differed to a statistically significant extent between groups.

Table 3.13. Streamline-weighted clustering differences between BD and HC groups across four-centres

Clustering Coefficient Region		**Healthy Control Mean ± SD**	**BD Mean ± SD**	**Group Comparison F[p value]**
Superior Frontal Gyrus	Left	53.04 ± 34.13	47.02 ± 32.79	6.885[0.073]
	Right	53.59 ± 37.15	44.49 ± 32.31	26.664[0.011]
Inferior Frontal Gyrus, orbital part	Left	18.68 ± 17.02	18.39 ± 15.48	0.041[0.852]
	Right	-	-	
Anterior Cingulate Gyrus	Left	42.04 ± 32.77	36.17 ± 27.52	2.145[0.238]
	Right	40.72 ± 31.91	35.27 ± 29.43	3.618[0.151]
Middle Cingulate Gyrus	Left	48.12 ± 33.38	41.27 ± 33.71	22.669[0.013]
	Right	51.73 ± 36.47	45.41 ± 36.41	14.222[0.026]
Posterior Cingulate Gyrus	Left	38.78 ± 38.72	35.88 ± 37.32	2.997[0.172]
	Right	38.65 ± 39.89	35.48 ± 38.30	1.671[0.281]
Superior Parietal Gyrus	Left	34.07 ± 21.09	32.48 ± 21.88	2.930 [0.183]
	Right	33.77 ± 25.21	32.25 ±23.36	2.681 [0.191]
Superior Occipital Gyrus	Left	38.05 ± 34.98	33.81 ± 32.20	4.614[0.117]
	Right	41.31 ± 33.83	41.83 ± 36.26	0.114[0.757]

Table 3.13 Legend. Patients display reduced clustering in the right superior frontal gyrus and bilateral middle cingulate gyri. Findings not withstanding correction for multiple testing.

Table 3.14. FA-weighted local efficiency differences between BD and HC groups across four-centres

Local Efficiency Region		Healthy Control Mean ± SD	BD Mean ± SD	Group Comparison F[pvalue]
Superior Frontal Gyrus	Left	0.33 ± 0.023	0.32 ± 0.033	7.349[0.007]*
	Right	0.33 ± 0.022	0.32± 0.029	6.698[0.010]
Inferior Frontal Gyrus, orbital part	Left	0.27 ± 0.033	0.27 ± 0.032	0.497[0.481]
	Right	-	-	-
Anterior Cingulate Gyrus	Left	0.30 ± 0.022	0.30 ± 0.024	6.215[0.013]
	Right	0.30 ± 0.023	0.29 ± 0.025	9.483[0.002]*
Middle Cingulate Gyrus	Left	0.31 ± 0.024	0.30 ± 0.027	9.454[0.002]*
	Right	0.32 ± 0.024	0.31 ± 0.029	5.444[0.020]
Posterior Cingulate Gyrus	Left	0.32 ± 0.031	0.31 ± 0.035	5.553[0.019]
	Right	0.33 ± 0.034	0.32 ± 0.037	6.082[0.014]
Superior Parietal Gyrus	Left	0.30 ± 0.032	0.29 ± 0.034	7.214[0.008]*
	Right	0.29 ± 0.036	0.28 ± 0.037	3.833[0.051]
Superior Occipital Gyrus	Left	0.29 ± 0.044	0.28 ± 0.041	5.949[0.015]
	Right	0.30 ± 0.041	0.29 ± 0.038	4.566[0.033]

Table 3.14 Legend. Features of local efficiency differ statistically significant extent between patients and controls among frontal, cingulate and parietal connections.

Table 3.15. Streamline-weighted local efficiency differences between BD and HC groups across four-centres

Local Efficiency Region		**Healthy Control Mean ± SD**	**BD Mean ± SD**	**Group Comparison F[pvalue]**
Superior Frontal Gyrus	Left	83.53 ± 51.78	75.42 ± 51.46	4.939 [0.107]
	Right	88.51 ± 59.57	73.64 ± 53.01	16.729 [0.025]
Inferior Frontal Gyrus, orbital part	Left	27.68 ± 25.94	26.98 ± 24.17	0.010 [0.926]
	Right	-	-	-
Anterior Cingulate Gyrus	Left	64.23 ± 48.07	55.81 ± 41.04	2.194 [0.234]
	Right	60.65 ± 46.29	53.42 ± 43.12	3.650 [0.0.150]
Middle Cingulate Gyrus	Left	72.35 ± 52.71	62.85 ± 53.79	23.255 [0.012]*
	Right	82.41 ± 59.43	75.57 ± 49.08	14.087[0.026]
Posterior Cingulate Gyrus	Left	57.76 ± 54.75	53.35 ± 52.66	3.438 [0.152]
	Right	56.75 ± 56.77	51.39 ± 52.99	1.707[0.280]
Superior Parietal Gyrus	Left	48.69 ± 34.84	46.21 ± 36.00	4.474 [0.110]
	Right	49.06 ± 41.97	45.63 ± 37.53	1.778 [0.271]
Superior Occipital Gyrus	Left	53.19 ± 51.00	48.09 ± 47.94	4.436 [0.121]
	Right	58.11 ± 51.00	57.90 ± 52.79	0.061 [0.820]

Table 3.15 Legend. Reductions in local efficiency were identified in fronto-limbic connections in patients, with deficits in the right superior frontal gyrus and bilateral middle cingulate gyri.

Relationship between graph properties and clinical characteristics across four-centres

Clinical characteristics of the patient group in the four-centre study were not associated with longer characteristic path length. No association was found between path length and illness duration (r=-0.186, p=0.150), age of onset (r=0.191, p=0.140), or YMRS measures (r=-0.085, p=0.51) and HDRS measures (r=0.002, p=0.98).

Characteristic Path Length findings were not explained by medication use of the primary medication load (r=-0.369, p=0.369), medication dose (r=0.064, p=0.881).

Global connectivity across three-centres

When the analysis was restricted to a three-centre study, due to the identical scanner and acquisition sequence parameters, patients of the three-centres exhibited longer characteristic path length compared to controls ($F=7.58$, $p<0.006$) [Table 3.16-3.17; Figure 3.4]. No global differences were identified across further graph theory global metrics. Longer characteristic path length has been a consistent feature in patients across research studies.

Figure 3.4. Differences in Characteristic Path Length in BD and HC groups in the study across three-centres

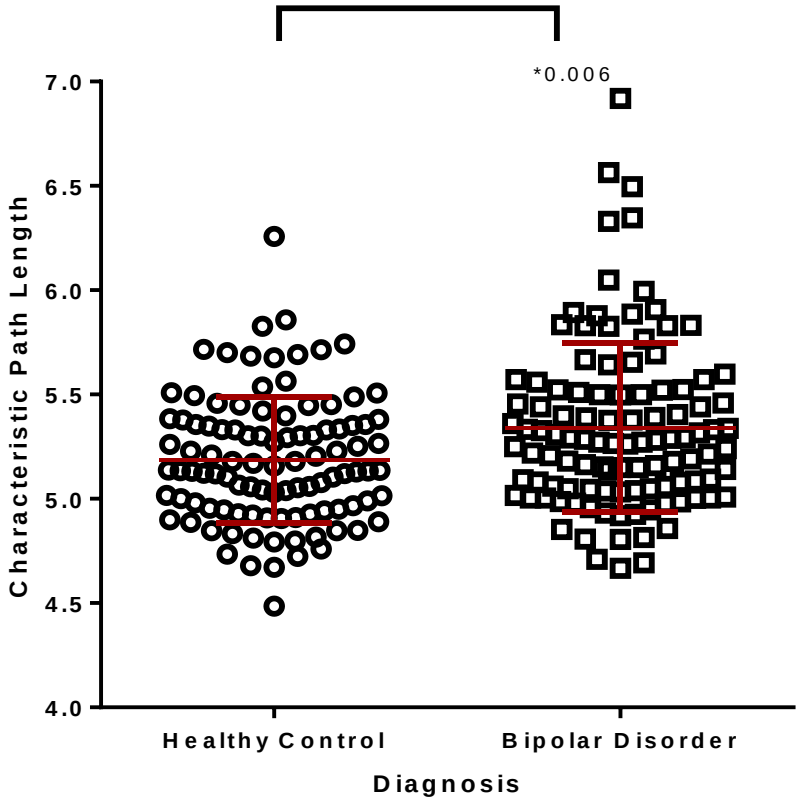

Figure 3.4 Legend. The BD group displayed longer characteristic path length compared to the HC group when connectivity matrices were weighted by the FA connection weight. Global connectivity was preserved when connected matrices were weighted by the number of streamlines.

Table 3.16. FA-weighted global measures across three-centres

Global Measures	**Healthy Control Mean ± SD**	**BD Mean ± SD**	**Group Comparison F [pvalue]**
Degree	25.69 ± 2.52	25 ± 2.97	1.09[0.296]
Density	0.299 ± 0.028	0.292 ± 0.033	1.06[0.303]
Characteristic Path Length	5.18 ± 0.30	5.33± 0.40	7.58[0.006] *
Global Efficiency	0.213± 0.020	0.209 ± 0.0189	1.9[0.169]
Clustering Coefficient	0.214 ± 0.016	0.212 ± 0.015	1.79[0.182]

Table 3.16 Legend. One measure of global integration was statistically significantly different between patients and controls, while four global measures were preserved in patients.

Table 3.17. Streamline-weighted global measures across three-centres

Global Measures	**Healthy Control Mean ± SD**	**BD Mean ± SD**	**Group Comparison F [pvalue]**
Degree	25.60 ± 2.63	24.99 ± 2.97	0.659[0.418]
Density	0.298 ± 0.029	0.292 ± 0.033	0.632 [0.427]
Characteristic Path Length	0.07 ±0.026	0.07 ± 0.039	1.144[0.286]
Global Efficiency	36.12 ± 9.16	33.56 ± 10.93	1.778[0.0184]
Clustering Coefficient	18.81 ± 4.91	17.87 ± 4.46	2.448[0.119]

Regional connectivity across three-centres

Regional deficits were identified in the clustering coefficient and local efficiency measure. Regions restricted for further investigation were those affected in a prior tractography analysis that included connections of the left anterior portion of the arcuate fasciculus, left cingulum bundle, and splenium(Sarrazin et al. 2014). Dysconnectivity was identified in the left middle cingulate gyrus in patients compared to controls in both the clustering coefficient metric and local efficiency metric [Table 3.18-3.21].

Table 3.18. FA-weighted clustering differences between BD and HC groups across three-centres

Clustering Coefficient Region		Healthy Control Mean ± SD	BD Mean ± SD	Group Comparison F [pvalue]
Inferior Frontal Gyrus, Orbital Part	Left	0.200 ± .057	0.203 ± .047	0.027 [.870]
Anterior Cingulate Gyrus	Left	0.199 ± .026	0.196 ± .029	0.595 [.441]
Middle Cingulate Gyrus	Left	0.198 ± .029	0.188 ± .032	6.542 [.011]*
Posterior Cingulate Gyrus	Left	0.201 ± .026	0.198 ± .030	1.980 [.161]
Superior Parietal Gyrus	Left	0.235 ± .047	0.231 ± .040	2.163 [.143]
	Right	0.226 ± .045	0.220 ± .037	1.596 [.208]
Superior Occipital Gyrus	Left	0.205 ± .037	0.200 ± .033	2.512 [.115]
	Right	0.208 ± .036	0.203 ± .031	1.994[.159]

Table 3.18 Legend. Patients displayed significantly reduced clustering in the left middle cingulate compared to controls when defined by the FA connection weight.

Table 3.19. Streamline-weighted clustering differences between BD and HC groups across three-centres

Clustering Coefficient Region		Healthy Control Mean ± SD	BD Mean ± SD	Group Comparison F [pvalue]
Inferior Frontal Gyrus, Orbital Part	Left	10.58 ± 9.74	10.83 ± 6.28	0.045[0.832]
Anterior Cingulate Gyrus	Left	24.39 ± 10.01	21.96 ± 10.21	1.219[0.271]
Middle Cingulate Gyrus	Left	32.51 ± 16.93	26.67 ± 13.48	6.711[0.010]*
Posterior Cingulate Gyrus	Left	16.52 ± 8.11	15.54 ± 8.74	0.737[0.392]
Superior Parietal Gyrus	Left	25.32 ± 14.81	23.67 ± 12.19	1.688[0.195]
	Right	22.27 ± 13.34	22.55 ± 13.27	0.239 [0.626]
Superior Occipital Gyrus	Left	18.08 ± 10.53	16.10 ± 8.71	2.186[0.141]
	Right	22.00 ± 13.03	22.37 ± 13.35	0.184[0.668]

Table 3.19 Legend. Patients display significantly reduced clustering in the left middle cingulate gyrus compared to healthy controls when defined by the number of streamlines.

Table 3.20. FA-weighted local efficiency differences between BD and HC groups across three-centres

Local Efficiency Region		Healthy Control Mean ± SD	BD Mean ± SD	Group Comparison F [pvalue]
Inferior Frontal Gyrus, Orbital Part	Left	0.260 ± .061	0.264 ± .048	0.200[.655]
Anterior Cingulate Gyrus	Left	0.307 ± .024	0.302 ± .025	2.673[.104]
Middle Cingulate Gyrus	Left	0.313 ± .027	0.303 ± .029	8.072 [.005]*
Posterior Cingulate Gyrus	Left	0.323 ± .036	0.315 ± .038	2.547 [.112]
Superior Parietal Gyrus	Left	0.289 ± .045	0.285 ± .034	1.721 [.191]
	Right	0.272 ± .042	0.270 ± .032	0.313 [.576]
Superior Occipital Gyrus	Left	0.272 ± .035	0.269 ± .035	1.40[.238]
	Right	0.278 ± .042	0.277 ± .030	0.141 [.707]

Table 3.20 Legend. Reduced clustering and efficiency were regionally specific to the left middle cingulate gyrus in patients compared to controls.

Table 3.21. Streamline-weighted local efficiency differences between BD and HC groups across three-centres

Local Efficiency Region		Healthy Control Mean ± SD	BD Mean ± SD	Group Comparison F [pvalue]
Inferior Frontal Gyrus, Orbital Part	Left	14.16 ± 11.80	14.47 ± 8.06	0.0842 [0.772]
Anterior Cingulate Gyrus	Left	37.31 ± 12.77	33.76 ± 14.67	1.284 [0.258]
Middle Cingulate Gyrus	Left	45.82 ± 20.78	38.14 ± 16.70	7.429 [0.007]*
Posterior Cingulate Gyrus	Left	25.71 ± 11.86	23.97 ± 12.12	0.779 [0.379]
Superior Parietal Gyrus	Left	30.22 ± 15.65	28.37 ± 13.93	1.475 [0.226]
	Right	26.47 ± 14.42	26.54 ± 13.95	0.264 [0.608]
Superior Occipital Gyrus	Left	22.83 ± 11.99	20.62 ± 10.44	1.80 [0.181]
	Right	27.85 ± 15.06	28.23 ± 15.30	0.127 [0.722]

Table 3.21. Legend. Reduced local efficiency was regionally identified in the left middle cingulate gyrus in patients compared to controls. This deficit was supported when edges were defined by both FA and number of streamlines.

Figure 3.5. Group differences in left middle cingulate gyrus defined by regional connectivity

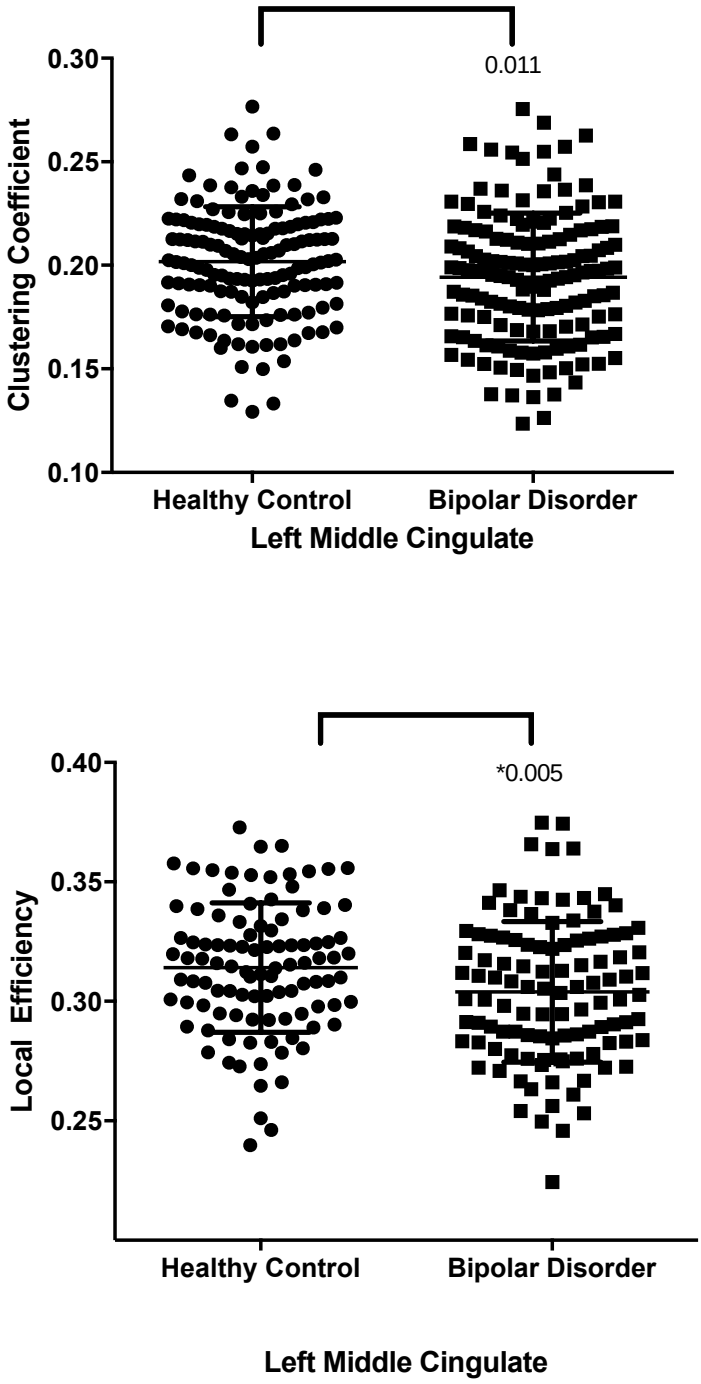

Figure 3.5. Legend. Patients display reduced clustering patterns and local efficiency patterns compared to healthy volunteers in the left middle cingulate. Differences in regional connectivity were most prominent using the FA connection weight.

Analysis of global and regional connectivity across three international centres of patients with BD demonstrated that widespread dysconnectivity is a feature of BD, as indicated by longer characteristic path length in the patient group compared to healthy control group. Additionally, upon further analysis of regional connectivity, differences suggest impaired connectivity of the left middle cingulate across two regionally specific features of segregation.

Relationship between graph properties and clinical characteristics

Clinical measures of symptoms and severity were not related to global dysconnectivity measures. The statistically significant difference in characteristic path length was not associated with clinical measures of illness duration ($r=-0.186$, $p=0.15$), age of onset($r=0.191$, $p=0.140$), and symptom ratings defined by YMRS($r=0.070$, $p=0.590$) and HDRS($r=0.002$, $p=0.989$).

Path length differences were not explained by medication load ($r=-0.103$, $p=0.424$), dose($r=0.059$, $p=0.734$).

Next, we explored sub-network connectivity features in patients with BD and healthy volunteers.

Sub-network analysis

Results of the sub-network analysis in the Galway Bipolar Study

Findings of sub-network analysis show topological clusters among the set of supra-threshold edges as evidence against the null hypothesis. Here we report two outputs of the sub-network analysis defining both the set of connections comprised in the graph component found to show a significant effect as well as a corresponding p-value for each component [Figure 3.6; Table 3.22].The BD group displayed weaker connected components compared to controls across varying supra-threshold connections (t=2, p=0.015); (t=2.5, p=0.017); (t=3, p=0.020), in which a single dysconnected network comprised of multiple dysconnections was identified for each threshold. We identified collective network dysconnectivity differences between groups with supra-threshold connections t=2, consisting of frontal, parietal and occipital connections. Higher supra-threshold connections (t=2.5, t=3) indicate consistency in findings with reduced structural connectivity among parietal and occipital connections in patients compared to healthy controls. Additionally, we investigated the magnitude of the edge weight effects. Higher t-statistic values indicate edges with a greater magnitude of an effect. No significant differences were identified when edges were defined by number of streamlines.

Figure 3.6. Density of nodal connections in participant groups

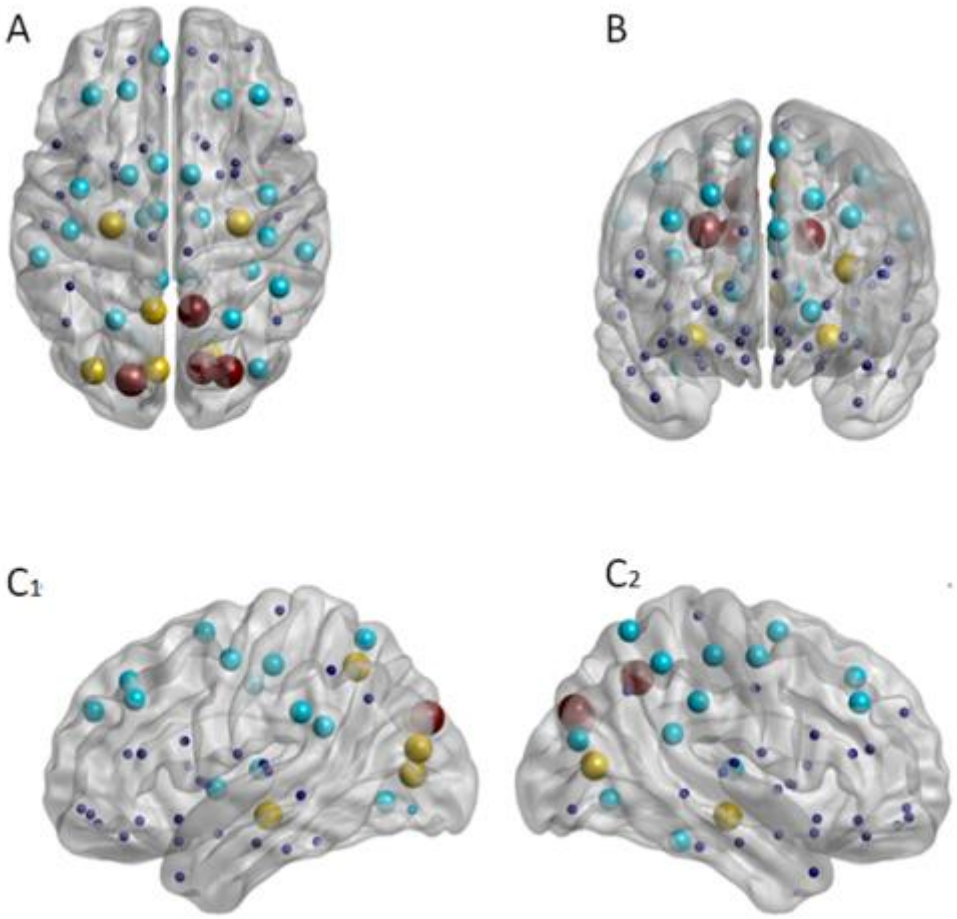

Figure 3.6 Legend. Nodal alterations identified in Network Based Statistic toolbox (NBS) with color and size of sphere indicating increasing t-statistic thresholds. Dark blue nodes indicate AAL nodes which did not significantly differ at any threshold. Light blue nodes (T=2) identify a reduction in density of connections in the BD group compared to control group. Similarly, yellow nodes (T=2.5) and red nodes (T=3) represent reduced density of connections in the BD group at higher thresholds. A) Axial B) Coronal C1) Left Sagittal and C2) Right Sagittal orientations.

Table 3.22. Magnitude of edge weights across supra-threshold connections

Supra-threshold connections	**T-stat >2.5 P=0.018**	**T-stat >3**
Hippocampus Left to Hippocampus Right	2.52	
Hippocampus Right to Calcarine Left	3.12	
Hippocampus Left to Calcarine Right	2.53	
Hippocampus Right to Calcarine Right	2.78	
Hippocampus Left to Superior Occipital Left	2.58	
Cuneus Right to Superior Occipital Left	2.59	
Hippocampus Right to Superior Occipital Right	2.68	
Calcarine Right to Superior Occipital Right	2.77	
Cuneus Right to Superior Occipital Right	3.07	3.07
Superior Occipital Left to Superior Occipital Right	3.10	3.10
Calcarine Right to Middle Occipital Left	2.91	
Superior Occipital Right to Middle Occipital Left	2.74	
Hippocampus Right to Precuneus Left	2.76	
Superior Occipital Right to Precuneus Left	2.63	
Hippocampus Right to Precuneus Right	2.74	
Calcarine Right to Precuneus Right	2.88	
Cuneus Right to Precuneus Right	3.17	3.17
Superior Occipital Left to Precuneus Right	3.33	3.33
Superior Occipital Right to Precuneus Right	3.84	3.84
Hippocampus Left to Thalamus Left	2.60	

Table 3.22 Legend. The magnitude of the edge weights identifies the strongest weighted connections. Across highest supra-threshold connections, the strongest edge weights were identified between i. Right Cuneus to Right Superior Occipital Gyrus, ii. Left Superior Occipital Gyrus to Right Superior Occipital Gyrus, iii. Right Cuneus to Precuneus, iv. Left Superior Occipital Gyrus to Right Precuneus, v. Right Superior Occipital Gyrus to the Right Precuneus.

Sub-network analysis across four centres

Findings of the Network Based Statistic indicate reduced connectivity in the BD group compared to healthy controls in a sub-network connecting inferior fronto-temporal nodes. Comparison of network density revealed a sub-network consisting of 13 nodes and 16 edges disconnected in the patient group compared to healthy controls. Sub-network nodes are shown in Figure 3.7. No significant difference was observed when the number of streamlines edge weight was applied.

Figure 3.7. Density of nodal connections across four-centres

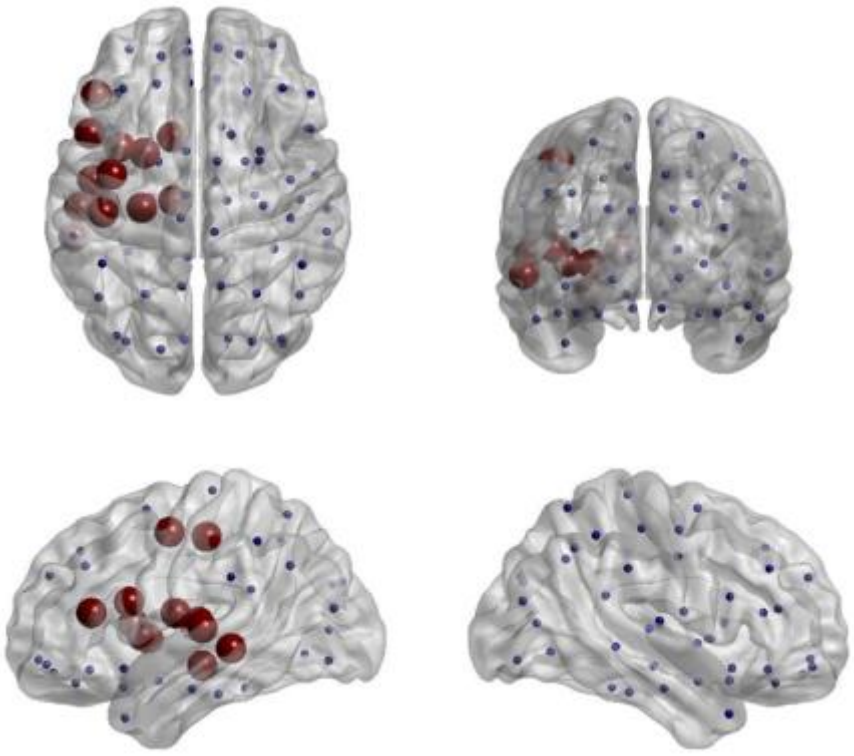

Figure 3.7 Legend. Group differences in connected components using FA connection weight. The results of the sub-network analysis show a topological cluster of connected regions. Connected component composed of 16 edges and 13 nodes, with statistically significant p value<0.033.

Sub-network analysis across three-centres

Sub-network analysis identified two connected components that differed between groups, with one component that differed significantly. The network component highly overlapped with deficits identified in Sarrazin et al., 2014. Analysis of connected components revealed group differences of a left fronto-temporal component in BD compared to controls comprised of 13 nodes and 17 edges. This collection of regions is FWER corrected [p=0.001] [Figure 3.9; Table 3.23]. This left hemispheric component comprised of the frontal inferior operculum, frontal inferior triangularis, rolandic operculum, insula, caudate, putamen, thalamus, hippocampus, Heschl's gyrus, middle and superior temporal gyri, and pre and post central gyri. These included inferior frontal and temporal connections.

Network differences using FA edge weight indicate more subtle connectivity differences compared to streamline count among the same connections [Figure 3.8].

Figure 3.8. FA-weighted connected component differences across three-centres

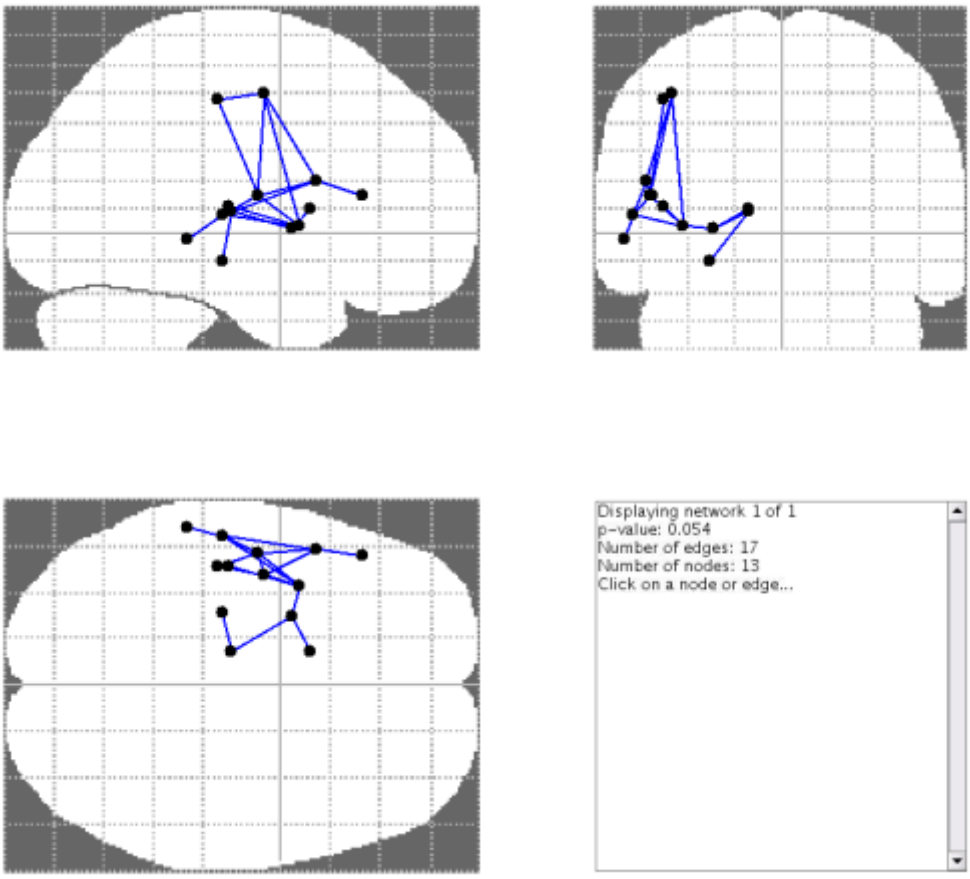

Figure 3.8 Legend. Statistically subtle effects identified between patients and controls using FA edge weight across three-centre participants. The sub-network differences show a connected component that is more weakly connected in patients compared to healthy controls. Weak inter-connections are denoted by the blue links.

Figure 3.9. Streamline-weighted connected component differences across three-centres

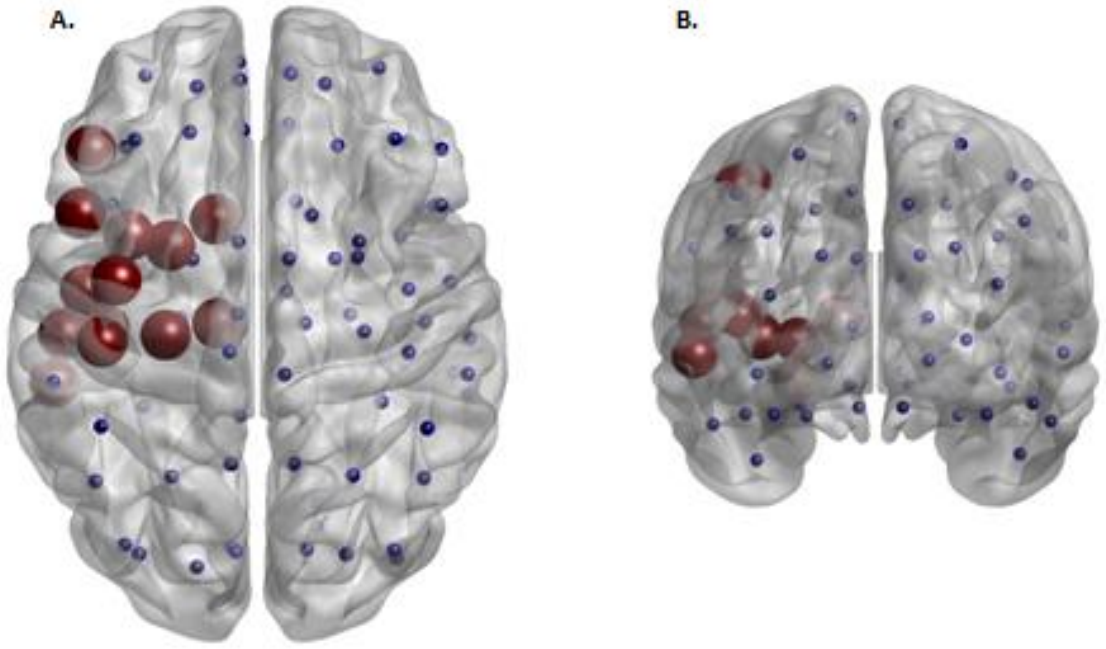

Figure 3.9 Legend. Inferior frontal and temporal connections were identified in the connected component which statistically differed between patients and controls defined by the number of streamlines.

Table 3.23. Magnitude of edge-weight connections compared across four and three centres

Supra-threshold connections >2	**Four Centre** Component p=0.021 Test Statistic	**Three Centre** Component p=0.001 Test Statistic
Precentral Left to Inferior Frontal Gyrus, Opercular part Left	66.72	9.81
Inferior Frontal Gyrus, Opercular Part Left to Inferior Frontal Gyrus, Triangularis Left	50.75	11.42
Precentral Left to Rolandic Operculum Left.	67.47	3.05
Inferior Frontal Gyrus, Opercular Part Left to Rolandic Operculum Left	55.41	6.33
Rolandic Operculum Left to Insula Left	71.40	4.39
Precentral Left to Postcentral Left	58.53	10.36
Rolandic Operculum Left to Postcentral Left	33.21	3.58
Insula Left to Putamen Left	70.17	14.03
Caudate Left to Putamen Left	78.95	17.13
Hippocampus Left to Thalamus Left	32.76	2.84
Putamen Left to Thalamus Left	65.47	12.32
Insula Left to Heschl Gyrus Left	39.59	4.74
Inferior Frontal Gyrus, Opercular Part Left to Superior Temporal Gyrus Left	28.90	2.10
Rolandic Operculum Left to Superior Temporal Gyrus Left	39.18	2.42
Insula Left to Superior Temporal Gyrus Left	58.46	2.20
Superior Temporal Left to Middle Temporal Gyrus Left	41.90	4.62

Table 3.23 Legend. The strongest magnitude of edge weights was identified in both supra-threshold connections greater than two. The number of streamlines edge weights were strongest in connections of the caudate to putamen, insula to putamen, putamen to thalamus, and the inferior frontal operculum to the inferior frontal triangularis. The greatest consistency in magnitude of connectivity is shown within the connections between the insula and putamen, and caudate and putamen.

History of Psychotic Features

Additionally, connected component differences were assessed between patients with a positive history of psychotic features and patients with an absent history of psychotic features. This analysis was completed for both FA and streamline count connection weights. Previously in the three-centre study Sarrazin and colleagues reported differences in FA when they assessed differences in patients with and without a history of psychotic features(Sarrazin et al. 2014). Across the multi-centre investigations, a post-hoc analysis compared patients with a positive history of psychotic features with patients without psychotic feature, with no observed differences between groups.

History of Psychotic Features in the Four-Centre Study

In the four-centre investigation, the post-hoc test comparing patients with psychotic features and healthy controls show no significant effects within a sub-set of the original component differences. Similarly, a post-hoc test displayed sub-network differences in patients without psychotic features compared with controls within a sub-set of the between group sub-network. [Figure 3.10-3.13]. In addition, when we compared connected components between patients without psychotic features and healthy controls differences were observed. Patients without psychotic features showed differences in connected components with an additional node included in the component. This encompassed 14 nodes and 18 edges; additionally involving the left supramarginal gyrus($p<0.031$)[Figure 3.12].

Figure 3.10. FA-weighted connected components in patients with psychotic features compared with patients without psychotic features

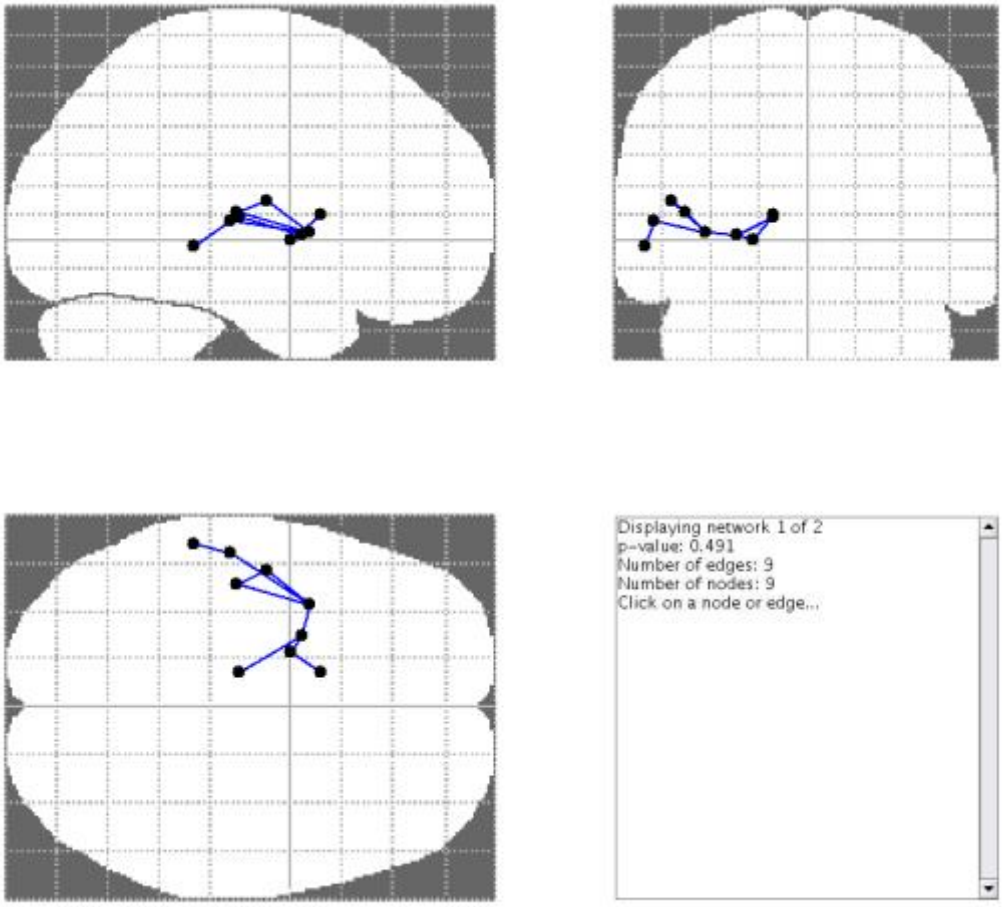

Figure 3.10 Legend. Inter-connections are denoted by the blue links. No differences were observed between patients with a positive history of psychotic features and patients with an absent history of psychotic features using FA connection weight, however the nodes included in the non-significant component form a subset of the overall comparison. These nodes comprised of the left caudate, pallidum, thalamus, putamen, insula, Heschl's gyrus, rolandic operculum, superior and middle temporal gyri.

Figure 3.11. FA-weighted connected component differences between patients without psychotic features and healthy controls

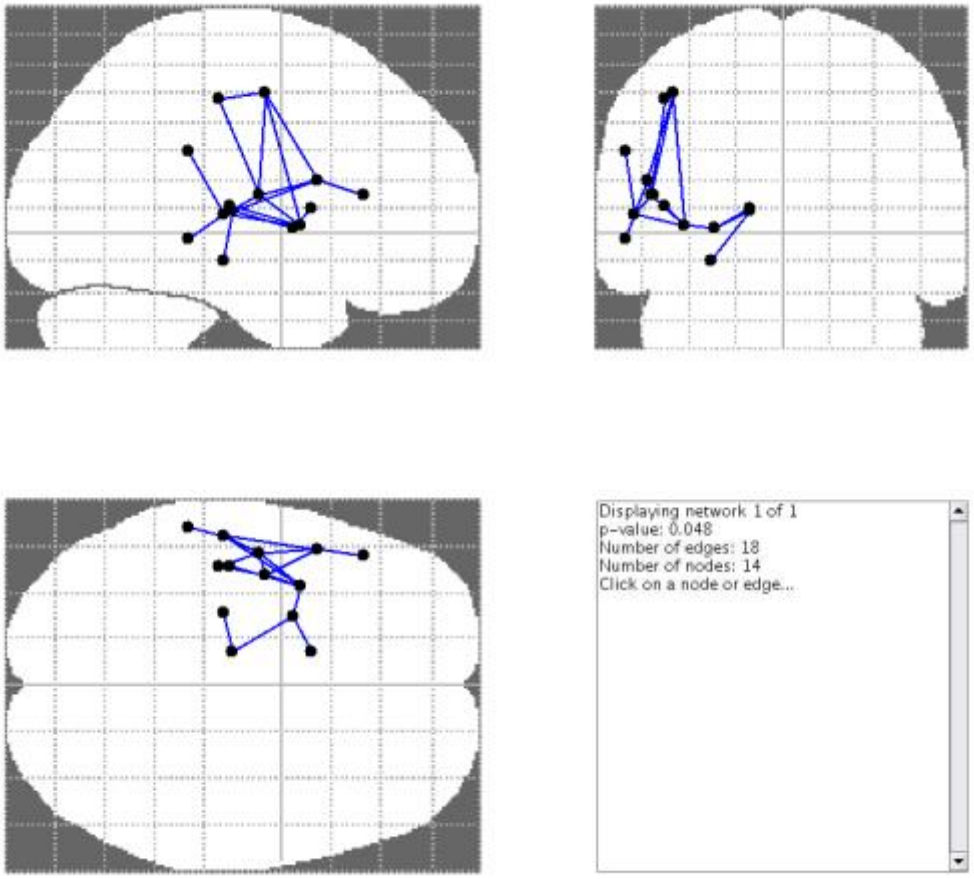

Figure 3.11 Legend. Patients without psychotic features display an altered component within fronto-temporal connections, with additional recruitment of the left supramarginal gyrus.

Figure 3.12. Streamline-weighted component differences between patients without psychotic features compared with healthy controls

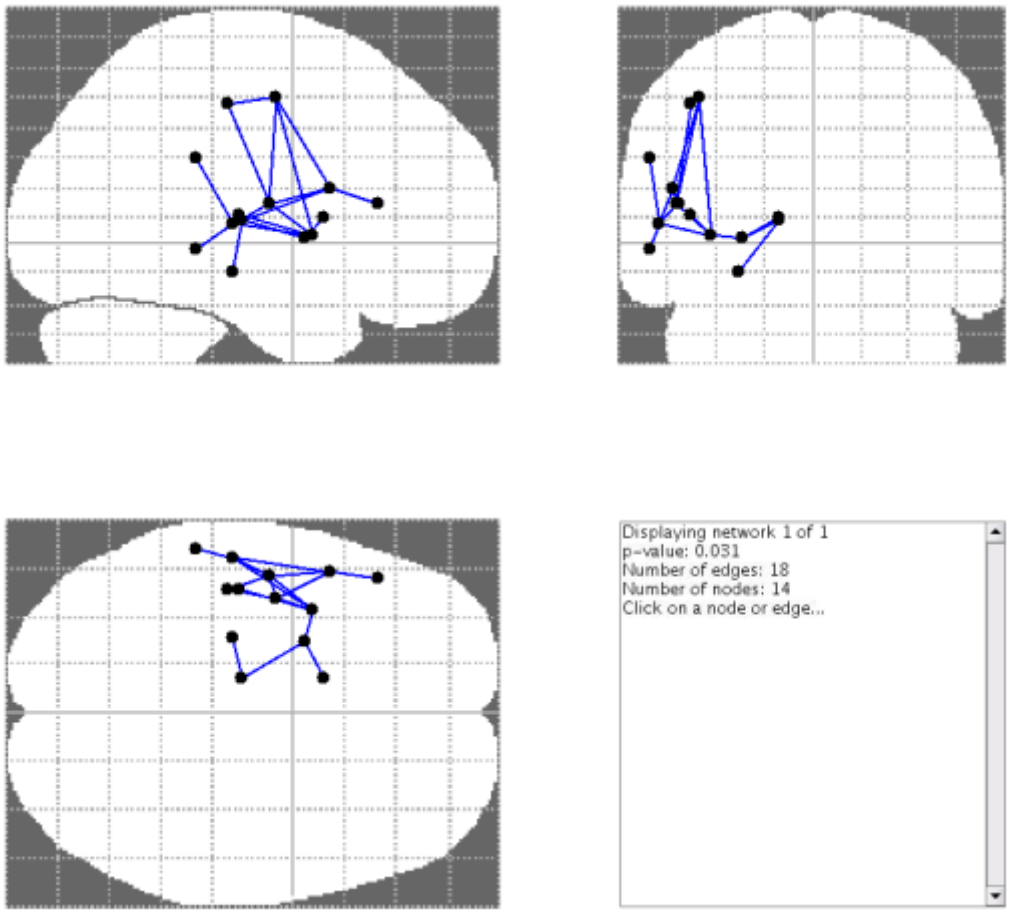

Figure 3.12 Legend. Patients without psychotic features indicate inclusion of the left supramarginal gyrus in this reduced sub-network.

We further investigated whether there were differences between patients with psychotic features and healthy controls.

Figure 3.13. FA-weighted component differences between patients with psychotic features and healthy controls

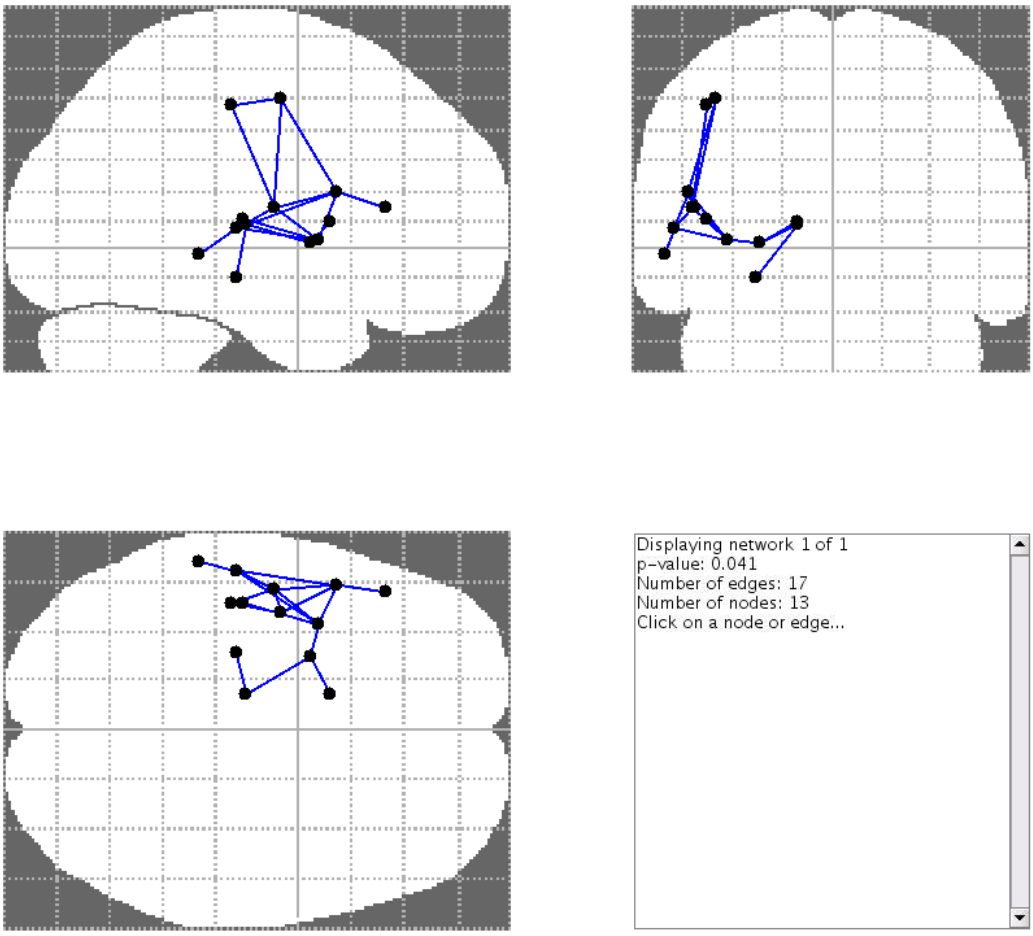

Figure 3.13 Legend. Patients with psychotic features display reduced connectivity compared to healthy controls.

Figure 3.14. Streamline-weighted component differences between patients with psychotic features and healthy controls

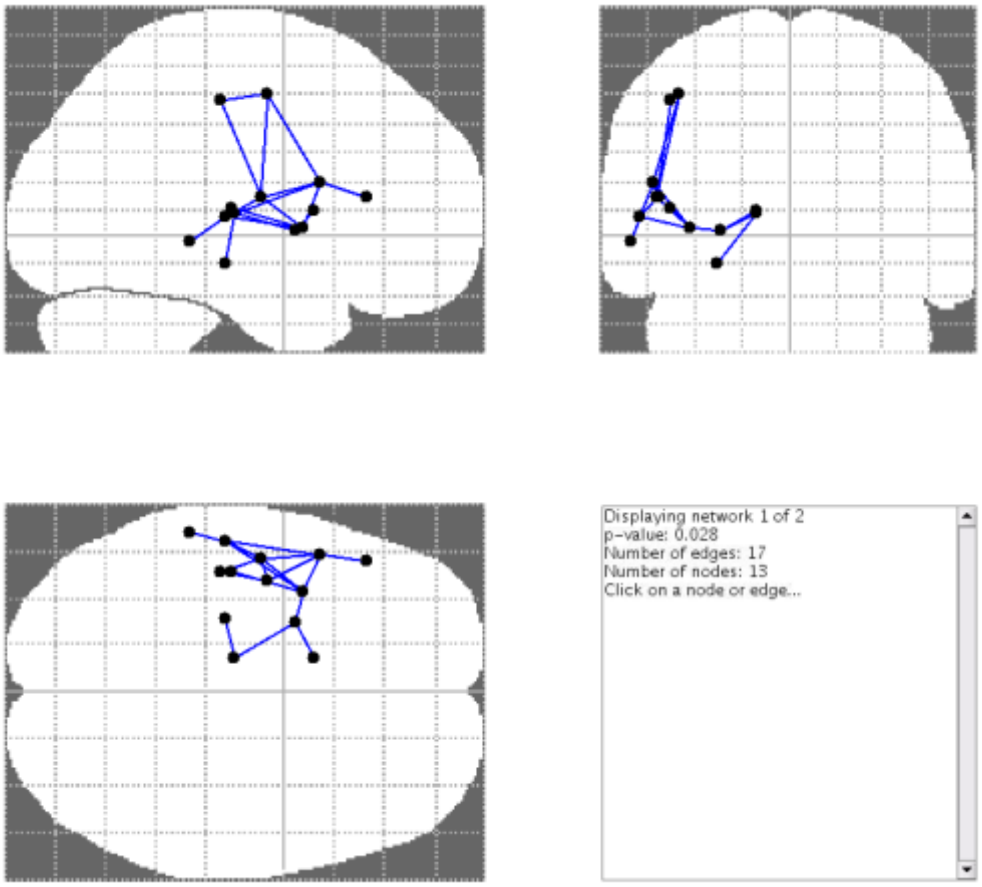

Figure 3.14 Legend. Connections weighted by number of streamlines indicated connected component differences between patients with psychotic features compared to healthy controls ($p<0.028$). This sub-network component comprised of the 13 nodes and 17 edges.

History of Psychotic Features in the Three-Centre Study

Figure 3.15. FA-weighted connected components in patients with and without psychotic features

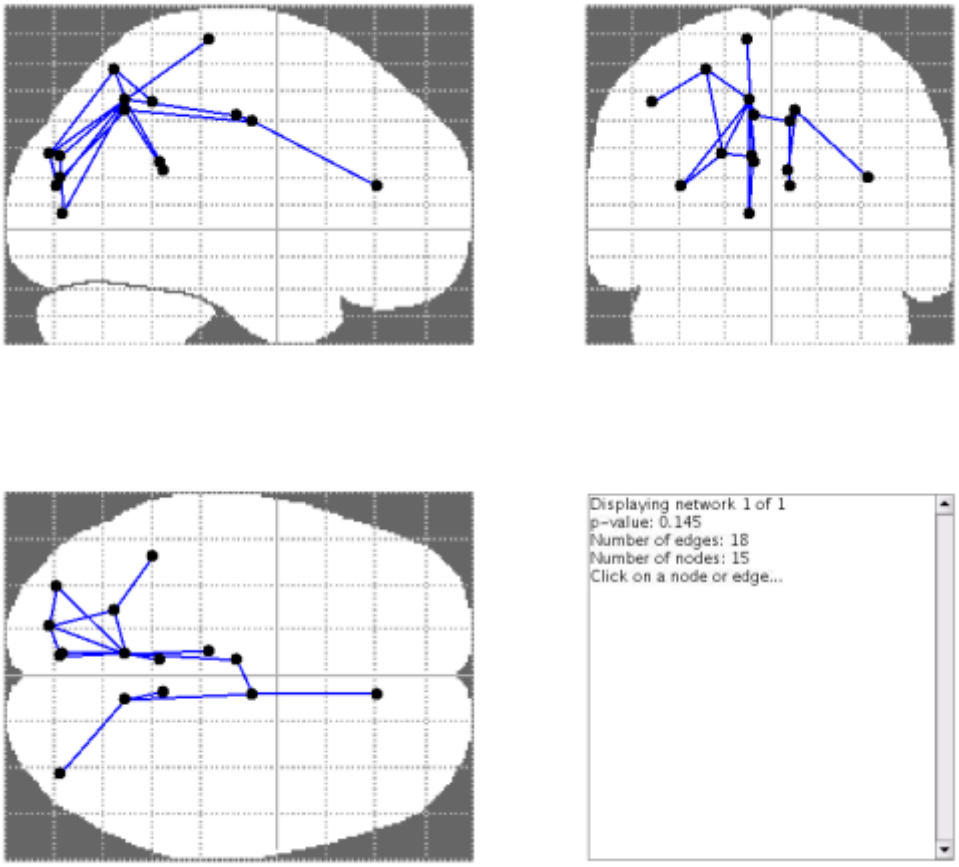

Figure 3.15 Legend. Components did not differ between patients with and without psychotic features, however sub-network identified show collected connections between posterior-limbic and parieto-occipital connections. This component of 15 nodes and 18 edges comprised of the following nodes: right anterior cingulate gyrus, bilateral middle cingulate gyri, left paracentral lobule, bilateral posterior cingulate gyri, right precuneus, bilateral middle occipital gyri, left cuneus, left precuneus, left calcarine, left superior occipital gyrus, left superior parietal, left inferior parietal lobule.

Figure 3.16. Streamline-weighted components in patients with and without psychotic features

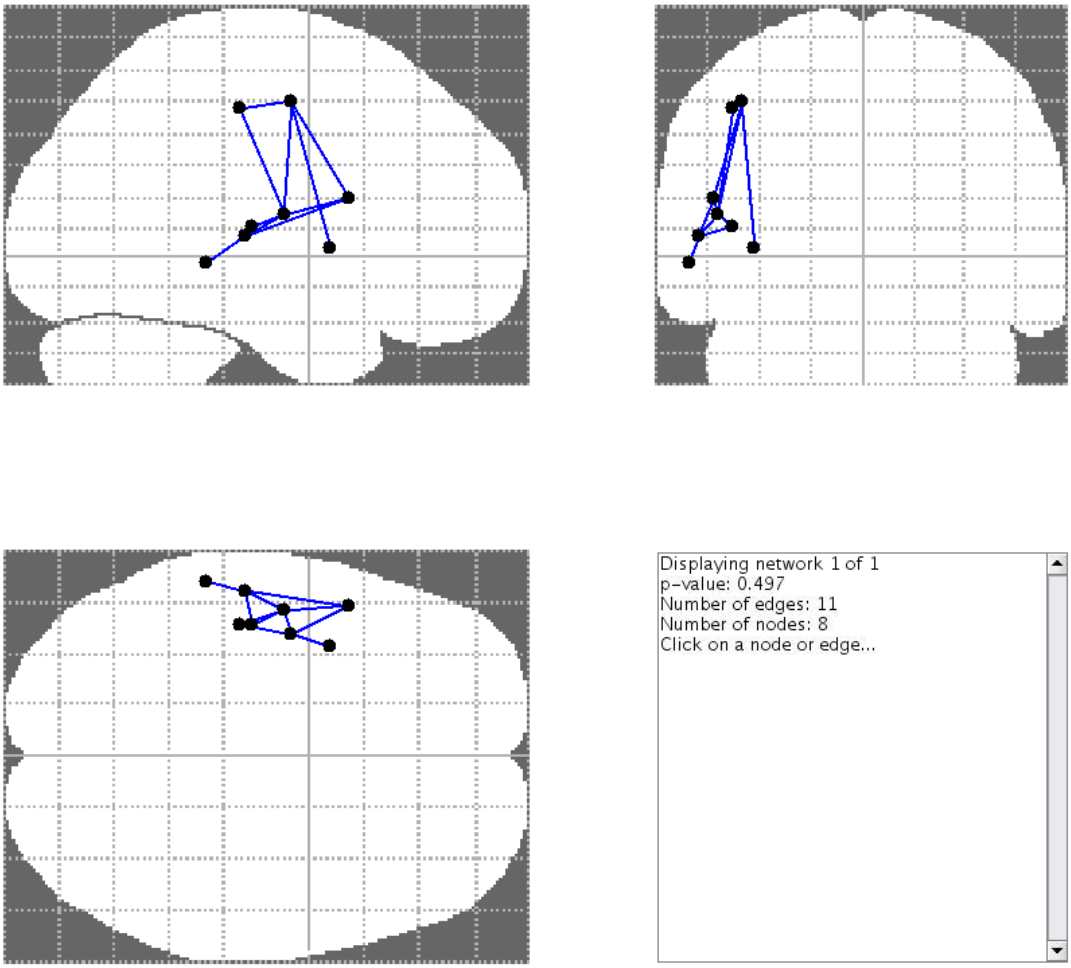

Figure 3.16 Legend. No significant differences were observed within the sub-network component using streamline count as the edge weight.

No further differences were observed in the three centre investigation between patients with psychotic features and healthy controls and patients without psychotic features compared with healthy controls.

Finally, we present a rich-club analysis investigating a sub-network of nodes that are rich in connections and densely inter-connected forming a club.

Normalized rich-club connections and rich-club membership

Results of rich-club analysis in the Galway Bipolar Study

Weighted rich-club connections ranged across *k* values of 27-64, while the weighted and normalized rich-club connections ranged across *k* values of 28-56. The rich-club connectivity effects were significant for *k* density values 55 and 56 before FDR multiple comparison correction (k=55, Z=-2.236, p=0.024; k=56, Z=-2.654, p=0.0067). After FDR correction for 28 possible densities, k=56 demonstrated a moderate to large effect size (Cohen's d=0.59).

Figure 3.17. Rich-club organization in patients and controls in GBS study

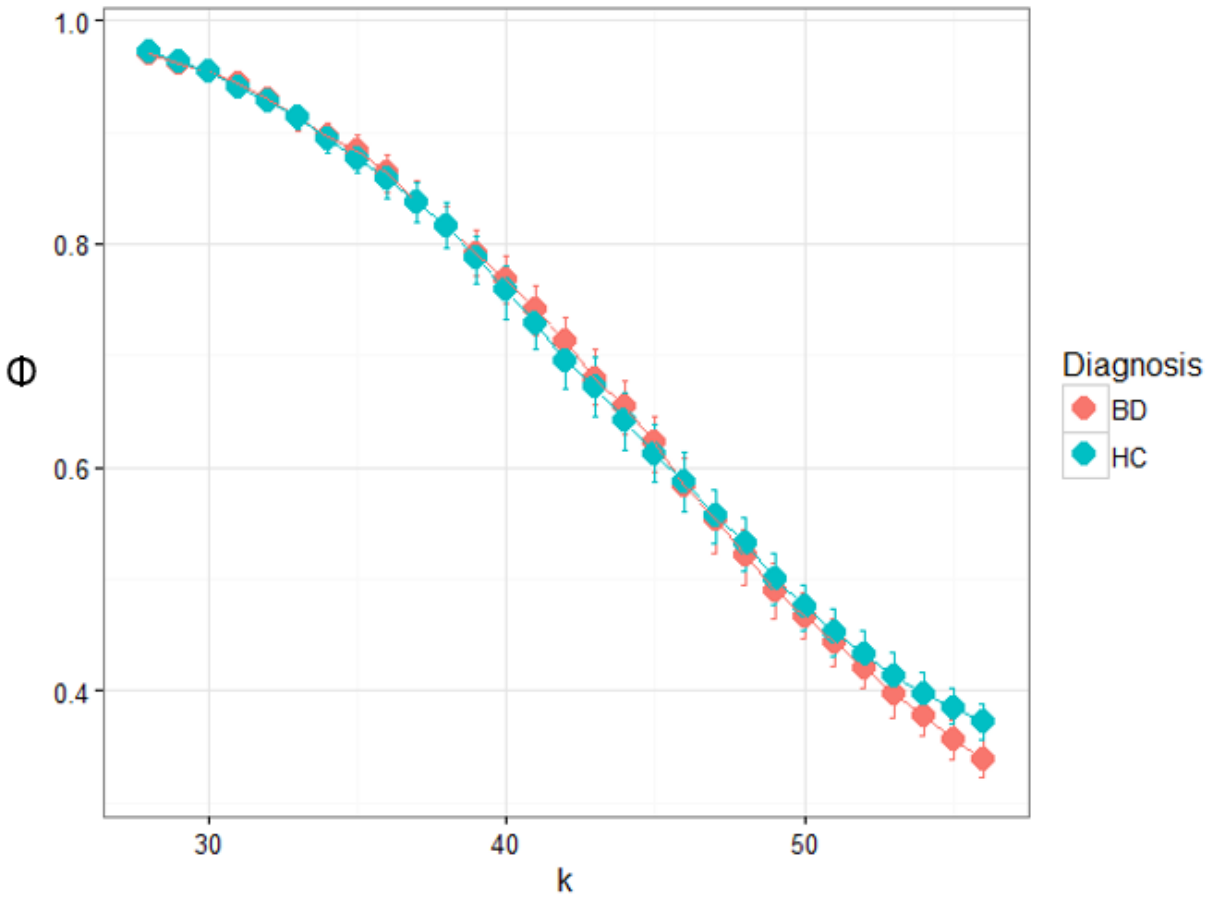

Figure 3.17 Legend. Rich-club density values shown across *k* densities 28-56 indicate BD patients have reduced rich-club connectivity compared to controls at *k* 56. Rich-club connectivity differences are reported above at k density 56 with bars representing 95% confidence interval.

Figure 3.18. Frequency of participants with rich-club organization

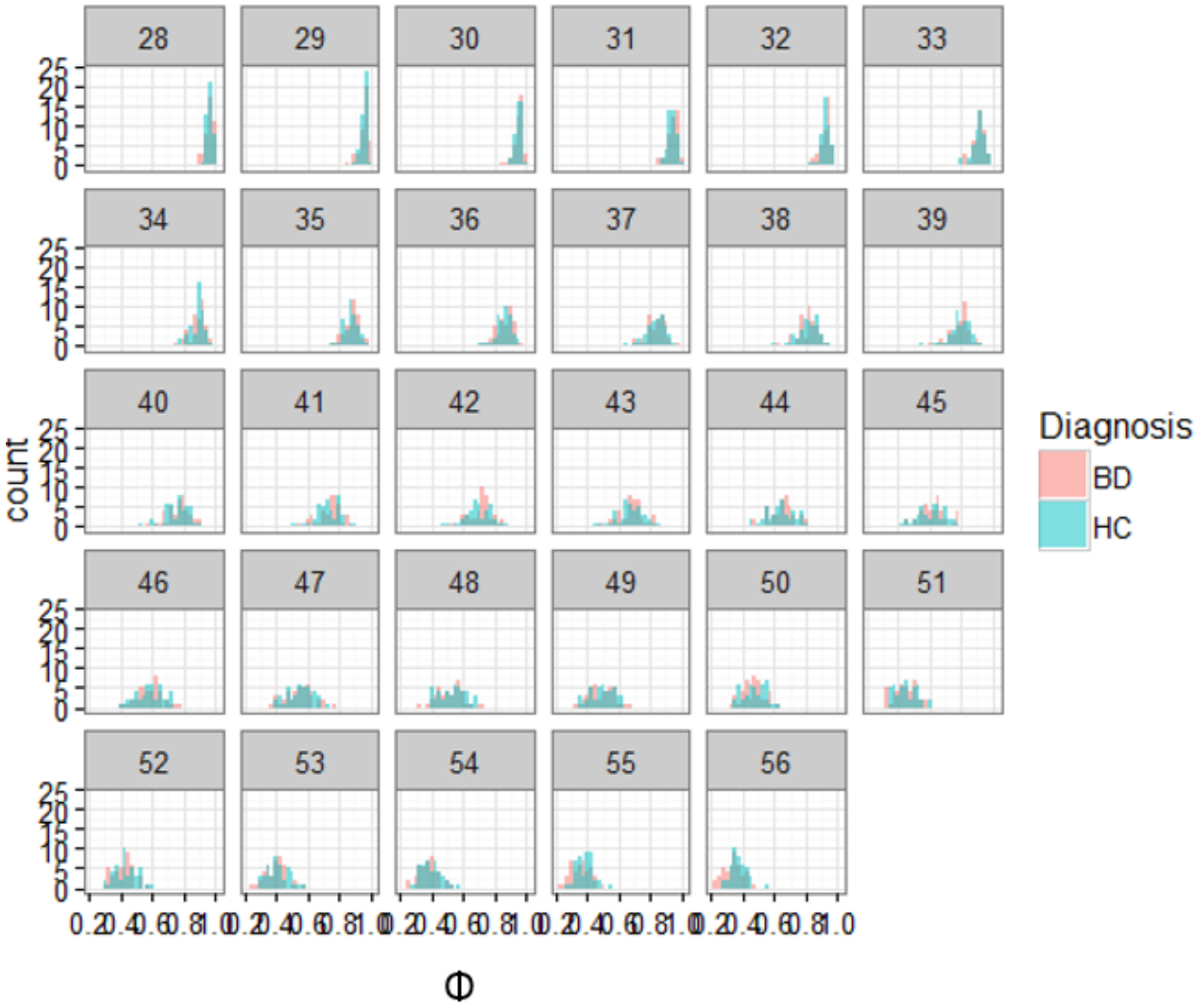

Figure 3.18 Legend. This demonstrates the frequency of participants across the 28 possible rich club densities *k* 28-56. The BD group in red show lower values of rich-club Φ across the range of *k* compared with the healthy control group in blue.

Results of rich-club membership of Galway Bipolar Study

Next, rich-club membership was assessed to determine if rich-club structures were differentially affected between groups. Rich-club membership was defined by the statistically significant pathway (Z=-2.654, p=0.0067) common to more than 60% of participants [Figure 3.17]. This analysis revealed the rich-club members connected by this pathway.

Additionally, analysis was repeated for the statistically significant pathway for 70% or more of participants [Figure 3.20]. Rich-club structures common to 60% of participants revealed the following hubs: superior frontal gyrus, middle cingulate gyrus, hippocampus, caudate, precuneus and thalamus [Figure 3.19]. Validation of rich-club nodes in this analysis also comprise the top 10 highest degree of nodes and top 12% of nodes(Collin et al. 2014; van den Heuvel & Sporns 2011). Rich-club membership differences between patients and controls are depicted in Figure 3.19 & 3.20.

Figure 3.19. Rich-Club Membership in participants of the Galway Bipolar Study

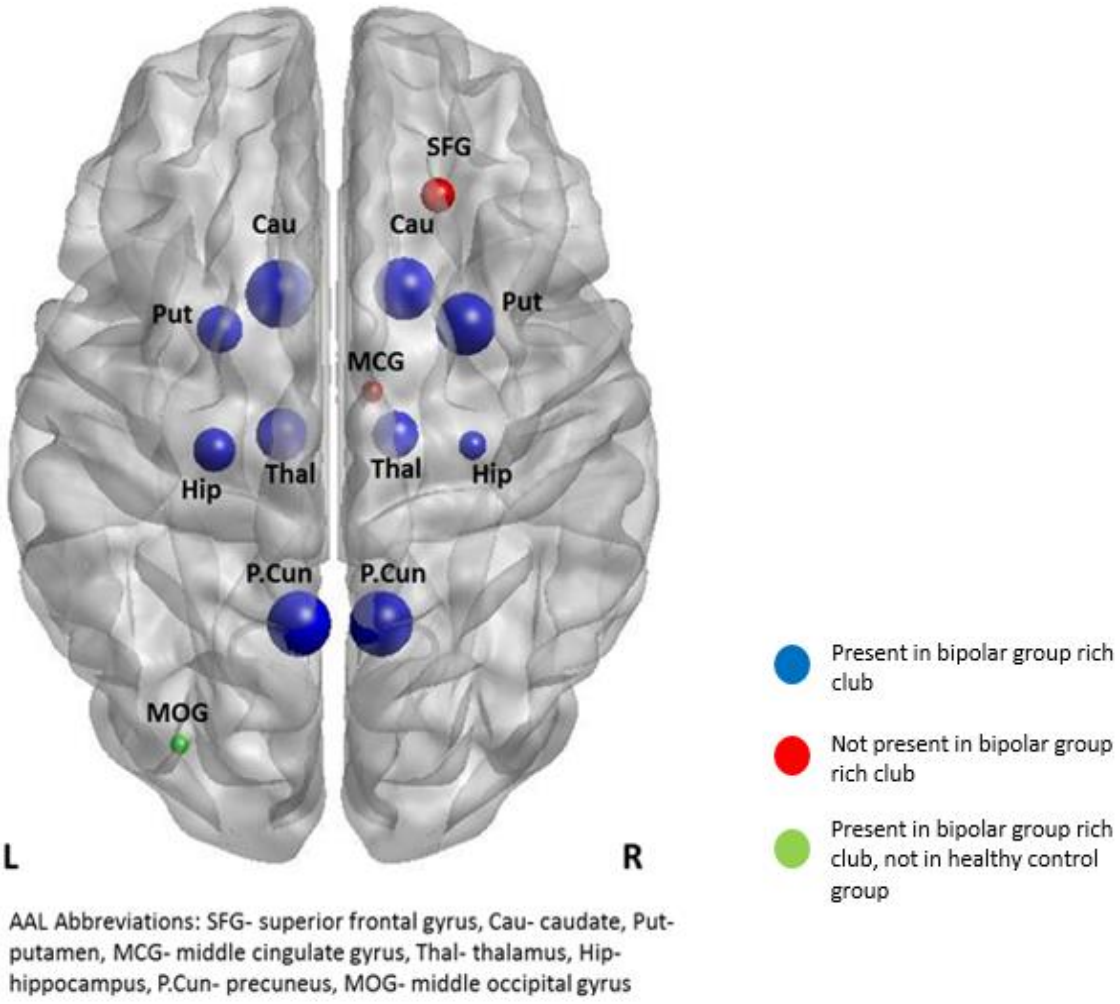

Figure 3.19 Legend. Nodes in blue and red were present in healthy control rich-club members, nodes in red were not present in the BD group rich-club, however the node in green was recruited in the BD rich-club and not present in HC rich-club.

Figure 3.20. Consistent rich-club membership differences in Galway Bipolar Study

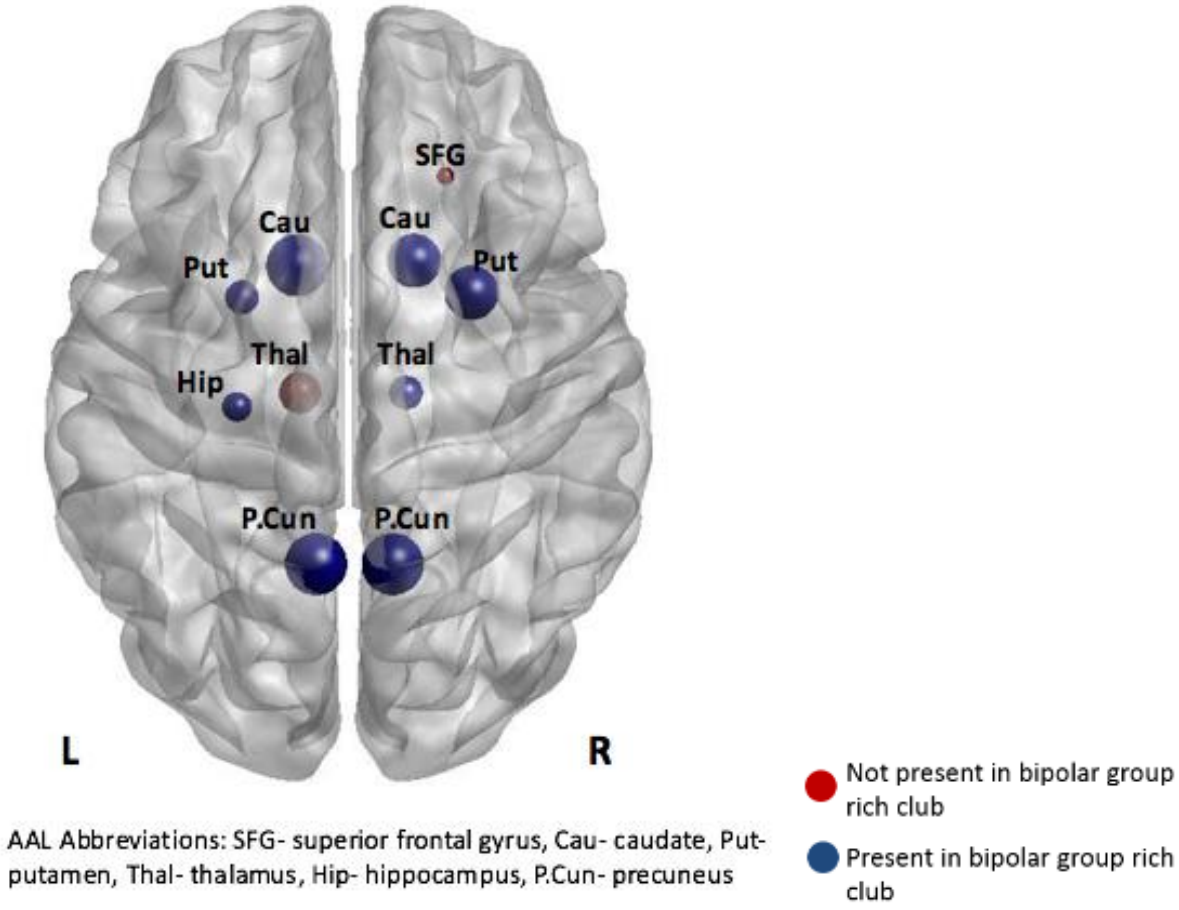

Figure 3.20 Legend. Rich-club membership at 70% most common pathway at rich-club density.

Rich-club membership in the bipolar group at group threshold 60% indicates the right frontal superior gyrus and right middle cingulate gyrus were not recruited, but the patients recruited the left middle occipital gyrus. Additionally, when the threshold was increased to 70%, the most notable differences include the absence of the right superior frontal gyrus and left thalamus as hubs in the bipolar patient group rich-club network compared to healthy volunteers, and in addition the left middle occipital gyrus was no longer recruited in patients (Figure 3.20). Of note, dysconnections identified by the network based statistics analysis above overlap with rich-club members, namely left hippocampus, precuneus and thalamus at the highest supra-threshold connections.

Taken together, the rich-club coefficient revealed trend-level connectivity effects as well as rich-club membership differences between groups.

Results of rich-club analysis across a four-centre study

Rich-club connections

Rich-club connectivity was assessed through the number of streamlines connection map, as definition of the rich-club membership examines connectivity deficits based on density of connections determined from the number of connections through a structure. Normalized rich club connectivity was investigated determining a rich-club regime across a range of *k* densities between *k* 21-*k*30. Across the range of *k* densities significant differences between Φ, the rich-club coefficient detected differences between groups across all ranges of *k*, however when adjusted for multiple comparisons, findings were no longer significant.

Figure 3.21. Rich-club organization across four-centres

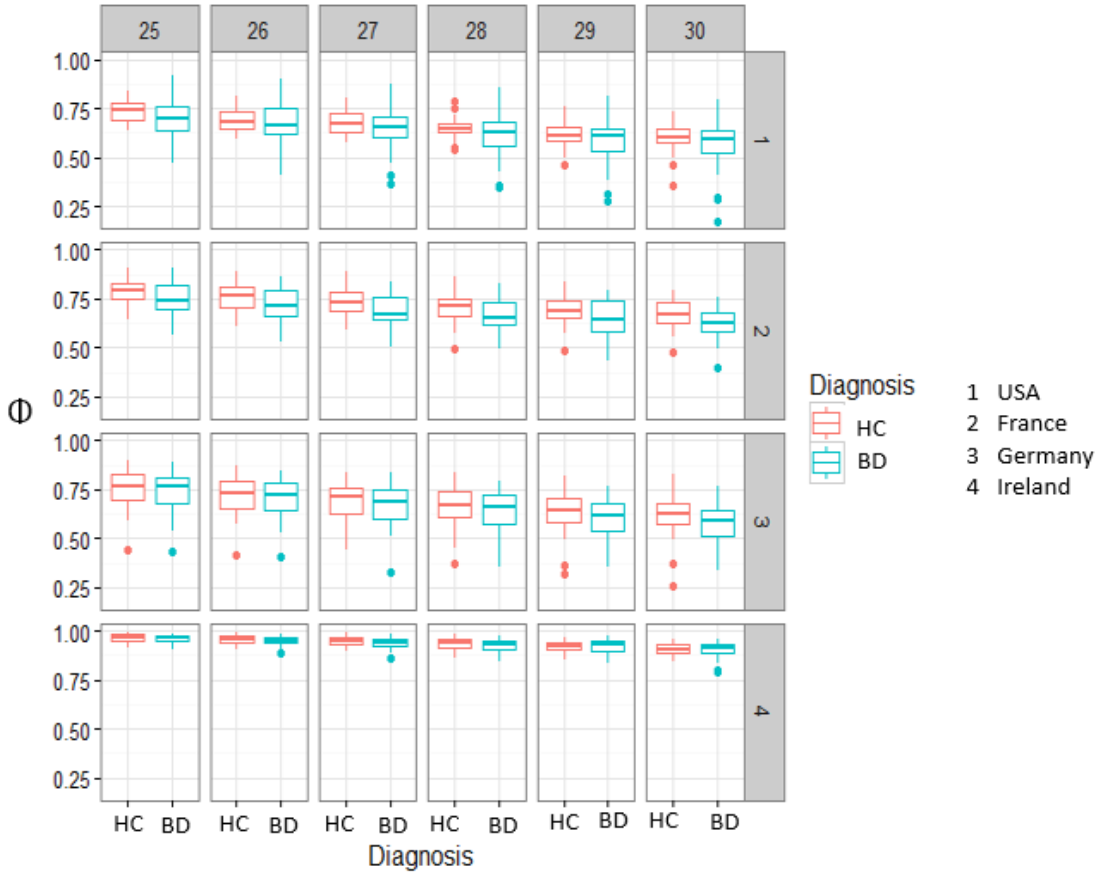

Figure 3.21 Legend. The four rows represent each research centre (1) USA, (2) France, (3) Germany, and (4) Ireland. The five colums represent higher values of rich club density *k*, and the y-axis shows the rich-club coefficient Φ which represents the level of inter-connectivity between the rich-club structures. At the top 5 highest rich-club density values, patients with BD are represented in blue and the HC group are represented in red. There is a consistent reduction between groups across values of k.

Figure 3.22. Rich-club organization defined by diagnosis and research centre

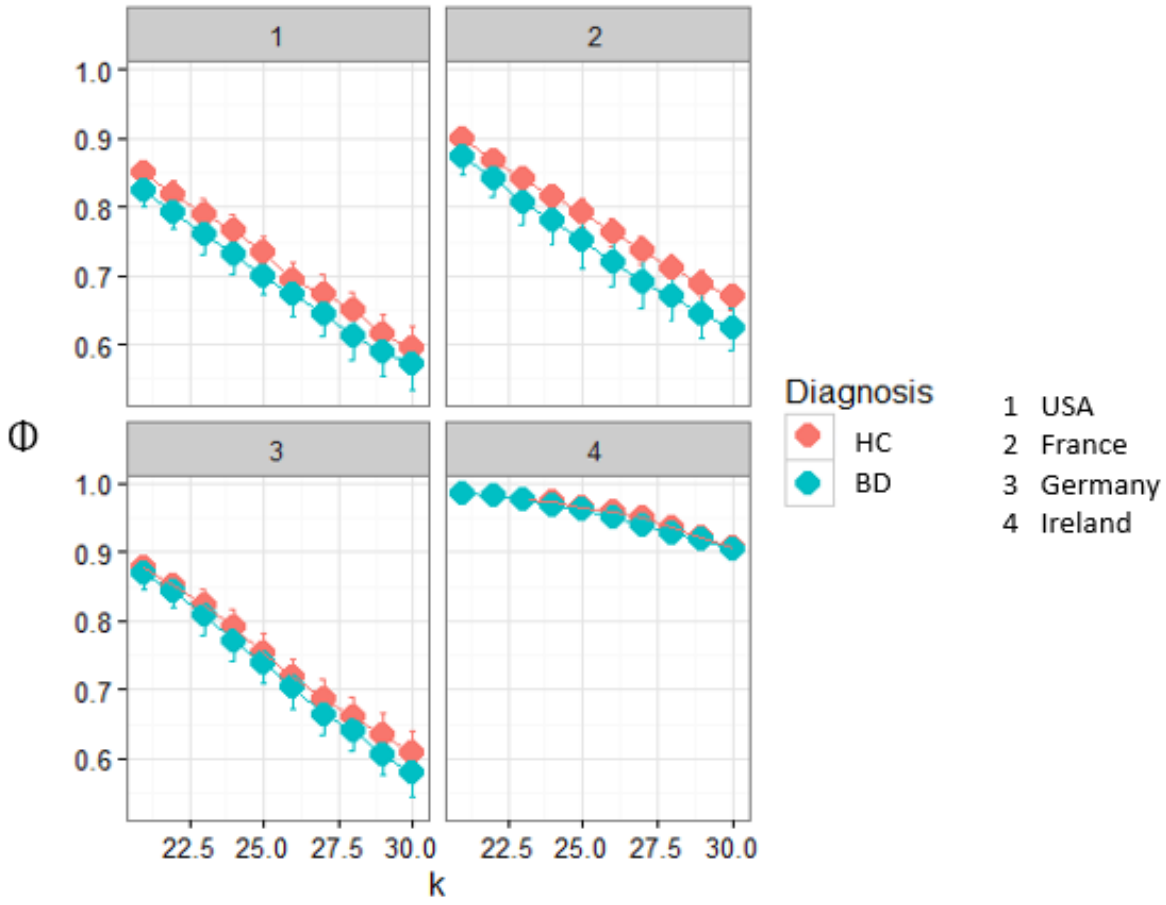

Figure 3.22 Legend. Additionally, this graph presents the rich-club coefficient for Φ and *k*. The four panels represent each research centre (1) USA, (2) France, (3) Germany, and (4) Ireland. The x-axis represent higher values of rich club density *k*, and the y-axis shows the rich-club coefficient Φ which represents the level of inter-connectivity between the rich-club structures. At the top 5 highest rich-club density values, patients with BD are represented in blue and the HC group are represented in red. This figure shows the similar relationship in rich club reductions in the three international centres with identical scanner model and protocol, while the Galway dataset demonstrates a similar reduction but at a different density level and weaker extent of connectivity.

Figure 3.23. Frequency of participants with rich-club organization across four-centres

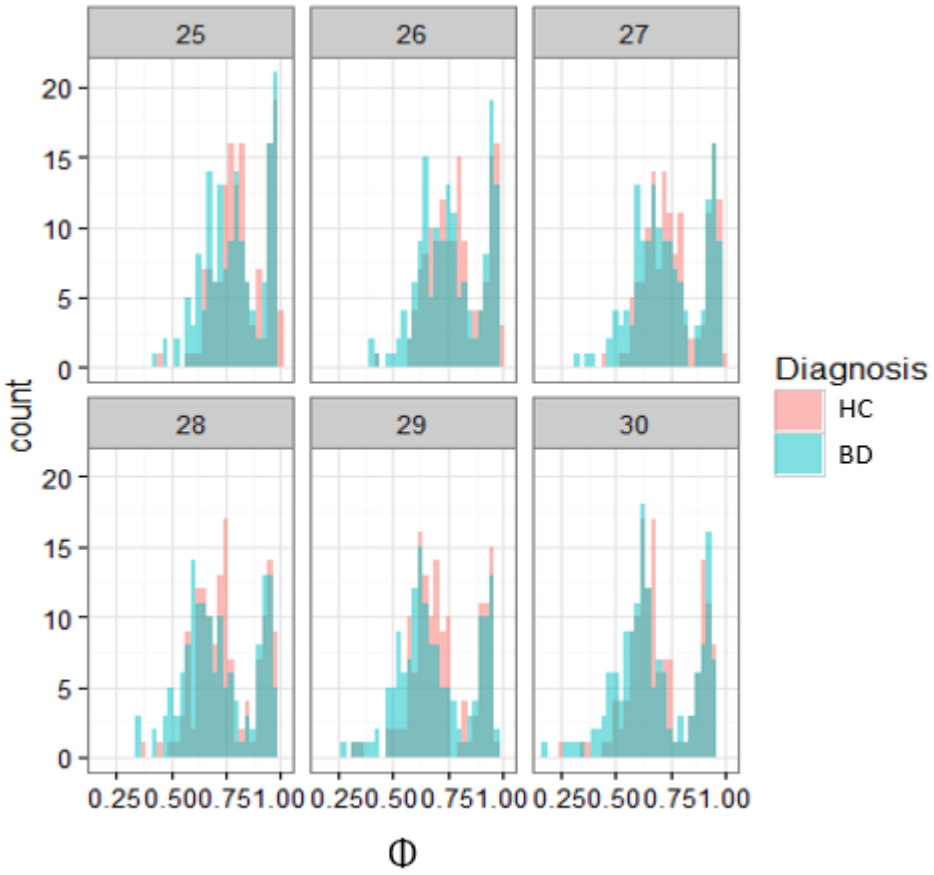

Figure 3.23 Legend. Here we report the frequency of participants according to rich club level Φ among high density values *k*. On average there is a greater propensity for the BD group to display lower values of Φ.

Rich-club membership across four-centres

Rich-club membership was defined as pathways connecting rich-club structures at *k* density > 25. The common pathway across 60% of participants was identified when connections were present in over 90 participants in patients and healthy controls.

Figure 3.24. Rich-club membership across four-centres

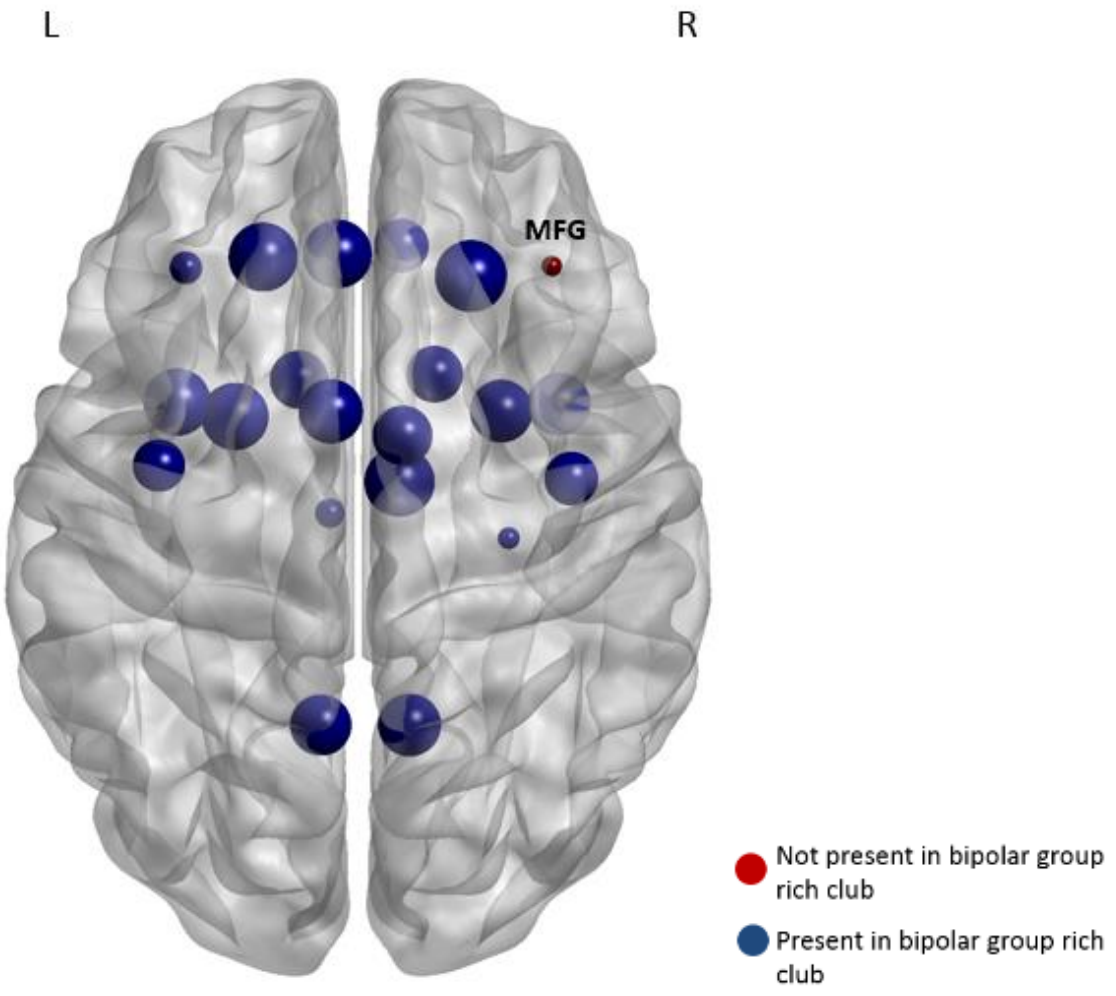

Figure 3.24 Legend. Rich-club membership evaluating rich-club structures connected by pathway *k* 21 common to 60% of participants reveals one membership difference, in which the right middle frontal gyrus is present in healthy controls and absent in patients.

Results of rich-club analysis across three-centres

Rich-club connections

A rich-club analysis was then implemented to investigate rich-club phenomenon in this largely powered study. Research centre was considered a factor with 3 levels, for each research centre. Participants report a different slope in *k* appeared to be differentiated by research centre. Then, we modeled *k* to vary by site. Predictors were then added to the random model, where *k* appears to have a direct effect on Φ. When we examine the interaction between k and diagnosis we see the biggest interaction. Therefore, our effect of *k* depends on diagnosis. Site effects did not explain the diagnosis effect, where Φ changes across levels of *k* depending on diagnosis.

Figure 3.25. Rich-club connectivity by diagnosis and research centre

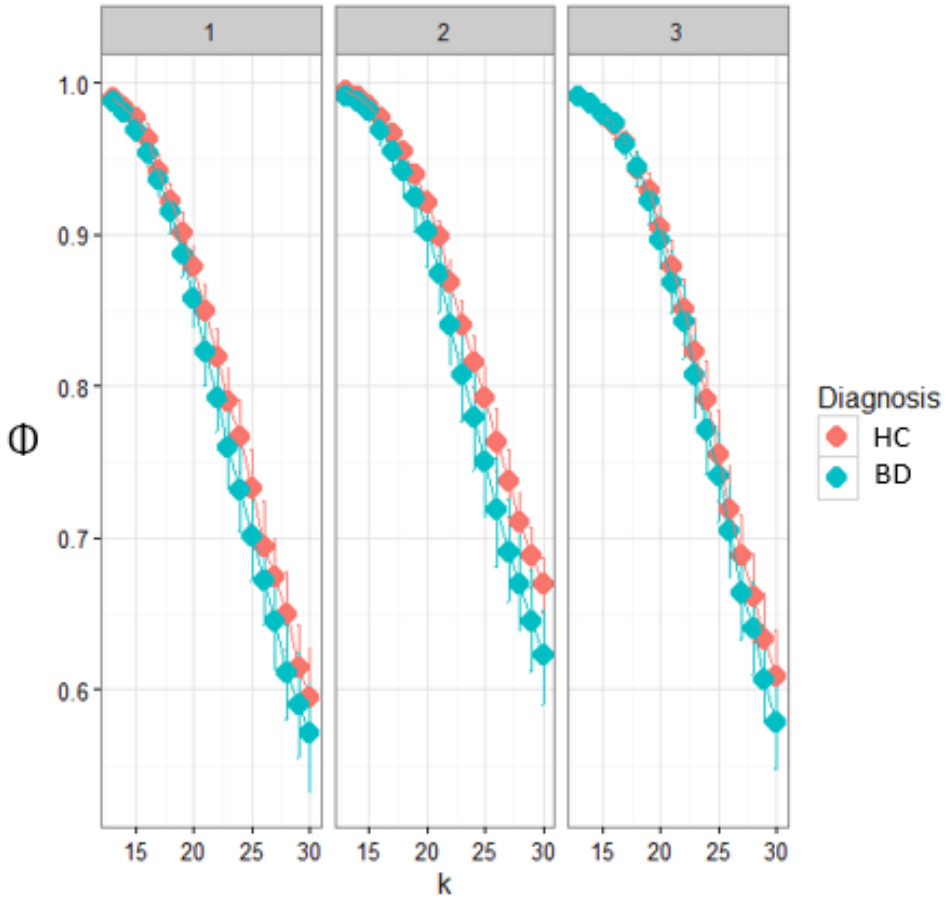

Figure 3.25. Legend. Rich-club coefficient across high values of *k* density defined by research centre. Additionally, this graph presents the rich-club coefficient for Φ and *k*. The 3 colums represent each research centre (1) USA, (2) France, (3) Germany. The x-axis represents higher values of rich club density *k*, and the y-axis shows the rich-club coefficient Φ which represents the level of inter-connectivity between the rich-club structures. Across the range of rich-club density values, patients with BD are represented in blue and the HC group are represented in red.

Figure 3.26. Frequency of participants rich-club connectivity at high density k values

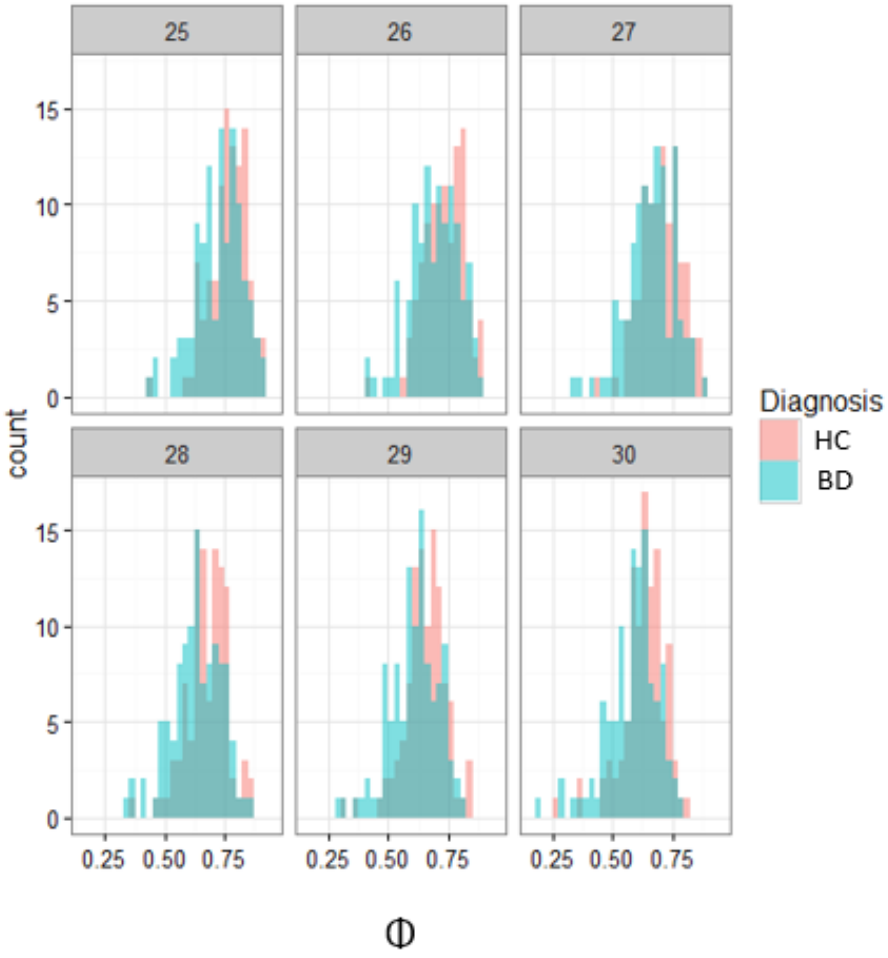

Figure 3.26 Legend. Frequency shows most patients with BD exhibit lower Φ across values *k* compared to controls.

A normalized rich-club at *k* densities 13-30 was revealed in this analysis. A linear mixed model analysis was implemented in R software to determine a between group difference. With multiple comparison correction, this analysis identified a range of rich-club densities which statistically differed between groups. These findings withstand multiple comparison correction $p<0.001$.

Rich-club membership across three-centres

Rich Club membership of this analysis indicates rich-club recruitment differed between groups among the right middle frontal gyrus, and the left hippocampus at 60% participant threshold.

Figure 3.27. Rich-club membership across three-centres

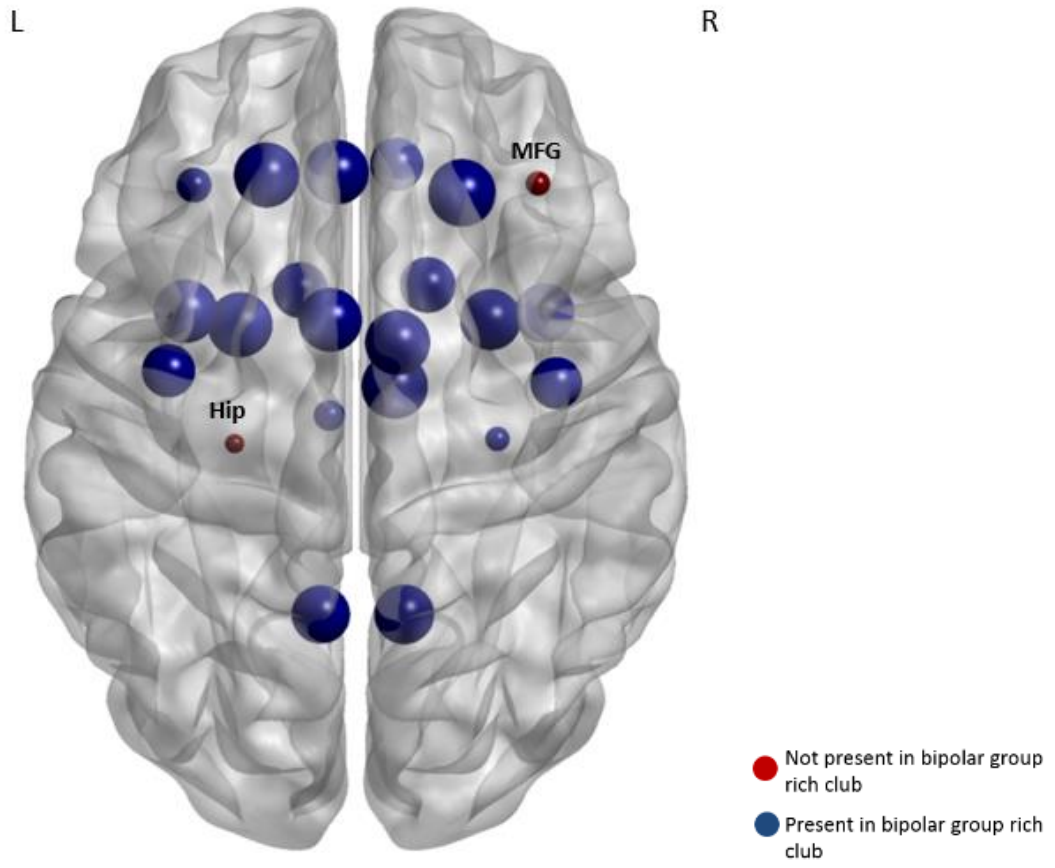

Figure 3.27 Legend. Rich-club membership indicates the right middle frontal gyrus and left hippocampus are present in healthy controls and absent in patients with BD.

Summary of the main findings

In this chapter, dysconnectivity was investigated through three methodological approaches. In general, patients with BD had substantial abnormalities in global integration characterized by longer characteristic path length compared with healthy controls. Global connectivity patterns in the Galway Bipolar Study findings point to longer characteristic path length, reduced global efficiency and reduced mean clustering, as features of BD. When the re-analysed Galway Bipolar Study cohort was included in the four-centre analysis, patients with BD displayed longer characteristic path length, reduced global efficiency and clustering compared with healthy controls. When the investigation was restricted across three centres, longer characteristic path length was a consistent feature of impaired global integration in patients with BD.

Converging results from analysis of regions based on predefined nodes across the Galway Bipolar Study and four-centre study indicate segregation is impaired in frontal, limbic and parieto-occipital regions when assessed by clustering and local efficiency properties in BD compared with healthy controls. Segregation of the left middle cingulate gyrus was impaired in patients when assessed with local efficiency and clustering coefficient measures using both FA and streamline count connection weights. Taken together, the BD group displayed reduced properties of segregation in frontal, limbic and parietal regions.

In the second methodological approach, sub-networks appear to be more weakly connected in BD when FA was employed as the connection weight across cohorts the Galway Bipolar Study and study across four-centres. Within the Galway Bipolar Study patients, sub-networks were more weakly connected across posterior parietal and occipital connections when examined at

higher connection thresholds. When sub-networks were examined at lower density thresholds, fronto-limbic dysconnectivity was affected bilaterally in the BD group. In the four and three centre investigations, sub-networks were predominantly impaired within left fronto-temporal circuitry.

In the third methodological approach, rich-club connectivity and structural membership differences were investigated in patients BD compared with healthy controls. We identified subtle connectivity differences between patients and controls in the Galway Bipolar Study cohort. When the re-analysed Galway data was included with the four-centre study, similarly the reduced density in patients did not withstand correction for multiple testing. When rich-club connectivity was assessed in the three centre study, there were statistically significant reductions in connectivity across a range of rich-club densities between patients and controls.

In addition to testing for differences in rich-club connectivity, another facet to the rich-club analysis was to investigate differences in structures involved in rich-club membership. Across each dataset, differential hub involvement was evident in regions participating in the patient and healthy control rich-clubs. In the Galway Bipolar Study, the superior frontal gyrus was present in rich-club members in healthy controls, however was absent in the patients' rich-club. The left middle occipital gyrus was additionally included in the patient group rich-club, but not present in the healthy control group. When the Galway study data was re-analysed and combined with the four-centre study, the rich-club membership also showed differential rich-club membership, as the patients' rich-club membership did not include the right middle frontal gyrus. Within the three-centre study, patients' rich-club membership did not include the right middle frontal gyrus and left hippocampus, as was present in healthy controls. In contrast to the three-centre

investigation, the left hippocampus was not a participating rich-club structure in either healthy participants or patients in the study across four centres. Finally, no differences were detected between graph measures in the patient groups and psychotropic medications, illness duration, and age of onset.

Chapter 4

Discussion

This chapter summarizes the main results from each methodological approach to synthesize what the findings mean when taken together. This chapter then discusses how network findings tie with current models of BD. Finally, I explore the methodological considerations, challenges, and future recommendations.

Integration and Segregation

Global Dysconnectivity

The first aim of this research was to assess global and regional measures of integration and segregation as features of neuroanatomical dysconnectivity in BD. This study provides novel evidence of distributed neuroanatomical dysconnectivity, using graph theory metrics, as a trait based feature of BD. Across the cohorts with BD, impaired integration and segregation was identified in patients compared with controls indicating abnormal connectivity patterns in BD. In the Galway Bipolar Study and the study across four-centres longer characteristic path length, reduced global efficiency, and lower mean clustering coefficient demonstrated widespread anatomical dysconnectivity. Consistent with the prior analyses of the thesis, impaired global integration was also evident when the analysis was restricted to the three international centres with identical scanner protocol. In contrast to the Galway Bipolar Study and the study across

four-centres, global efficiency was not significantly reduced in the three-centre investigation, which potentially indicates subtle differences between the mathematically similar measure path length. One explanation is that path length is largely influenced by longer paths, while global efficiency is primarily influenced by shorter paths (Rubinov & Sporns 2010; Bullmore & Sporns 2009). The pathophysiological mechanisms related to differences in path length are still unknown and represents an area requiring further research.

Impaired global integration identified in this thesis is consistent with three studies which identified reduced global efficiency in BD (Leow et al. 2013; Gadelkarim et al. 2014; Collin et al. 2015). However two other graph analysis studies in BD reported connectivity to be preserved globally (Forde et al. 2015; Wheeler et al. 2015). In contrast with the present investigations which used volumetric parcellation, one of these studies that defined its nodes by cortical thickness did not detect differences in connection density between patients with BD and healthy volunteers (Wheeler et al. 2015). The lack of standardization in network composition represents one of the challenges when interpreting the findings across the existing literature. Moreover, the association between cortical volume and thickness is still unknown, therefore further studies employing multiple node definitions are required to interpret whether BD is affected primarily by volumetric cortico-subcortical networks compared with a thickness-based cortical networks.

Disrupted anatomical integration has also been identified in schizophrenia and may be a general pathophysiological feature across other neuropsychiatric disorders(Crossley et al. 2014; Fornito et al. 2015); therefore probing further properties of regional dysconnectivity may be particularly informative in relation to mood disorders specifically.

Regional Dysconnectivity

In the Galway Bipolar Study and the study across four-centres, uncorrected regional analyses of clustering and local efficiency identified widespread reductions among fronto-limbic, parietal and occipital connections, consistent with some other studies(Gadelkarim et al. 2014; Leow et al. 2013; Forde et al. 2015). Furthermore, regional dysconnectivity of the left middle frontal gyrus and right superior medial frontal gyrus has been supported in a recent investigation in patients from families multiply affected with BD(Forde et al. 2015).

Connectivity of bilateral anterior, middle and posterior cingulate gyri was also impaired in the larger four-centre study. Cingulate cortex deficits are reported in neuroimaging investigations in BD due to its role in the limbic system(Emsell & McDonald 2009; Vederine et al. 2011; Ellison-Wright & Bullmore 2010). Although, a review of two meta-analysis suggests cingulate deficits are inconsistent in BD(Houenou et al. 2011). Previously, a published tractography analysis of the Galway Bipolar Study cohort reported reduced fractional anisotropy along the cingulum bundle and callosal genu and splenium(Emsell, Leemans, et al. 2013). Similarly, leftward reductions in FA in the cingulum bundle and splenium have been found previously in the three international centres (Sarrazin et al. 2014). The consistency of these tractography deficits in the four-centre investigation provide additional evidence for impaired connectivity of the cingulum as a feature of BD. In the three centre investigation, significantly decreased regional clustering and efficiency were detected in the left middle cingulate gyrus in patients, that is consistent with

the study by Sarrazin and colleagues who also reported lower FA in the left dorsal cingulum segment(Sarrazin et al. 2014).

The heterogeneous functionality of the cingulate cortex is contributed by multiple cytoarchitectural divisions (Yu et al. 2011). Many afferent and efferent projections of the cingulate cortex contribute to the heterogeneity in defining its anatomical and functional subdivisions. Recently, Jones and colleagues (Jones et al. 2013) identified distinctive subdivisions of the connections of the cingulum bundle, which described connections of the dorsal cingulum fibres traversing through the temporal lobe close to the splenium(Jones et al. 2013). These temporal and splenium connections were also regionally impaired in this cohort. The middle cingulate gyrus has been related to action execution, response selection, error detection, competition monitoring, anticipation and working memory (Cole & Schneider 2007). Deficits in these functions have been associated with BD. Future studies collecting cognitive and behavioral information alongside neuroimaging parameters could assess whether such dysfunction is related to cingulate gyrus abnormalities.

These deficits in the left middle cingulate gyrus were identified in both FA-weighted networks and streamline-weighted networks. The results survived correction for global connectivity, indicating results were not dependent upon increases or decreases in density alone. This finding highlights the consistency in identifying impaired focal microstructural organization and its extent on regional connectivity through complex network analysis.

Impaired segregation was also identified across posterior parietal and occipital regions in BD. Parietal and default mode network dysconnectivity has been corroborated by an investigation of path length associated community estimation(Gadelkarim et al. 2014).This analysis indicated

that connectivity abnormalities in BD appear to extend beyond fronto-limbic regions to further association tracts of the brain(Nortje et al. 2013; Vederine et al. 2011; Wise et al. 2015).

Taken together, global and regional neuroanatomical dysconnectivity is a relatively consistent feature in patients with BD. We identified disrupted integration between communities across multiple network systems supporting BD as a dysconnection syndrome. Measures of integration and segregation represent potential trait related biomarkers in these remitted patients with BD, with properties of segregation revealing regionally discrete white matter dysconnectivity in BD.

Comparison of differences between FA and streamline count

The current work revealed differences in integration and segregation depending on the edge weights employed. This section addresses what potentially accounts for these differences when connection matrices are weighted using either number of streamlines or FA.

Streamline count has been the most commonly used edge weight in studies employing graph analysis(Fornito et al. 2013). Potentially, this represents an attractive measure of connectivity as pathways are considered to link nodes to each other(Sporns et al. 2000). When the ellipsoidal direction changes voxel-by-voxel a trajectory is formed representing a fibre tract. The criteria at which the trajectory terminates is based on a number of parameters, one of them being FA thresholding. The streamline is terminated when the diffusion become more isotropic, and the primary eigenvalues approaches 1 which is equivalent to FA approaching 0. The number of these reconstructed streamlines is then used to infer anatomical connectivity in graph analysis.

Both connection weights present challenges for interpreting brain networks. Streamline count is not representative of individual axons(Fornito et al. 2013). Alternatively, FA presents a voxel-wise index of microstructural organization that is averaged across the streamlines connecting two nodes. Therefore, presenting the average FA can mask localized differences in microstructural organization.

An advantage of network analysis that extends prior diffusion analysis techniques such as TBSS, is the ability to probe multiple measures of neuroanatomical connectivity *in vivo*. Differences between groups observed in the current work may be related to reductions in fractional anisotropy collectively as deficits were identified in the connections defined by fractional anisotropy rather than the number of streamlines between nodes. Based on the results in the current work, FA may be a more robust measure of neuroanatomical connectivity compared with the number of streamlines. The pathophysiological mechanism related to differences in FA and streamline count are still unresolved.

Network analysis not only examines integration and segregation based on white matter microstructural alone, but also examines the influence of topological position of nodes. The influence of topological position of nodes will be discussed further in this chapter.

Sub-Networks in BD

The second aim of the work was to assess sub-networks in BD, with the hypothesis that reductions in connected sub-networks may underlie the neural circuitry related to mood disorders. In the Galway Bipolar Study, three impaired connected components were identified and encompassed fronto-limbic and parietal/occipital connections. Differences between the highest densities of connections suggest further posterior dysconnectivity in BD. The highest density threshold for defining the set of supra-threshold connections revealed dysconnectivity among the cuneus, precuneus, and superior occipital connections. Investigation into the structural core of the cerebral cortex suggests there is an above average connectivity in posterior brain regions, which may support these high density connections identified in these participants with BD (Hagmann et al. 2008). Interestingly, evidence from functional connectivity analyses support a model of affected posterior default mode network as well as parieto-occipital dysconnectivity(Strakowski et al. 2011). Strakowski proposed that self-referential thinking and interpretation of visual stimuli is affected in disturbances of this network namely by altered functional connectivity of the precuneus and cuneus(Strakowski et al. 2000; Strakowski et al. 2002). These structures are topologically central with high degree, which may be particularly affected in brain disorders(Crossley et al. 2014). Weaker connectivity of network components in patients indicates these connections interact collectively, supporting BD as a dysconnection syndrome(O'Donoghue et al. 2015).

The sub-network identified in the four-centre and three-centre studies supported the investigation by Sarrazin and colleagues' that identified reduced FA in left fronto-temporal white matter in

patients compared with healthy controls. The impaired sub-network consisted of 16 nodes and 13 edges connecting deep frontal regions and deep temporal regions. Due to the impaired fronto-temporal connectivity, it may be that the uncinate fasciculus is affected as it connects cortico-limbic pathways. Impaired microstructural organization of the uncinate fasciculus has been reported to represent a biological marker of psychotic illness(Versace et al. 2008; Emsell et al. 2014; Houenou et al. 2007; Linke et al. 2013). Moreover, connections of the uncinate within the lateral orbitofrontal cortices and anterior temporal lobe are thought to modulate episodic memory, language and social-emotional processing(Versace et al. 2008).

Moreover, studies suggest the inferior frontal gyrus is associated with appropriate attention, placing emotional meaning, and affect labeling (Wegbreit et al. 2014; Hajek et al. 2013). Few studies have investigated language deficits in mood disturbances, and the neurobiological role of the inferior frontal gyrus in BD has been controversial (Phillips & Swartz 2014). There appears to be limited reports of impaired white matter connectivity within these inferior frontal cortices in BD(Kubicki et al. 2011). This may potentially be due to the compacted anatomical structure of the inferior frontal gyrus. Therefore, novel DTI tractography analysis of U-fibres may elucidate the impaired connectivity between these tightly connected structures(Zhang et al. 2014).

In the study across four-centres the greatest magnitude of connectivity differences was located in connections between the caudate and putamen, as well as the rolandic operculum and the insula. Fronto-striatal dysconnectivity has been supported in the fMRI investigations in BD due to its role in the reward system. The reward system is highly associated with dysfunction in the striatum and appears to be a major functional deficit in patients with BD(Yip et al. 2014; Strakowski et al. 2005; Mason et al. 2014). Of note, features of anhedonia and reward deficits are

also associated with these left ventrolateral prefrontal cortex (VLPFC) deactivations, which represent supported characteristics of mood disorders(Phillips et al. 2008; Phillips & Swartz 2014).

In the three centre study, the greatest magnitude of connectivity differences was located between connections of the left rolandic operculum to the left insula and left rolandic operculum to the left superior temporal gyrus. Reduced functional activation of language related regions in the inferior frontal gyrus and superior temporal gyrus was lateralized in first episode schizophrenia patients(van Veelen et al. 2011). The rolandic operculum has been shown to be involved in sensory-motor networks involved in speech production(Behroozmand et al. 2015), which may be impaired as a feature of psychomotor dysfunction in BD.

When inter-connections of sub-networks were assessed in patients with a positive history of psychotic features and absent history of psychotic features there were no differences between patient groups in both the study across four centres and three centres. This finding is in contrast to the more prominent focal differences in FA in those with a history of psychosis previously observed in the three centre cohort(Sarrazin et al. 2014).

In the four-centre investigation, patients without psychotic features displayed weaker sub-networks compared with healthy controls in the same regions, with the inclusion of an additional connection in the supramarginal gyrus. When patients with a positive history of psychotic features were compared with healthy controls, the original component differences were consistent in the left fronto-temporal connections. Of interest, the additional region included in the sub-network differences between patients without psychotic features additionally included a region, known to be affected in high risk psychosis. The supramarginal gyrus is critical for

auditory and visual processing, and has been reported to be affected in populations of high risk individuals for psychosis(Fusar-Poli et al. 2011). Weaker connectivity was identified in the supramarginal gyrus in patients without psychotic features, and not shown in patients with psychosis, could potentially be driven by its inter-connectivity with fronto-striatal regions. Inclusion of the supramarginal gyrus in the component supports posterior parietal dysconnectivity in patients with BD.

This current investigation supports aberrant left hemispheric ventral-limbic dysconnectivity as evidenced by the reduced connectivity in sub-networks in the BD group. These deep fronto-temporal network deficits are associated with features of disrupted language processing and is also a common feature of psychomotor dysfunction in BD. Potentially, reduced connectivity in sub-networks involved in language production, thought processing, and reward systems may represent more trait-like abnormalities in BD. Taken together, sub-network analyses across the GBS and multi-centre studies show impaired integration of fronto-limbic-striatal dysconnectivity in BD. This methodological approach for investigating sub-networks appears to be a sensitive technique for identifying inter-connectivity in BD.

Rich-Club Connectivity and Membership in BD

In the final methodological approach, we investigated rich-club density and rich-club structural differences between patients and healthy controls. When the analysis was restricted to the three-centre study, significantly reduced rich-club density was identified in the patient group compared with healthy controls. These differences in density survived multiple comparison correction across the possible range of rich-club densities, demonstrating this as the first study to identify rich-club deficits in BD. In the Galway Bipolar Study and study across four-centres, analysis of rich-club density revealed subtle connectivity effects in the bipolar group. Rich-club density effects did not withstand multiple comparison correction in either study. Interpreting why these statistically robust differences were present in the three-centre and not the four-centre investigations could be an effect of the imaging protocol, however the findings were corrected for research centre and employed a fisher-pitman permutation test for non-normally distributed data to account for differences contributed by different research centres. The subtle connectivity effects in the Galway Bipolar Study could potentially have masked the significant effects identified in the three-centre investigation. The subtle effects identified in the Galway Bipolar Study and four-centre investigations indicate that rich-club density in BD may be impaired to a lesser extent than more severe psychotic illnesses like schizophrenia, where lower levels of rich-club connectivity have been reported in schizophrenia, as well as in unaffected siblings of patients with schizophrenia compared with controls(van den Heuvel et al. 2013; G. Collin et al. 2015; Collin et al. 2014). Only one other study has examined rich-club connectivity in BD and reported preservation compared with controls(Collin et al. 2015). This study investigated rich-club connections in BD when the rich-club was defined by the top 10% betweenness centrality

and highest degree regional connections(Collin et al. 2015). The current rich-club investigations assessed normalized rich-club organization, which explored the above average connectivity and non-random organization between these hubs. The rich-club members were also validated as the top 10% highest degree nodes.

As addressed in the **Methods** chapter, the importance of the limbic system argues for the inclusion of sub-cortical structures in network maps when investigating psychiatric illnesses(van Erp et al. 2015). Collin and colleagues (2015) in their rich-club connectivity study in BD confined their rich-club network to cortico-cortical connections(Collin et al. 2015). Therefore, these network comparisons are substantially different and would result in an alternative cortical rich-club network, rather than cortico-subcortical rich-club network explored in this thesis.

Across the cohorts, structures recruited as part of the rich-club do appear to be differentially affected in BD compared to controls. In the Galway Bipolar Study, the superior frontal gyrus was absent from the bipolar group rich-club, suggesting dysconnectivity is present in this densely interconnected frontal structure. This absence was maintained when the rich-club membership was considered by pathway common to the top 60% of participants or 70% of participants(de Reus & van den Heuvel 2013a). In the Galway Bipolar Study, rich-club members connected by the pathway common to more than 60% of participants indicated above average connectivity of the right middle cingulate gyrus in healthy controls, which was absent in the bipolar group. Moreover, the bipolar group appeared to recruit the left middle occipital gyrus, which may potentially represent a compensatory effect from disrupted frontal rich-club connectivity(Griffa et al. 2013). In the study by Collin and colleagues(Collin et al. 2015), rich-club connectivity was examined through multiple hub classifications. These hubs consisted of portions of bilateral

cingulate, precuneus, superior frontal, parietal and temporal gyri, as well as pre and post central gyri and insular cortices (Collin et al. 2015). Overlapping rich-club members in the present work propose cingulate, precuneus and superior frontal connections to be most reproducible across investigations and hub definitions.

Nodes anatomically connected with the superior frontal gyrus, also present in the rich-club network, include the caudate and thalamus(Li et al. 2013; Haznedar et al. 2005). These deficits are consistent with pathophysiology incorporating the anterior thalamic radiation in BD (Sussman, BDs 2009). While thalamic function has been implicated previously in BD, volumetric analyses of the thalamus have been varied(Hallahan et al. 2011).

In the four-centre study, the right middle frontal gyrus was absent in patients and present in healthy control rich-club members. Similarly, the three-centre study identified rich-club membership differences whereby the right middle frontal gyrus and left hippocampus were absent in patient rich-club members and present in healthy control rich-club members. This indicates that the right middle frontal gyrus and its' connections emerge as vulnerable hubs across investigations. Volumetric analyses of the hippocampus have reported left hippocampal reductions in patients with BD compared to healthy volunteers(Quigley et al. 2015). However, a mega-analysis of hippocampal volume in BD reported variations between studies with overall preserved hippocampal volume(Hallahan et al. 2011). Impaired integration of the hippocampus as a hub structure may indicate disruption of the cortico-limbic network. Future work that includes sub-cortical structures in network pipelines may address the inconsistencies in hippocampal dysconnectivity in BD.

Differential hub involvement in the right middle frontal gyrus have been supported in functional connectivity studies reporting deactivation in the right middle frontal gyrus in patients with BD (Houenou et al. 2011). The superior frontal gyrus is anatomically connected to the middle frontal gyrus and inferior frontal gyrus through the anterior portion of the arcuate(Li et al. 2013). Therefore, these right frontal and middle deficits may indicate impaired integration in the DLPFC and contribute to extended dysconnectivity through the rich-club network. These central hubs in the frontal lobe are involved in attention, reappraisal, working memory and voluntary emotional regulation, which is impaired in BD(Phillips et al. 2008). Therefore, abnormal frontal hub organization may be a potentially vulnerable region of impaired emotional regulation and cognitive control in BD.

Similar rich-club members were previously identified as hubs in both healthy volunteers and patients with schizophrenia, defined by betweenness centrality, when network maps were reconstructed using the equivalent structural atlas(van den Heuvel et al. 2010). Specifically, hub organization in schizophrenia revealed a less central role in frontal hubs when nodes were defined by the automated anatomical labeling atlas(van den Heuvel et al. 2010). Hubs defined in the study of schizophrenia correspond with rich-club members of the current analysis; consistent with shared dysconnectivity of frontal hubs across the range of psychotic illnesses (van den Heuvel et al. 2010). Validation of this parcellation scheme highlights the consistency of these structures as critical hubs in cortico-subcortical networks.

The relationship between aberrant rich-club organization and functional hypo or hyper-activation requires further study. A meta-analysis of functional MRI data in schizophrenia reported that functional over or under-activations were more likely to be located in rich-club hub nodes

(Crossley et al. 2015). A functional MRI meta-analysis of response inhibition in individuals with BD indicated hyper-activation of the right middle frontal gyrus in fMRI studies in patients with BD compared with controls (Hajek et al. 2013). Similarly, two meta-analyses in patients with BD reported increased activation in the right middle frontal gyrus and reduced activation in the right superior frontal gyrus compared with healthy controls (Houenou et al. 2011). Our findings of impaired hub organization are supported in these few functional meta-analyses and are in line with Crossley and colleagues (Crossley et al. 2015) findings that functional over- and under-activations are more likely to be reported in rich-club hubs in individuals with psychotic illnesses. Therefore, findings of the current research support impaired hub organization is a feature of BD.

Taken together, patients with BD display aberrant rich-club organization that might be affected by subtle reductions in rich-club density. Across the cohorts, rightward frontal rich-club organization is impaired in patients with BD compared to healthy controls. Abnormal frontal hub organization may underpin impaired emotional regulation and cognitive control in BD.

Clinical Outcomes in BD

To explain the lack of significant findings in the investigation of clinical measures and graph theory properties, it is important to highlight the clinical cohort were mostly in remission in the presented investigations. The Galway Bipolar Study participants were prospectively confirmed as euthymic; therefore, they had low ratings on clinical mood rating scales of mania and depression. The patients from the three international centres included patients with higher HDRS

scores; however, these patients were also largely in remission. Given this lack of symptom variability, it is unsurprising that there were no associations between mood rating symptoms and graph measures. In addition, there were no differences in graph measures related to illness duration. This is a consistent finding across current network investigations in BD(Forde et al. 2015; Leow et al. 2013; Collin et al. 2015). This potentially highlights the difference between BD and its commonly associated psychotic illness, schizophrenia, as schizophrenia characterized by more progressive neurobiological abnormalities, where patients exhibit more severe network abnormalities with longer illness duration(Sun et al. 2015; van den Heuvel et al. 2013; Collin et al. 2015). This suggests neuroanatomical dysconnectivity is an inherent trait related marker rather than a state dependent marker in BD. These neuroanatomical deficits may be contributed by genetic heritability, as evidenced by intermediate levels of dysconnectivity identified in unaffected relatives with BD (Forde et al. 2015), and more prominently, in unaffected siblings of patients with schizophrenia(Collin et al. 2014; G. Collin et al. 2015).

A potential source of clinical heterogeneity includes the high proportion of individuals with BD also experiencing features of psychosis. There was a positive history of psychotic features in over half the participants in both the three centre study and four centre studies. There were no connectivity differences between patients with a positive history of psychotic features and patients with an absent history of psychotic features. Differences were observed when sub-networks were compared between patients with a positive history of psychotic features and healthy controls. Patients with an absent history of psychotic features additionally included the left supramarginal gyrus in the weaker sub-network compared with healthy controls. This may indicate more distinct connectivity deficits in patients with an absent history of psychotic

features with BD. Direct comparison of individuals with and without psychotic features may elucidate features of the illness contributed by psychotic symptoms.

Integration of research findings

Considering commonalities of the various analyses conducted, this work supports disrupted anatomical integration, reduced regional connectivity, left lateralized sub-network dysconnectivity, and differential rich-club organization as features of impaired structural integration in BD. In this novel research area, the relationship of graph analysis measures to pathophysiological mechanisms in brain disorders is an active area of examination (Fornito et al. 2013). This section aims to relate features of dysconnectivity identified by this work to the ventral-limbic and dorsal-cognitive models of BD, and then assesses how topology is used to assess neuroanatomical connectivity. We then explore the caveats of the current research by reviewing clinical and methodological considerations, and concluding with future recommendations.

Ventral –limbic and dorsal-cognitive systems

Recent research suggests BD arises from impaired functioning of two systems: the ventral/limbic system which is involved in aberrant reward processing, and the dorsal/cognitive network, which when impaired is believed to contribute to cognitive dysfunction associated with BD(Houenou et al. 2011; Phillips & Swartz 2014). It has been suggested that an overactive left ventral-striatal-ventrolateral and orbitofrontal cortical circuitry results in clinical and cognitive deficits shown in patients with BD(Phillips & Swartz 2014). Functional connectivity studies have shown

increased activation in the left ventral-limbic network, with decreased activation in the cortical-cognitive network in the right hemisphere(Houenou et al. 2011; Lois et al. 2014).

In the current work, impaired regional and sub-network connections are consistent with the studies supporting impaired reward circuitry in BD. The reward system integrates information through the ventral striatum and amygdala circuitry, managing emotional processing and valence(Trost et al. 2014). Both symptoms of mania and depression have been associated with impaired reward processing(Phillips & Swartz 2014; Wessa et al. 2014). Dysconnectivity of the VLPFC as a model of BD is supported by impaired integration of cortico-limbic pathways identified in the current work. Grey matter reductions in frontal, subcortical, and temporal regions, along with major tract deficits in frontal-subcortical structures support abnormalities of this system in BD(Phillips & Swartz 2014). Models of BD suggest aberrant activation of the reward system, resulting in symptoms such as anhedonia in individuals with BD (Phillips et al. 2008; Trost et al. 2014). Clinical studies support anhedonia as a common withdrawal symptom that might be more trait-like and persistent(Velthorst & Meijer 2012). The VLPFC manages processing of emotional stimuli, and is related to impaired interpretation of facial expressions in patients with BD(Wessa & Linke 2009). The findings provide additional evidence for current neural network models of impaired emotional and reward processing, and potentially represent a structural model for functional hyper or hypo activations in individuals with BD. The findings also support left-ward asymmetry of fronto-limbic and frontal-striatal connectivity as a consistent marker of aberrant reward processing(Phillips & Swartz 2014).

Cognitive control networks comprise the anterior cingulate cortex, presupplementary motor area, dorsolateral prefrontal cortex, inferior frontal junction, anterior insular cortex, dorsal pre-motor

cortex, and posterior parietal cortex(Cole & Schneider 2007). Impaired segregation identified in the current investigations are consistent with impaired connectivity of this system in BD. Dorsolateral prefrontal and posterior parietal connections were impaired in segregation measures of clustering and local efficiency in patients with BD compared with controls in both the Galway Bipolar Study and study across four centres. Frontal regions in the cognitive control networks were identified as hubs in the multi-centre rich-club analyses.

Cognitive networks relay information between dorsolateral prefrontal cortex and ventral networks, and connect with the anterior cingulate cortex (ACC), which is responsible for attention and cognitive processing(Cole & Schneider 2007). Interestingly, studies indicate that voluntary behavioral control of positive and negative emotions include specifically the right DLPFC and left VLPFC, as these areas are involved in regulating emotional behaviours (Phillips et al. 2008). The findings of the current work converge with this hypothesis of an imbalance in left VLPFC and right DLPFC integration. This was demonstrated by differential right frontal rich-club organization, and impaired sub-network connectivity in the left inferior frontal gyrus identified in patients with BD compared with controls. Taken together, the findings from the current work support and extend these current models of BD through complex network approaches.

How can topology explain neuroanatomical connectivity and spatial embedding?

Network science has extended the knowledge of neuroanatomical wiring through complex patterns of organization. Investigation into healthy brain networks has identified a structural core of the cerebral cortex, identifying structures which are more densely interconnected (Hagmann et al. 2008). Analysis of sub-networks has revealed collections of inter-connected regions based on density(Zalesky, Fornito & Bullmore 2010). In addition, investigations have proved the rich-club identifies a group of regions with above average features of integration (van den Heuvel & Sporns 2011). A majority of the research to date has focused on impaired integration between structures rather than examination of a structures topological position in a network(Roberts et al. 2016). Here we attempt to address the topology of vulnerable nodes exhibiting impaired connectivity in patients with BD.

Spatial embedding

Spatial embedding speaks to the topological organization of a node in a network. Topological position is a factor to consider when evaluating regional communities, sub-networks, and rich-club connections. As brain networks are constrained by physical properties, spatial embedding is important for evaluating connections between neighboring nodes (Bullmore & Sporns 2012; Bullmore & Sporns 2009). The spatial embedding of brain networks allows for a hierarchical arrangement in which the brain can be organized into communities upon further sub-communities(Bassett et al. 2008; Bassett et al. 2010). The topological position of a node in a

network is then important to elucidate how the patterns of integration, within and between, sub-systems support behaviour and cognition.

Given the importance of integrative hub networks in healthy models of the human connectome (Hagmann et al. 2008; van den Heuvel & Sporns 2011; van den Heuvel & Sporns 2013), it is evident topological position as well as efficient connectivity are critical for healthy brain function.

Aberrant integration and segregation in patients with BD may be related to topological vulnerability. This is supported by the evidence that findings are unchanged after correcting for global connectivity. Global connectivity correction highlights regional deficits are not only affected by reductions or increases in connection density, but their topological position in the network contributes to their structural vulnerability in BD.

Implications of the current work

The current work identified disrupted neuroanatomical integration in individuals with BD. Longer characteristic path length was identified in patients with BD across the cohorts, and therefore reflects a consistent marker in BD. Reductions in measures of integration and segregation are consistent with the structural, diffusion and functional neuroimaging literature to date. Impaired neuroanatomical connectivity may represent a structural basis for emotional and reward processing.

Disrupted neuroanatomical integration is evident when patients are in remission indicating persistent structural deficits are present as traits in individuals with BD.

Investigation of both FA and streamline count highlights the distinction in connection weights and their utility in detecting abnormal integration in brain networks. While the number of reconstructed streamlines is more widely reported, FA may be more robust and anatomically sensitive than the number of reconstructed streamlines. Further work is needed to determine the relationship between FA and streamline count, and how these properties might differ in the same pathway.

Furthermore, topological location of affected nodal connectivity may be distinctive in BD. Graph theory extends previous DTI techniques to probe the influence of a region's connectivity on its neighboring connections. Regions remained impaired after correction for global dysconnectivity suggesting topological position is a critical feature of complex neural networks. In addition, analysis of rich-club structural membership differences identified differential organization of frontal rich-club structures across the cohorts in BD. While the rich-club connection density was weakly impaired across the two major cohorts, the absence of right frontal hubs in rich-club members in BD was consistent across all investigations. Potentially, impaired right frontal hub organization is a more pervasive trait deficit, which is confirmed by previous aberrant functional activation in these regions in BD.

This work demonstrates that fronto-limbic, posterior parietal dysconnectivity, left VLPFC, and right DLPFC may be more likely to be affected in BD due to their topological position being involved in many regulatory processing and sensory networks.

Strengths of the study

This complex network investigation in BD makes a significant contribution to the field's knowledge. This investigation was carried out first in a moderately sized cohort of clinically homogenous euthymic patients with BD, and further assessed in large population of individuals from international research centres. In addition, the scanner and acquisition protocols from all research centres were implemented for high quality data resolution. The three international centres employed the same model scanner and identical image acquisition protocol. In relation to study pre-processing there were a number of advantages to the techniques chosen. All images underwent subjection motion and eddy current correction. The DTI data included rotation of the b-matrix during subject motion correction. Failure to rotate the b-matrix can cause errors in reconstruction in the orientation of the diffusion tensor(Leemans & Jones 2009). In addition, the data underwent optimized quality assessment protocol. All images were visually inspected for potential artefacts. Quality assessment rating scores were provided from the international centres and then moderate to severe images were re-assessed to benchmark the data quality.

The multi-centre study investigations employed a further up-dated software for pre-processing and generation of network matrices compared with the Galway Bipolar Study investigation. *ExploreDTI*v.4.8.4 included recursive calibration of the response function(Tax et al. 2014). Recursive calibration is employed during tractography and aims to better resolve partial volume effects within voxels(Tax et al. 2014).

This study took advantage of high resolution tractography reconstruction techniques. Constrained Spherical Deconvolution (CSD) was employed using deterministic tractography to

reconstruct multiple diffusion directions within each voxel. CSD has proved optimal in resolving tract propagation in voxels with high crossing fibres(Tournier et al. 2007; Jeurissen et al. 2011). CSD may propagate spurious reconstructed streamlines; however, stringent tracking angle and FA thresholds should limit this possibility.

Another advantage of the current work was the inclusion of multiple connection weights. Of interest, there were few cases of consensus in findings when using both FA and number of streamlines connection weights. FA weighted connections appeared to be more robust when detecting an effect in regional measures, although when connection matrices were weighted by number of streamlines findings were consistent with FA in the sub-network analyses in the multi-centre investigations. In future work, connectivity-to-length mapping might resolve some of the variability when using the number of reconstructed streamlines. Of note, reconstructed streamlines between nodes were not adjusted for tract volume, which can be dependent on voxel size. In addition, some studies correct for ROI volume, due to the fact that streamline count may be larger in some regions due to larger node size and therefore a greater number of projections tracking through those regions(de Reus & van den Heuvel 2013b). These challenges are unresolved in network analysis, and may be clarified by future studies.

The investigation applied graph thresholding to resolve possible spurious streamline count that may arise from tractography algorithms. When choosing an optimal graph thresholding approach it is important to consider how graph thresholding might affect the results(Drakesmith et al. 2015). Some studies implement group thresholds, where only connections identified in a majority of participants should be included for analysis(de Reus & van den Heuvel 2013a). In addition, as was explained in the **Methods** chapter, graph thresholding provides the options of

connection-weight threshold or a graph density threshold. A connection-weight threshold identifies a minimum number of streamline counts traversing a node to be included for analysis. A density-based threshold applies a density for the entire graph to be benchmarked. When connection-weight thresholds are implemented these definitions might limit the minimum connections which may on average be lower in the patient group by virtue of hypothesized impaired integration common to brain disorders(Fornito et al. 2012). In addition, one could weight by a density-based threshold. This would allow moderate densities to be approximately equal between groups, but allow connection densities to vary between groups. In this case it would allow lower values present in patients to be reconstructed. Density-based thresholding was used to allow connection-weights to vary between groups. Selection of graph thresholding is largely inconsistent, however was cautiously considered in this work.

A strength of the current analysis is the parcellation scheme employed in the brain-mapping pipeline. The scale at which the brain should be accurately mapped to be most biological meaningful is not yet standardized(Fornito et al. 2013). This study benefits from a cortical and subcortical parcellation. A majority of complex network analyses limit their connectome maps to cortical connection maps, while this analysis extended to cortico-subcortical mapping. Differences in subcortical volume in BD has a substantial body of literature to support its role in the aetiology of BD and as a trait feature of the illness(Quigley et al. 2015; Houenou et al. 2012; Strakowski et al. 2012; Vargas et al. 2013; van Erp et al. 2015; Hibar et al. 2016).

The current work utilized the AAL atlas which associates a template volume for each structure and for each participant. The AAL atlas is optimal as it is timely and efficient, and allows for comparable differences in techniques such as the network based statistic, as all data is registered

to a common coordinate space. Most investigations attempt to replicate analyses over multiple parcellation schemes, which can be intensively laborious(Collin et al. 2015). When anatomically sensitive parcellation schemes can be implemented reliably, there may be greater consistency identified across investigations.

Finally, a major strength of the study is in the replication of some findings in that this work reproduced major deficits identified in the local Galway Bipolar Study in the separate and independent multi-centre cohort using a similar methodological approach. Impaired global integration identified in the Galway Bipolar Study was identified in the multi-centre investigations. Reduced FA in left fronto-temporal pathways and callosal splenium was identified in both the four-centre and three-centre investigation. The findings are largely consistent with a majority of DTI meta-analyses in BD, and supported in major meta-analyses of structural neuroimaging to date in BD(Houenou et al. 2011; Vederine et al. 2011). Aberrant hub connectivity reported in this investigation has been supported to be hyper and hypo-activated in meta-analysis of functional connectivity findings in BD(Hajek et al. 2013).

Medication use

The patients with BD were taking a range of medications from standard mood stabilizers to antipsychotics, antidepressants and benzodiazapines (to control anxiety symptoms) at time of scanning. The most widely prescribed pharmacological treatment for BD is lithium. Lithium reduces the risk of recurring both manic and depressive episodes. A majority of the patients were

taking mood stabilizers and antipsychotics. Of these, lithium use is known to cause an increase in brain volume(Sassi et al. 2002; Hallahan et al. 2011). Medication status tested considered whether patients were on lithium or not. Medication load was categorized to assess the variety and dose of multiple medications taken by patients. Across the cohorts, there was no association between measures of medication status, years of lithium duration, and medication load with measures of integration and segregation. Neither lithium status nor medication load affected the resulting findings.

In general, the lack of associations identified between the network abnormalities and clinical measures or medication use supports the presence of anatomical dysconnectivity as a trait related featuere of bipolar disorder, possibly related to genetic or developmental risk. Longitudinal studies will be required to confirm this.

Methodological Limitations

Methodological limitations must also be considered when interpreting these network findings(Fornito et al. 2013; de Reus & van den Heuvel 2013b). As network analyses lack standardized recommendations around methodological processes at this point; this study carries challenges in interpreting and reconciling results across investigations(Fornito et al. 2013). Methodological considerations carrying uncertainty include the specific choice of parameters for white matter tract reconstruction, edge weights of fractional anisotropy measures and streamline count. Advancing from previous research by use of more biologically relevant connection

weights as well as a template cortical parcellation may identify less variable effects(Fornito et al. 2013). The field would benefit from some degree of standardization in these approaches, which would assist in directly comparing results as they emerge from research groups.

In this study, differences in scanner and acquisition protocols may confound the interpretation of findings across sites. A strength of the collaborative multi-centre study across three-centres was the data collection protocol. The data of three centre study was acquired with same model scanner and identical acquisition protocol, although differences in hardware would account for subtle differences in connection densities. Fortunately, the data was highly comparable, and there were no main effects due to scanner. A methodological study investigated the reproducibility of structural connectome reconstructions from diffusion data. Larger white matter pathways such as corpus callosum and the superior longitudinal fasciculus remained highly correlated across time points and scanners(Bonilha et al. 2015). In this analysis a linear mixed model analysis was employed to account for the inherent differences due to scanner variation. After inclusion of the re-analysed Galway data, it was expected the connection density from research centres with identical scanner protocol behaved more similarly compared to the initial MRI acquisition employed in the Galway Bipolar Study.

Combining data from multiple image acquisition sites requires implementing standardized quality assessment. To improve quality control of the multi-centre study investigations, quality assessment of poor DW images by slice number was reported from the multi-centre study. This allowed us to benchmark quality control ratings across centres. Unfortunately, some datasets included poor image acquisition, and about 10 participant DW images were removed from analysis.

Another potential limitation was the template parcellation scheme employed. Its advantages included cortico-subcortical mapping; although, a subject-specific parcellation would be ideal under further investigation to improve anatomical sensitivity. When using parcellations from Freesurfer each resulting brain network is within its own coordinate space and requires further registration to compare connectivity between groups in network analysis such as the network based statistic. Outside the scope of the thesis, a Freesurfer based parcellation was explored but identified challenges that require further exploration. One such investigation should explore tractography angle threshold to probe the angle at which the reconstructed streamlines propagate through a node. Previously, angle thresholds in complex network analyses in BD report angle thresholds of 65° (Leow et al. 2013). Further work is needed to identify a reliable subject-specific parcellation method. In addition, points at which streamlines propagate through a node will vary individually and cause inherent differences in streamline count for each individual. The current investigation may benefit from a Freesurfer analysis to determine the relationship between white matter connectivity patterns and volumetric differences previously reported in BD(Leow et al. 2013; Ajilore et al. 2015; Gadelkarim et al. 2014; Collin et al. 2015). Subject-specific parcellation schemes could assist in elucidating more pervasive features of dysconnectivity in BD through improved anatomical sensitivity.

A challenge when designing a study using complex graph analysis is the variety of graph measures available. The Brain Connectivity toolbox consists of over 20 graph measures(Rubinov & Sporns 2010). To elucidate trait biomarkers, it is crucial to identify clinically relevant measures of neuroanatomical connectivity. This study limited the measures of integration and segregation to the top 4-5 most standardized measures employed in psychiatric illnesses. A number of investigations report the use of in-house metrics, this potentially limits its ability to be

compared across studies. Graph measures previously reported to be affected in BD include inter and intra hemispheric path length. Inter-hemispheric dysconnectivity was not specifically examined in this analysis, where it has been supported as a feature of psychotic illnesses in previous structural network investigations (Leow et al., 2013, Caeyenbergh et al., 2014; GadElkarim et al., 2014; Collin et al., 2015).

Future Recommendations

Characterizing neuroanatomical connectivity across large cohorts of participants was a challenging feat. There were multitudes of parameters to consider from study design to pre-processing, analysis and statistical inference. This investigation aimed to proceed with the optimal and reliable techniques available. As this is a quickly advancing field there are a number of future recommendations to consider.

The clinical cohort investigated in this work comprised of mostly well patients with BD. The underlying neurobiology of mood phases of the illness is still unclear. A longitudinal design to scan patients at multiple time points would help to identify whether distinctive neuroanatomical connectivity patterns are apparent at various phases of the illness course. Longitudinal investigations would unravel the mood state versus trait characteristics in BD.

Standardization of data acquisition would improve the field as large collaborative study designs (ENIGMA and Human Connectome Projects) become more mainstream. Standardization of clinical variables used in assessment would allow us to probe how neuroanatomical

dysconnectivity is associated with clinical outcome or mood state in large cohorts. For example, the Galway Bipolar Study databases included information about number of hospitalizations due to mania or depression, in addition to the total number of hospitalizations. When the data was combined, only a small number of clinical measures overlapped between research centres. This confined analysis of clinical outcome to age of onset and illness duration in the multi-centre investigations.

Dysconnectivity reported in the current work was not associated with clinical outcome or mood rating scores, therefore these represent more trait related features. These neuroanatomical deficits could potentially be associated with genetic risk for the illness. Future work collecting genetic data in the Galway Bipolar Study is underway. Further genetic data from the multiple collaborative international centres could identify potential risk phenotypes in BD and its association with neuroanatomical dysconnectivity.

Future recommendations for network based investigations should include improved subject-specific parcellation with appropriately standardized tractography parameters. Further investigation of connectivity through multiple parcellation schemes would confirm the consistency of the results beyond the choice of nodes.

Most studies normalize graph measures in order to have a reference network and identify these connectivity patterns as non-random features of organization(van den Heuvel et al. 2009). A limitation of the randomization occurs as the connection matrices lose their spatial constraints after re-wiring(Roberts et al. 2016). Subsequently graphs could be thresholded or thereby constrained to the original model in the form of surrogate modeled networks(Roberts et al. 2016). Various methodological selections allow for variations between graph theory

investigations. Further standardization of the components of networks and its subsequent computational models will allow for improved interpretation between investigations.

The regions implicated in aberrant hub organization in this work is consistent with abnormal functional activations in the literature. Recently, complex network analysis has expanded to elucidating the structure-function relationship through measures of connectivity in psychiatric cohorts(van den Heuvel et al. 2013; Fornito & Bullmore 2014; Cocchi et al. 2014). The acquisition of multimodal data to examine structural-functional associations in more depth would help to elucidate the biological implications of the structural connectivity abnormalities.

Conclusion

This multifaceted analysis employing graph theory metrics provides substantial additional evidence for anatomical dysconnectivity representing a trait feature of BD. This study supports impaired integration and segregation through reductions in global efficiency and regional connectivity in neuroanatomical networks. The techniques employed in the present investigations have a number of advantages over the current literature, namely a cortico-subcortical network approach to confirm and support the literature identifying aberrant microstructural organization in fronto-limbic tracts.

The aim of the thesis was to clarify the extent of impaired connectivity in brain networks in individuals with BD. Three different methodological approaches were employed to characterize various features of neuroanatomical topology, including global and regional properties, sub-

network analysis, and rich-club connectivity and membership analysis. Some of these approaches allowed for *a priori* hypotheses to be tested to explore areas we expected to identify greater dysconnectivity defined by prior tractography analysis carried out in these cohorts. Additionally, techniques such as the Network Based Statistic and rich-club connectivity did not include an *a priori* assumption regarding the extent of dysconnectivity. This allowed for disrupted neuroanatomical connectivity in regions that might not have been previously investigated or reported to be identified.

Differences in results by connection weights employed suggest FA may be a more robust measure of neuroanatomical dysconnectivity. This also suggests the prior literature reporting negative findings may be limited by the edge weight employed.

In addition, the topological organization of frontal hubs and cingulate regions were identified as abnormal in patients with BD. Major frontal hubs and cingulate regions withstood correction for global density indicating these regions are topologically critical in the network for information transfer.

This investigation reports the largest cortico-subcortical graph theory based network investigation to date. This is the first network analysis study in BD to investigate sub-network circuitry using Network Based Statistics. Furthermore, differential hub recruitment in frontal rich-club members is a novel finding in the literature examining rich-club connectivity in BD.

To identify a clinically relevant biomarker a measure must be biologically informative and efficient. These novel analytical techniques are of considerable interest for the application in epidemiological study designs into the aetiopathogenesis of psychotic illness. They can be

potentially analysed on large, representative cohorts of patients with psychotic illness since they can be acquired from clinical MR scanners in a reasonable timeframe and processed using automated methodology. The interpretations as to what impaired graph properties might represent in relation to aberrant function are somewhat speculative. The findings suggest impaired inter-connectivity between critical functional sub-units may provide a structural basis for functional dysconnectivity, but this explanation can only be further assessed through structural-functional modeling.

This thesis presents a novel series of investigations across multiple cohorts to describe neuroanatomical dysconnectivity in BD. The findings from the current research contribute to the field and should inspire further complex network analysis studies to examine cortico-subcortical dysconnectivity in BD. This would not only elucidate neurobiological markers in psychotic illnesses, but also standardize more accurate models in connectome research.

Bibliography

Achard, S. & Bullmore, E., 2007. Efficiency and cost of economical brain functional networks. *PLoS Computational Biology*, 3(2), pp.0174–0183.

Ajilore, O. et al., 2015. Connectome signatures of neurocognitive abnormalities in euthymic bipolar I disorder. *Journal of Psychiatric Research*, 68, pp.37–44. Available at: http://linkinghub.elsevier.com/retrieve/pii/S0022395615001697.

APA, 1994. *Diagnostic and statistical manual of mental disorders (4th ed.)*,

Ashburner, J. & Friston, K.J., 2000. Voxel-based morphometry--the methods. *NeuroImage*, 11(6 Pt 1), pp.805–821.

Bassett, D.S. et al., 2009. Cognitive fitness of cost-efficient brain functional networks. *Proceedings of the National Academy of Sciences of the United States of America*, 106(28), pp.11747–52. Available at: http://www.pubmedcentral.nih.gov/articlerender.fcgi?artid=2703669&tool=pmcentrez&rendertype=abstract.

Bassett, D.S. et al., 2010. Efficient physical embedding of topologically complex information processing networks in brains and computer circuits. *PLoS Computational Biology*, 6(4).

Bassett, D.S. et al., 2008. Hierarchical organization of human cortical networks in health and schizophrenia. *The Journal of neuroscience : the official journal of the Society for Neuroscience*, 28(37), pp.9239–48. Available at: http://www.pubmedcentral.nih.gov/articlerender.fcgi?artid=2878961&tool=pmcentrez&rendertype=abstract [Accessed March 28, 2016].

Beaulieu, C., 2002. The basis of anisotropic water diffusion in the nervous system - A technical review. *NMR in Biomedicine*, 15(7-8), pp.435–455.

Behroozmand, R. et al., 2015. Sensory-motor networks involved in speech production and motor control: an fMRI study. *NeuroImage*, 109, pp.418–28. Available at: http://www.ncbi.nlm.nih.gov/pubmed/25623499 [Accessed June 23, 2016].

Belmaker, R.H., 2004. Bipolar disorder. *The New England journal of medicine*, 351(5), pp.476–486.

Benedetti, F. et al., 2011. Disruption of white matter integrity in bipolar depression as a possible structural marker of illness. *Biological Psychiatry*, 69(4), pp.309–317. Available at: http://dx.doi.org/10.1016/j.biopsych.2010.07.028.

Benjamini, Y. & Hochberg, Y., 1995. Controlling the False Discovery Rate: A Practical and Powerful Approach to Multiple Testing. *Journal of the Royal Statistical Society. Series B (Methodological)*, 57(1), pp.289 – 300. Available at: http://www.jstor.org/stable/2346101.

Bonilha, L. et al., 2015. Reproducibility of the structural brain connectome derived from diffusion tensor imaging. *PLoS ONE*, 10(9), pp.1–17.

Bullmore, E. & Sporns, O., 2009. Complex brain networks: graph theoretical analysis of structural and functional systems. *Nature reviews. Neuroscience*, 10(3), pp.186–98. Available at:

http://www.ncbi.nlm.nih.gov/pubmed/19190637 [Accessed July 9, 2014].

Bullmore, E. & Sporns, O., 2012. The economy of brain network organization. *Nature reviews. Neuroscience*, 13(5), pp.336–49. Available at: http://www.ncbi.nlm.nih.gov/pubmed/22498897 [Accessed January 21, 2014].

Caeyenberghs, K. & Leemans, A., 2014. Hemispheric lateralization of topological organization in structural brain networks. *Human Brain Mapping*, 35, pp.4944–4957.

Chen, C.H. et al., 2011. A quantitative meta-analysis of fMRI studies in bipolar disorder. *Bipolar Disorders*, 13, pp.1–15.

Chiang, S. et al., 2015. Time-dependence of graph theory metrics in functional connectivity analysis. *NeuroImage*, 125, pp.601–15. Available at: http://www.ncbi.nlm.nih.gov/pubmed/26518632 [Accessed November 3, 2015].

Cocchi, L. et al., 2014. Disruption of structure-function coupling in the schizophrenia connectome. *NeuroImage: Clinical*, 4, pp.779–787. Available at: http://dx.doi.org/10.1016/j.nicl.2014.05.004.

Cole, M.W. & Schneider, W., 2007. The cognitive control network: Integrated cortical regions with dissociable functions. *NeuroImage*, 37(1), pp.343–360. Available at: http://dx.doi.org/10.1016/j.neuroimage.2007.03.071.

Collin, G. et al., 2015. Brain network analysis reveals affected connectome structure in bipolar I disorder. *Human Brain Mapping*, 00(July), p.n/a–n/a. Available at: http://doi.wiley.com/10.1002/hbm.23017.

Collin, G. et al., 2015. Connectome organization is related to longitudinal changes in general functioning, symptoms and IQ in chronic schizophrenia. *Schizophrenia Research*, 38(1), p.9. Available at: http://www.researchgate.net/publication/274405885_Connectome_organization_is_related_to_longitudinal_changes_in_general_functioning_symptoms_and_IQ_in_chronic_schizophrenia.

Collin, G. et al., 2014. Impaired rich club connectivity in unaffected siblings of schizophrenia patients. *Schizophrenia Bulletin*, 40(2), pp.438–448.

Collin, G. et al., 2013. Structural and Functional Aspects Relating to Cost and Bene fi t of Rich Club Organization in the Human Cerebral Cortex. , (September), pp.2258–2267.

Craddock, N., O'Donovan, M.C. & Owen, M.J., 2005. The genetics of schizophrenia and bipolar disorder: dissecting psychosis. *Journal of medical genetics*, 42(3), pp.193–204.

Crossley, N. a et al., 2013. Cognitive relevance of the community structure of the human brain functional coactivation network. *Proceedings of the National Academy of Sciences of the United States of America*, 110, pp.11583–8. Available at: http://www.pubmedcentral.nih.gov/articlerender.fcgi?artid=3710853&tool=pmcentrez&rendertype=abstract.

Crossley, N. a. et al., 2014. The hubs of the human connectome are generally implicated in the anatomy of brain disorders. *Brain*. Available at: http://www.brain.oxfordjournals.org/cgi/doi/10.1093/brain/awu132 [Accessed July 14, 2014].

Crossley, N.A. et al., 2015. Altered Hub Functioning and Compensatory Activations in the Connectome : A Meta-Analysis of Functional Neuroimaging Studies in Schizophrenia. *Schizophrenia Bulletin*, 42(2), pp.1–9.

Cui, L. et al., 2011. Overlapping clusters of gray matter deficits in paranoid schizophrenia and psychotic bipolar mania with family history. *Neuroscience letters*, 489(2).

Daianu, M. et al., 2015. Rich club analysis in the Alzheimer's disease connectome reveals a relatively undisturbed structural core network. *Human Brain Mapping*, 00(October 2014), p.n/a–n/a. Available at: http://doi.wiley.com/10.1002/hbm.22830.

Debnath, L., 2010. A brief historical introduction to Euler's formula for polyhedra, topology, graph theory and networks. *International Journal of Mathematical Education in Science and Technology*, 41(6), pp.769–785.

Derrible, S. & Kennedy, C., 2011. Applications of graph theory and network science to transit network design. *Transport Reviews*, 31(4), pp.495–519.

Drakesmith, M. et al., 2015. Overcoming the effects of false positives and threshold bias in graph theoretical analyses of neuroimaging data. *NeuroImage*, 118, pp.313–333. Available at: http://dx.doi.org/10.1016/j.neuroimage.2015.05.011.

Dunayevich, E. & Keck, P.E., 2000. Prevalence and description of psychotic features in bipolar mania. *Current psychiatry reports*, 2(4), pp.286–290.

Ellison-Wright, I. & Bullmore, E., 2010. Anatomy of bipolar disorder and schizophrenia: a meta-analysis. *Schizophrenia research*, 117(1), pp.1–12. Available at: http://www.ncbi.nlm.nih.gov/pubmed/20071149 [Accessed July 17, 2014].

Ellison-Wright, I. & Bullmore, E., 2009. Meta-analysis of diffusion tensor imaging studies in schizophrenia. *Schizophrenia research*, 108(1-3), pp.3–10. Available at: http://www.ncbi.nlm.nih.gov/pubmed/19128945 [Accessed August 24, 2014].

Emsell, L., Leemans, A., et al., 2013. Limbic and callosal white matter changes in euthymic bipolar I disorder: an advanced diffusion magnetic resonance imaging tractography study. *Biological psychiatry*, 73(2), pp.194–201. Available at: http://www.ncbi.nlm.nih.gov/pubmed/23158457 [Accessed November 1, 2013].

Emsell, L., Langan, C., et al., 2013. White matter differences in euthymic bipolar I disorder: A combined magnetic resonance imaging and diffusion tensor imaging voxel-based study. *Bipolar Disorders*, 15, pp.365–376.

Emsell, L. et al., 2014. White matter microstructural abnormalities in families multiply affected with bipolar I disorder: a diffusion tensor tractography study. *Psychological medicine*, 44(10), pp.2139–50. Available at: http://journals.cambridge.org/abstract_S0033291713002845 [Accessed April 18, 2016].

Emsell, L. & McDonald, C., 2009. The structural neuroimaging of bipolar disorder. *International review of psychiatry (Abingdon, England)*, 21(785026916), pp.297–313.

van Erp, T.G.M. et al., 2015. Subcortical brain volume abnormalities in 2028 individuals with schizophrenia and 2540 healthy controls via the ENIGMA consortium. *Molecular Psychiatry*, (October 2014), pp.1–7. Available at: http://www.nature.com/doifinder/10.1038/mp.2015.63.

Van Essen, D.C., 2011. The Human Connectome Project. *Journal of Vision*, 11, pp.8–8.

Van Essen, D.C. et al., 2013. The WU-Minn Human Connectome Project: An overview. *NeuroImage*, 80, pp.62–79.

Fischl, B., 2012. FreeSurfer. *NeuroImage*, 62(2), pp.774–781.

Forde, N.J. et al., 2015. Structural brain network analysis in families multiply affected with bipolar I disorder. *Psychiatry Research - Neuroimaging*, 234(1), pp.44–51. Available at: http://dx.doi.org/10.1016/j.pscychresns.2015.08.004.

Fornito, A. et al., 2012. Schizophrenia, neuroimaging and connectomics. *NeuroImage*, 62(4), pp.2296–2314. Available at: http://dx.doi.org/10.1016/j.neuroimage.2011.12.090.

Fornito, A. & Bullmore, E.T., 2014. Reconciling abnormalities of brain network structure and function in schizophrenia. *Current opinion in neurobiology*, 30C, pp.44–50. Available at: http://www.ncbi.nlm.nih.gov/pubmed/25238608 [Accessed January 7, 2015].

Fornito, A., Zalesky, A. & Breakspear, M., 2013. Graph analysis of the human connectome: promise, progress, and pitfalls. *NeuroImage*, 80, pp.426–44. Available at: http://www.ncbi.nlm.nih.gov/pubmed/23643999 [Accessed November 1, 2013].

Fornito, A., Zalesky, A. & Breakspear, M., 2015. The connectomics of brain disorders. *Nature Reviews Neuroscience*, 16(3), pp.159–172. Available at: http://dx.doi.org/10.1038/nrn3901.

Fusar-Poli, P. et al., 2011. Altered brain function directly related to structural abnormalities in people at ultra high risk of psychosis: Longitudinal VBM-fMRI study. *Journal of Psychiatric Research*, 45(2), pp.190–198. Available at: http://dx.doi.org/10.1016/j.jpsychires.2010.05.012.

Gadelkarim, J.J. et al., 2014. Investigating brain community structure abnormalities in bipolar disorder using path length associated community estimation. *Human Brain Mapping*, 35(April 2013), pp.2253–2264.

Gollo, L.L. et al., 2015. Dwelling quietly in the rich club: brain network determinants of slow cortical fluctuations. *Philosophical transactions of the Royal Society of London. Series B, Biological sciences*, 370(1668), p.20140165–. Available at: http://rstb.royalsocietypublishing.org/content/370/1668/20140165.abstract.

Griffa, A. et al., 2013. Structural connectomics in brain diseases. *NeuroImage*, 80, pp.515–526. Available at: http://dx.doi.org/10.1016/j.neuroimage.2013.04.056.

Hagmann, P. et al., 2008. Mapping the structural core of human cerebral cortex. *PLoS Biology*, 6(7), pp.1479–1493.

Hajek, T. et al., 2013. Functional neuroanatomy of response inhibition in bipolar disorders - Combined voxel based and cognitive performance meta-analysis. *Journal of Psychiatric Research*, 47(12), pp.1955–1966. Available at: http://dx.doi.org/10.1016/j.jpsychires.2013.08.015.

Hallahan, B. et al., 2011. Structural magnetic resonance imaging in bipolar disorder: an international collaborative mega-analysis of individual adult patient data. *Biological psychiatry*, 69(4), pp.326–35. Available at: http://www.ncbi.nlm.nih.gov/pubmed/21030008 [Accessed November 1, 2013].

Hamilton, M.C., 1960. Hamilton Depression Rating Scale (HAM-D). *REDLOC*, 23, pp.56–62.

Haznedar, M.M. et al., 2005. Fronto-thalamo-striatal gray and white matter volumes and anisotropy of their connections in bipolar spectrum illnesses. *Biological psychiatry*, 57(7), pp.733–42. Available at: http://www.ncbi.nlm.nih.gov/pubmed/15820230 [Accessed August 9, 2013].

He, Y., Chen, Z.J. & Evans, A.C., 2007. Small-world anatomical networks in the human brain revealed by cortical thickness from MRI. *Cerebral Cortex*, 17(10).

Heilbronner, S.R. & Haber, S.N., 2014. Frontal Cortical and Subcortical Projections Provide a Basis for Segmenting the Cingulum Bundle: Implications for Neuroimaging and Psychiatric Disorders. *Journal of Neuroscience*, 34(30), pp.10041–10054. Available at: http://www.jneurosci.org/cgi/doi/10.1523/JNEUROSCI.5459-13.2014.

van den Heuvel, M.P. et al., 2010. Aberrant frontal and temporal complex network structure in schizophrenia: a graph theoretical analysis. *The Journal of neuroscience : the official journal of the Society for Neuroscience*, 30(47), pp.15915–15926.

van den Heuvel, M.P. et al., 2013. Abnormal rich club organization and functional brain dynamics in schizophrenia. *JAMA psychiatry*, 70(8), pp.783–92. Available at: http://www.ncbi.nlm.nih.gov/pubmed/23739835 [Accessed July 24, 2014].

van den Heuvel, M.P. et al., 2009. Efficiency of functional brain networks and intellectual performance. *The Journal of neuroscience : the official journal of the Society for Neuroscience*, 29(23), pp.7619–7624.

van den Heuvel, M.P. & Sporns, O., 2013. Network hubs in the human brain. *Trends in Cognitive Sciences*, 17(12), pp.683–696. Available at: http://dx.doi.org/10.1016/j.tics.2013.09.012.

van den Heuvel, M.P. & Sporns, O., 2011. Rich-club organization of the human connectome. *The Journal of neuroscience : the official journal of the Society for Neuroscience*, 31(44), pp.15775–86. Available at: http://www.ncbi.nlm.nih.gov/pubmed/22049421 [Accessed July 10, 2014].

Hibar, D.P. et al., 2016. Subcortical volumetric abnormalities in bipolar disorder. *Molecular psychiatry*. Available at: http://www.ncbi.nlm.nih.gov/pubmed/26857596.

Houenou, J. et al., 2007. Increased white matter connectivity in euthymic bipolar patients: diffusion tensor tractography between the subgenual cingulate and the amygdalo-hippocampal complex. *Molecular psychiatry*, 12, pp.1001–1010.

Houenou, J. et al., 2012. Neuroimaging biomarkers in bipolar disorder. *Front Biosci (Elite Ed)*, 4, pp.593–606. Available at: http://www.ncbi.nlm.nih.gov/pubmed/22201897.

Houenou, J. et al., 2011. Neuroimaging-based markers of bipolar disorder: evidence from two meta-analyses. *Journal of affective disorders*, 132(3), pp.344–55. Available at: http://www.ncbi.nlm.nih.gov/pubmed/21470688.

IBM SPSS Amos, 2012. IBM SPSS Amos. *IBM Software Business Analytics*, YTD03114-U, pp.1–8.

Jbabdi, S. & Johansen-berg, H., 2013. Europe PMC Funders Group Tractography - where do we go from here ? *Brain Connect.*, 1(3), pp.169–183.

Jeurissen, B. et al., 2011. Probabilistic fiber tracking using the residual bootstrap with constrained spherical deconvolution. *Human Brain Mapping*, 32(3), pp.461–479. Available at: http://doi.wiley.com/10.1002/hbm.21032.

Johansen-Berg, H. et al., 2004. Changes in connectivity profiles define functionally distinct regions in human medial frontal cortex. *Proceedings of the National Academy of Sciences of the United States of America*, 101(36), pp.13335–40. Available at: http://www.ncbi.nlm.nih.gov/pubmed/15340158.

Johansen-Berg, H. & Behrens, T.E.J., 2006. Just pretty pictures? What diffusion tractography can add in clinical neuroscience. *Current opinion in neurology*, 19(4), pp.379–385.

Jones, D.K., 2010. Challenges and limitations of quantifying brain connectivity in vivo with diffusion MRI. , 2, pp.341–355.

Jones, D.K. et al., 2013. Distinct subdivisions of the cingulum bundle revealed by diffusion MRI fibre tracking: Implications for neuropsychological investigations. *Neuropsychologia*, 51(1), pp.67–78. Available at: http://dx.doi.org/10.1016/j.neuropsychologia.2012.11.018.

Jones, D.K., 2008. Studying connections in the living human brain with diffusion MRI. *Cortex*, 44(8), pp.936–952.

Jones, D.K. & Cercignani, M., 2010. Twenty-five pitfalls in the analysis of diffusion MRI data. *NMR in Biomedicine*, 23(7), pp.803–820.

Jones, D.K., Knösche, T.R. & Turner, R., 2013. White matter integrity, fiber count, and other fallacies: The do's and don'ts of diffusion MRI. *NeuroImage*, 73, pp.239–254. Available at: http://dx.doi.org/10.1016/j.neuroimage.2012.06.081.

Kenney, J. et al., 2015. Cognitive course in first-episode psychosis and clinical correlates: A 4year longitudinal study using the MATRICS Consensus Cognitive Battery. *Schizophrenia Research*. Available at: http://linkinghub.elsevier.com/retrieve/pii/S0920996415004764.

Kirkpatrick, B. et al., 2008. Is schizophrenia a syndrome of accelerated aging? *Schizophrenia bulletin*, 34(6), pp.1024–32. Available at: http://schizophreniabulletin.oxfordjournals.org/content/34/6/1024 [Accessed March 28, 2016].

Kocher, M. et al., 2015. Individual variability in the anatomical distribution of nodes participating in rich club structural networks. *Frontiers in neural circuits*, 9(April), p.16.

Kraepelin, E., 1904. Lecture XXIX: Morbid personalities. *Lectures on clinical psychiatry.*, p.282.

Kubicki, M. et al., 2011. Stochastic tractography study of Inferior Frontal Gyrus anatomical connectivity in schizophrenia. *NeuroImage*, 55(4), pp.1657–1664.

Laidi, C. et al., 2015. Cerebellar volume in schizophrenia and bipolar I disorder with and without psychotic features. *Acta psychiatrica Scandinavica*, 131(3), pp.223–33. Available at: http://www.pubmedcentral.nih.gov/articlerender.fcgi?artid=4329064&tool=pmcentrez&rendertype=abstract [Accessed April 24, 2016].

Langan, C. & McDonald, C., 2009. Neurobiological trait abnormalities in bipolar disorder. *Molecular psychiatry*, 14(9), pp.833–846. Available at: http://dx.doi.org/10.1038/mp.2009.39.

Leemans, A. et al., 2009. ExploreDTI: a graphical toolbox for processing, analyzing, and visualizing diffusion MR data. In *Proceedings 17th Scientific Meeting, International Society for Magnetic Resonance in Medicine*. p. 3537. Available at: http://www.mendeley.com/research/exploredti-a-graphical-toolbox-for-processing-analyzing-and-visualizing-diffusion-mr-data/\nhttp://www.exploredti.com/ref/ExploreDTI_ISMRM_2009.pdf.

Leemans, A. & Jones, D.K., 2009. The B-matrix must be rotated when correcting for subject motion in DTI data. *Magnetic Resonance in Medicine*, 61(6), pp.1336–1349.

Leonhard, K., 1957. Pathogenesis of manic-depressive disease. *Der Nervenarzt*, 28(6), pp.271–2. Available at: http://www.ncbi.nlm.nih.gov/pubmed/13451870 [Accessed July 1, 2016].

Leow, A. et al., 2013. Impaired inter-hemispheric integration in bipolar disorder revealed with brain network analyses. *Biological psychiatry*, 73(2), pp.183–93. Available at: http://www.ncbi.nlm.nih.gov/pubmed/23122540 [Accessed August 15, 2013].

Levitt, J.J. et al., 2012. Fractional anisotropy and radial diffusivity: diffusion measures of white matter abnormalities in the anterior limb of the internal capsule in schizophrenia. *Schizophrenia research*, 136(1-3), pp.55–62. Available at: http://www.ncbi.nlm.nih.gov/pubmed/22019073.

Li, W. et al., 2013. Subregions of the human superior frontal gyrus and their connections. *NeuroImage*, 78, pp.46–58. Available at: http://dx.doi.org/10.1016/j.neuroimage.2013.04.011.

Linke, J. et al., 2013. Impaired anatomical connectivity and related executive functions: Differentiating vulnerability and disease marker in bipolar disorder. *Biological Psychiatry*, 74(12), pp.908–916. Available at: http://dx.doi.org/10.1016/j.biopsych.2013.04.010.

Lois, G., Linke, J. & Wessa, M., 2014. Altered Functional Connectivity between Emotional and Cognitive Resting State Networks in Euthymic Bipolar I Disorder Patients. *PLoS ONE*, 9(10), p.e107829. Available at: http://dx.plos.org/10.1371/journal.pone.0107829.

Lu, L.H. et al., 2011. White matter microstructure in untreated first episode bipolar disorder with psychosis: Comparison with schizophrenia. *Bipolar Disorders*, 13, pp.604–613.

Marneros, A. et al., 2009. Bipolar i disorder with mood-incongruent psychotic symptoms: A comparative longitudinal study. *European Archives of Psychiatry and Clinical Neuroscience*, 259(3), pp.131–136.

Mason, L. et al., 2014. Decision-making and trait impulsivity in bipolar disorder are associated with reduced prefrontal regulation of striatal reward valuation. *Brain*, 137, pp.2346–2355.

McAuley, J.J., da Fontoura Costa, L. & Caetano, T.S., 2007. Rich-club phenomenon across complex network hierarchies. *Applied Physics Letters*, 91(8), p.084103. Available at: http://scitation.aip.org/content/aip/journal/apl/91/8/10.1063/1.2773951 [Accessed July 24, 2014].

McColgan, P. et al., 2015. Selective vulnerability of Rich Club brain regions is an organizational principle of structural connectivity loss in Huntington's disease. *Brain : a journal of neurology*, 138(Pt 11), pp.3327–44. Available at: http://brain.oxfordjournals.org/content/138/11/3327 [Accessed March 28, 2016].

McDonald, C. et al., 2004. Association of genetic risks for schizophrenia and bipolar disorder with specific and generic brain structural endophenotypes. *Archives of general psychiatry*, 61(10), pp.974–84. Available at: http://www.ncbi.nlm.nih.gov/pubmed/15466670.

Meskaldji, D.E. et al., 2013. Comparing connectomes across subjects and populations at different scales. *NeuroImage*, 80, pp.416–425. Available at: http://dx.doi.org/10.1016/j.neuroimage.2013.04.084.

Mohlenkamp, M.J., 2011. A User ' s Guide to Spherical Harmonics.

Montgomery, S.A. & Asberg, M., 1979. A new depression scale designed to be sensitive to change. *The British journal of psychiatry : the journal of mental science*, 134, pp.382–9. Available at: http://www.ncbi.nlm.nih.gov/pubmed/444788 [Accessed March 19, 2015].

Neuhäuser, M. & Manly, B.F.J., 2004. The Fisher-Pitman permutation test when testing for differences in mean and variance. *Psychological reports*, 94(1), pp.189–94. Available at: http://www.ncbi.nlm.nih.gov/pubmed/15077763 [Accessed April 24, 2016].

Newman, M.E.J. & Girvan, M., 2004. Finding and evaluating community structure in networks. *Physical Review E - Statistical, Nonlinear, and Soft Matter Physics*, 69, pp.1–15.

Nortje, G. et al., 2013. Systematic review and voxel-based meta-analysis of diffusion tensor imaging studies in bipolar disorder. *Journal of affective disorders*, 150(2), pp.192–200. Available at: http://www.ncbi.nlm.nih.gov/pubmed/23810479 [Accessed July 17, 2014].

O'Donnell, L.J. & Pasternak, O., 2015. Does diffusion MRI tell us anything about the white matter? An overview of methods and pitfalls. *Schizophrenia Research*, 161(1), pp.133–141. Available at: http://linkinghub.elsevier.com/retrieve/pii/S0920996414004733.

O'Donoghue, S. et al., 2015. Applying neuroimaging to detect neuroanatomical dysconnectivity in psychosis. *Epidemiology and psychiatric sciences*, pp.1–5. Available at: http://journals.cambridge.org/abstract_S2045796015000074.

Parker, C.S. et al., 2014. Consensus between Pipelines in Structural Brain Networks. *PLoS ONE*, 9(10).

Phillips, M., Ladouceur, C. & Drevets, W., 2008. Automatic and Volontary Regulation of Emotion. *Molecular Psychiatry*, 13(9), pp.829–857.

Phillips, M.L. & Swartz, H.A., 2014. A critical appraisal of neuroimaging studies of bipolar disorder: Toward a new conceptualization of underlying neural circuitry and a road map for future research. *American Journal of Psychiatry*, 171(8), pp.829–843.

Quigley, S.J. et al., 2015. Psychiatry Research : Neuroimaging Volume and shape analysis of subcortical brain structures and ventricles in euthymic bipolar I disorder. *Psychiatry Research: Neuroimaging*, 233(3), pp.324–330. Available at: http://dx.doi.org/10.1016/j.pscychresns.2015.05.012.

de Reus, M. a. & van den Heuvel, M.P., 2013a. Estimating false positives and negatives in brain networks. *NeuroImage*, 70, pp.402–409. Available at: http://dx.doi.org/10.1016/j.neuroimage.2012.12.066.

de Reus, M. a. & van den Heuvel, M.P., 2013b. The parcellation-based connectome: Limitations and extensions. *NeuroImage*, 80, pp.397–404.

Roberts, J.A. et al., 2016. The contribution of geometry to the human connectome. *NeuroImage*, 124, pp.379–393. Available at: http://dx.doi.org/10.1016/j.neuroimage.2015.09.009.

Rorden, C., Karnath, H.-O. & Bonilha, L., 2007. Improving lesion-symptom mapping. *Journal of cognitive neuroscience*, 19(7), pp.1081–1088.

RStudio, 2012. RStudio: Integrated development environment for R. *The Journal of Wildlife Management*, 75(8). Available at: http://www.rstudio.org.

Rubinov, M. & Bullmore, E., 2013. Schizophrenia and abnormal brain network hubs. *Dialogues in Clinical Neuroscience*, 15, pp.339–349.

Rubinov, M. & Sporns, O., 2010. Complex network measures of brain connectivity: uses and interpretations. *NeuroImage*, 52(3), pp.1059–69. Available at: http://www.ncbi.nlm.nih.gov/pubmed/19819337 [Accessed October 31, 2013].

Sarrazin, S. et al., 2014. A multicenter tractography study of deep white matter tracts in bipolar I disorder: psychotic features and interhemispheric disconnectivity. *JAMA psychiatry*, 71(4), pp.388–96. Available at: http://www.ncbi.nlm.nih.gov/pubmed/24522197 [Accessed July 18, 2014].

Sarrazin, S. et al., 2015. Corpus callosum area in patients with bipolar disorder with and without psychotic features: an international multicentre study. *Journal of psychiatry & neuroscience : JPN*, 40(5), pp.352–9. Available at: http://www.pubmedcentral.nih.gov/articlerender.fcgi?artid=4543098&tool=pmcentrez&rendertype=abstract [Accessed April 24, 2016].

Sassi, R.B. et al., 2002. *Increased gray matter volume in lithium-treated bipolar disorder patients*,

Scanlon, C. et al., 2014. Cortical thinning and caudate abnormalities in first episode psychosis and their association with clinical outcome. *Schizophrenia Research*.

Senden, M. et al., 2014. Rich club organization supports a diverse set of functional network configurations. *NeuroImage*, 96, pp.174–182.

Skudlarski, P. et al., 2013. Diffusion tensor imaging white matter endophenotypes in patients with schizophrenia or psychotic bipolar disorder and their relatives. *American Journal of Psychiatry*, 170(8), pp.886–898.

Smith, S.M. et al., 2006. Tract-based spatial statistics: Voxelwise analysis of multi-subject diffusion data. *NeuroImage*, 31(4), pp.1487–1505.

Soares, J.M. et al., 2013. A hitchhiker's guide to diffusion tensor imaging. *Frontiers in neuroscience*, 7, p.31. Available at: http://www.pubmedcentral.nih.gov/articlerender.fcgi?artid=3594764&tool=pmcentrez&rendertype=abstract [Accessed July 18, 2014].

Sporns, O., 2013a. Making sense of brain network data. *Nature methods*, 10(6), pp.491–3. Available at: http://www.ncbi.nlm.nih.gov/pubmed/23722207 [Accessed November 1, 2013].

Sporns, O., 2013b. Structure and function of complex brain networks. *Dialogues in clinical neuroscience*, 15(3), pp.247–62. Available at: http://www.pubmedcentral.nih.gov/articlerender.fcgi?artid=3811098&tool=pmcentrez&rendertype=abstract [Accessed March 21, 2016].

Sporns, O., 2013c. The human connectome: Origins and challenges. *NeuroImage*, 80, pp.53–61. Available at: http://dx.doi.org/10.1016/j.neuroimage.2013.03.023.

Sporns, O. & Van Den Heuvel, M.P., 2013. Network maps of the human brain's rich club. *Network Science*, (August), pp.1–3. Available at: http://www.journals.cambridge.org/abstract_S2050124213000088.

Sporns, O., Tononi, G. & Edelman, G.M., 2000. Connectivity and complexity: the relationship between neuroanatomy and brain dynamics. *Neural networks : the official journal of the International Neural Network Society*, 13(8-9), pp.909–22. Available at: http://www.ncbi.nlm.nih.gov/pubmed/11156201.

Sporns, O., Tononi, G. & Kötter, R., 2005. The human connectome: A structural description of the human brain. *PLoS*

Computational Biology, 1(4), pp.0245–0251.

Stejskal, E.O. & Tanner, J.E., 1965. Spin Diffusion Measurements: Spin Echoes in the Presence of a Time-Dependent Field Gradient. *The Journal of Chemical Physics*, 42(1), p.288. Available at: http://scitation.aip.org/content/aip/journal/jcp/42/1/10.1063/1.1695690.

Strakowski, S.M. et al., 2011. Functional magnetic resonance imaging brain activation in bipolar mania: Evidence for disruption of the ventrolateral prefrontal-amygdala emotional pathway. *Biological Psychiatry*, 69(4), pp.381–388. Available at: http://dx.doi.org/10.1016/j.biopsych.2010.09.019.

Strakowski, S.M. et al., 2000. Neuroimaging in bipolar disorder. *Bipolar disorders*, 2(3 Pt 1), pp.148–164.

Strakowski, S.M., Adler, C.M. & DelBello, M.P., 2002. Volumetric MRI studies of mood disorders: do they distinguish unipolar and bipolar disorder? *Bipolar disorders*, 4, pp.80–88.

Strakowski, S.M., Delbello, M.P. & Adler, C.M., 2005. The functional neuroanatomy of bipolar disorder: a review of neuroimaging findings. *Molecular psychiatry*, 10(1), pp.105–116.

Strakowski, S.S.M. et al., 2012. The functional neuroanatomy of bipolar disorder: a consensus model. *Bipolar disorders*, 14(4), pp.313–325. Available at: http://www.ncbi.nlm.nih.gov/pubmed/22631617.

Sun, Y. et al., 2015. Reduced Hemispheric Asymmetry of Brain Anatomical Networks Is Linked to Schizophrenia: A Connectome Study. , pp.1–14.

Sussmann, J.E. et al., 2009. White matter abnormalities in bipolar disorder and schizophrenia detected using diffusion tensor magnetic resonance imaging. *Bipolar Disorders*, 11(1), pp.11–18. Available at: http://www.ncbi.nlm.nih.gov/pubmed/19133962\nhttp://onlinelibrary.wiley.com/store/10.1111/j.1399-5618.2008.00646.x/asset/j.1399-5618.2008.00646.x.pdf?v=1&t=guv6xk6e&s=1931b1d7e9f20cf98b5d23951bf7758febe81882.

Sussmann, J.E. et al., 2009. White matter abnormalities in bipolar disorder and schizophrenia detected using diffusion tensor magnetic resonance imaging. *Bipolar Disorders*, 11(1), pp.11–8. Available at: http://www.ncbi.nlm.nih.gov/pubmed/19133962\nhttp://onlinelibrary.wiley.com/store/10.1111/j.1399-5618.2008.00646.x/asset/j.1399-5618.2008.00646.x.pdf?v=1&t=guv6xk6e&s=1931b1d7e9f20cf98b5d23951bf7758febe81882 [Accessed April 19, 2016].

Tax, C.M.W. et al., 2014. Recursive calibration of the fiber response function for spherical deconvolution of diffusion MRI data. *NeuroImage*, 86, pp.67–80. Available at: http://dx.doi.org/10.1016/j.neuroimage.2013.07.067.

Thomson, P., 2007. Physician's desk reference 61st ed. *Montvale, NJ*, p.3171.

Tournier, J., Mori, S. & Leemans, a, 2011. Diffusion Tensor Imaging and Beyond. *Magnetic Resonance in …*, 65(6), pp.1532–1556. Available at: http://onlinelibrary.wiley.com/doi/10.1002/mrm.22924/full.

Tournier, J.D., Calamante, F. & Connelly, A., 2007. Robust determination of the fibre orientation distribution in diffusion MRI: Non-negativity constrained super-resolved spherical deconvolution. *NeuroImage*, 35(4), pp.1459–1472.

Trost, S. et al., 2014. Disturbed Anterior Prefrontal Control of the Mesolimbic Reward System and Increased Impulsivity in Bipolar Disorder. *Neuropsychopharmacology : official publication of the American College of*

Neuropsychopharmacology, 39(October 2013), pp.1–37. Available at: http://www.ncbi.nlm.nih.gov/pubmed/24535101.

Tzourio-Mazoyer, N. et al., 2002. Automated anatomical labeling of activations in SPM using a macroscopic anatomical parcellation of the MNI MRI single-subject brain. *NeuroImage*, 15, pp.273–289.

Vargas, C., López-Jaramillo, C. & Vieta, E., 2013. A systematic literature review of resting state network--functional MRI in bipolar disorder. *Journal of affective disorders*, 150(3), pp.727–35. Available at: http://www.ncbi.nlm.nih.gov/pubmed/23830141 [Accessed November 1, 2013].

Vederine, F.-E. et al., 2011. A meta-analysis of whole-brain diffusion tensor imaging studies in bipolar disorder. *Progress in Neuro-Psychopharmacology and Biological Psychiatry*, 35(8), pp.1820–1826. Available at: http://dx.doi.org/10.1016/j.pnpbp.2011.05.009.

van Veelen, N.M.J. et al., 2011. Reduced language lateralization in first-episode medication-naive schizophrenia. *Schizophrenia Research*, 127(1), pp.195–201.

Velthorst, E. & Meijer, C., 2012. The association between social anhedonia, withdrawal and psychotic experiences in general and high-risk populations. *Schizophrenia Research*, 138(2), pp.290–294.

Versace, A. et al., 2008. Elevated left and reduced right orbitomedial prefrontal fractional anisotropy in adults with bipolar disorder revealed by tract-based spatial statistics. *Archives of general psychiatry*, 65(9), pp.1041–1052.

Wang, F. et al., 2009. Determined Through Diffusion Tensor Imaging. *British Journal of Psychiatry*, 193(2), pp.126–129. Available at: http://bjp.rcpsych.org/cgi/content/abstract/193/2/126.

Wegbreit, E. et al., 2014. Developmental Meta-analyses of the Functional Neural Correlates of Bipolar Disorder. *JAMA psychiatry*, 71(8), pp.926–35. Available at: http://www.ncbi.nlm.nih.gov/pubmed/25100166.

Wessa, M., Kanske, P. & Linke, J., 2014. Bipolar disorder: A neural network perspective on a disorder of emotion and motivation. *Restorative Neurology and Neuroscience*, 32, pp.51–62.

Wessa, M. & Linke, J., 2009. Emotional processing in bipolar disorder: behavioural and neuroimaging findings. *International review of psychiatry (Abingdon, England)*, 21(4), pp.357–367.

Wheeler, A.L. et al., 2015. Further Neuroimaging Evidence for the Deficit Subtype of Schizophrenia. *JAMA Psychiatry*, pp.1–10. Available at: http://archpsyc.jamanetwork.com/article.aspx?doi=10.1001/jamapsychiatry.2014.3020.

Wise, T. et al., 2015. Voxel-Based Meta-Analytical Evidence of Structural Disconnectivity in Major Depression and Bipolar Disorder. *Biological Psychiatry*, pp.1–10. Available at: http://linkinghub.elsevier.com/retrieve/pii/S000632231500195X.

Yip, S.W. et al., 2014. Hypoactivation of the Ventral and Dorsal Striatum During Reward and Loss Anticipation in Antipsychotic and Mood Stabilizer-Naive Bipolar Disorder. *Neuropsychopharmacology*, 40(3), pp.1–9. Available at: http://www.ncbi.nlm.nih.gov/pubmed/25139065.

Young, R.C. et al., 1978. A rating scale for mania: Reliability, validity and sensitivity. *British Journal of Psychiatry*, 133(11), pp.429–435.

Yu, C. et al., 2011. Functional segregation of the human cingulate cortex is confirmed by functional connectivity based neuroanatomical parcellation. *NeuroImage*, 54(4), pp.2571–2581. Available at: http://dx.doi.org/10.1016/j.neuroimage.2010.11.018.

Zalesky, A. et al., 2012. Connectivity differences in brain networks. *NeuroImage*, 60(2), pp.1055–62. Available at: http://www.ncbi.nlm.nih.gov/pubmed/22273567 [Accessed November 1, 2013].

Zalesky, A. et al., 2011. Disrupted axonal fiber connectivity in schizophrenia. *Biological psychiatry*, 69(1), pp.80–9. Available at: http://www.ncbi.nlm.nih.gov/pubmed/21035793 [Accessed November 1, 2013].

Zalesky, A., Fornito, A., Harding, I.H., et al., 2010. Whole-brain anatomical networks: does the choice of nodes matter? *NeuroImage*, 50(3), pp.970–83. Available at: http://www.ncbi.nlm.nih.gov/pubmed/20035887 [Accessed November 1, 2013].

Zalesky, A. & Fornito, A., 2009. A DTI-Derived Measure of Cortico-Cortical Connectivity. , 28(7), pp.1–12.

Zalesky, A., Fornito, A. & Bullmore, E.T., 2010. Network-based statistic: identifying differences in brain networks. *NeuroImage*, 53(4), pp.1197–207. Available at: http://www.ncbi.nlm.nih.gov/pubmed/20600983 [Accessed November 1, 2013].

Zhang, T. et al., 2014. Characterization of U-shape streamline fibers: Methods and applications. *Medical Image Analysis*, 18(5), pp.795–807.

Zivanovic, O. & Nedic, A., 2012. Kraepelin's concept of manic-depressive insanity: One hundred years later. *Journal of Affective Disorders*, 137(1), pp.15–24.

List of publications arising from this work

Published Abstracts

O'Donoghue S, Emsell L, Langan C, Forde N, Cannon DM and McDonald C (2014). An Investigation of Global Network Structure in Bipolar Disorder. *Frontiers in Neuroscience*. Conference Abstract: Neuroscience Ireland Young Neuroscientists Symposium 2014. doi: 10.3389/conf.fnins.2014.87.00032

S. O'Donoghue, N.J. Forde, S Sarrazin, C. Poupon, J. Houenou, M.L. Phillips, A. Versace, M. Wessa, J. Linke, D. M Cannon, Colm McDonald. Anatomical dysconnectivity in bipolar 1 disorder: A graph theory study across three centers, (2016), Posters. *Bipolar Disorders*, 18: 70–194. doi:10.1111/bdi.12407

Peer-Reviewed Journal Publications

S. O'Donoghue, D. M. Cannon, C. Perlini, P. Brambilla, and C. McDonald, "Applying neuroimaging to detect neuroanatomical dysconnectivity in psychosis.," *Epidemiology and Psychiatric Sciences.*, pp. 1–5, 2015. doi: 10.1017/S2045796015000074

S. O'Donoghue, L. Kilmartin, D. O'Hora, J.N. Forde, L. Emsell, C. Langan, A.Leemans, G.Barker, D.M.Cannon, C.McDonald. Anatomical Integration and Rich Club Connectivity in Euthymic Bipolar Disorder. *Psychological Medicine* (Revised draft under review)

S.O'Donoghue, L. Holleran, D.M.Cannon, C.McDonald. Anatomical dysconnectivity in bipolar disorder in comparison to schizophrenia: A review of structural network analyses using diffusion MRI. *Journal of Affective Disorders* (Revised draft under review)